

**Lakehead University**

**Experimental Study of Vertical and Oblique Particle Clouds in Water**

Submitted by

**Mohamad Moghadaripour**

A thesis submitted to the Faculty of Graduate Studies in partial  
fulfillment of the requirements for degree of Master of Science

in

Environmental Engineering  
Department of Civil Engineering

Fall 2016

Thunder Bay, Ontario

Advisor: Dr. Amir Azimi

Co-advisor: Dr. Siyamak Elyasi

***Abstract:***

Sand jets and particle clouds are common in many engineering areas such as marine bed capping, dredging, and artificial island construction. Because of the wide range of their application, a better understanding of particle cloud's behavior will lead to increase the efficiency of engineering systems and lead to an improvement in predicting the behavior of solid-liquid flows. There are many parameters that can control the behavior of particle clouds behavior such as nozzle diameter  $d_o$ , particle size  $D_{50}$ , released mass  $m$ , impact velocity of sand particles (at the surface)  $u_i$  and initial oblique angle of the particle cloud. Moreover, some characteristics of two-phase flows such as entrainment coefficient and drag coefficient can be very important for controlling the impact of the two-phase flow.

In this research, laboratory experiments were conducted to find the impact of controlling parameters on the dynamics of vertical and oblique particle clouds in the water media. For considering the impact velocity of sand particles on the surface, the  $u_i$  was varied by changing the release height  $H$ . Nozzle size and mass of particles were grouped to form a non-dimensional parameter as aspect ratio  $L_o/d_o$ , where  $L_o$  is a length of sand particles occupied in a pipe with a nozzle diameter of  $d_o$ . It was found that the modified initial energy and circulation are correlated with  $L_o/d_o$ . A direct correlation between the width and frontal velocity of particle clouds with  $L_o/d_o$  was found. These relationships were formulated power law equations and can be used for prediction of cloud size and its frontal velocity. A wide range of particle sizes ( $D_{50}=0.1375$  mm– $0.718$  mm) was used to study the effects of particle size on spreading of sand jets and particle clouds. Effects of  $L_o/d_o$  and particle size on the evolution of sand particles in water media was also investigated. It was found that particle clouds with small particle sizes ( $D_{50}=0.1375$  mm) formed a sphere shape whereas particle cloud with a large particle size ( $D_{50}=0.595$  mm) forms an arc shape. Wider particle clouds were observed for small particles due

to the tendency of small particles to follow eddies. Experimental results indicated that particle cloud dilute almost six times faster than sand jets with similar initial conditions. Effects of impact velocity of sand particles on spreading of particle clouds were investigated and results were compared with similar clouds with zero released heights. For small  $L_o/d_o$  ratios (i.e.,  $L_o/d_o \leq 1.5$ ) experimental results indicated a direct correlation between  $H$  and the width of particle clouds. This relationship was adverse for  $1.5 < L_o/d_o < 15$ .

For considering the dynamics of oblique particle cloud, laboratory experiments were carried out for different particle sizes ( $D_{50}=0.196, 0.275, 0.3895, \text{ and } 0.507$  mm), drop heights ( $H=0.25, 0.6$  and  $1$  m), sand mass of ( $m=5, 16.2, 30.4, 44.5$  and  $60.7$  grams) and drop angle ( $\alpha=15, 30, 45$  and  $60$  degree). It was observed that aspect ratio of particle cloud (i.e.,  $L_o/d_o$  ratio) affect the velocity and maximum horizontal displacement  $x_{max}$  of the oblique particle cloud. As the aspect ratio increases, the velocity and the  $x_{max}$  tend to increase. Moreover, regardless of aspect ratio and the particle size, the oblique particle clouds reach to the maximum horizontal displacement at almost  $t/T=3$ , where  $t$  is the elapsed time from the releasing point and  $T$  is the time of the initial phase. Increasing the particle size and the drop angle also increases the maximum horizontal displacement of clouds. Effect of drop height on the  $x_{max}$  of oblique particle cloud was also investigated. For the small aspect ratio (i.e.,  $L_o/d_o=1.2$ ), an increase in the height decreases the  $x_{max}$ ; while for the medium and large aspect ratios (i.e.,  $L_o/d_o=7.5, 11$  and  $15$ ), as the drop height increases, the  $x_{max}$  also increases. The entrainment velocity is proportional to the frontal velocity of particle clouds using entrainment coefficient. Based on the experimental results, equations are developed for predicting depth, width, and velocity of particle cloud along the time. Using the equations with respect to the definition of entrainment coefficient, an equation have been developed for predicting the entrainment coefficient. It was concluded that

the entrainment coefficient of the particle cloud with small particle sizes is greater than entrainment coefficient of plumes. It was also observed that for the vertical particle cloud, the cloud with larger aspect ratio has smaller drag coefficient. Moreover, for quantifying the resistance of particle cloud in the water media, an equation for the drag coefficient of particles in the cloud has been developed.

## **Acknowledgements**

Foremost, I would like to express my sincere gratitude to my advisor Dr. Amir Azimi for the continuous support of my master study and research. I would like to thank my co-advisor, Dr. Siyamak Elyasi, who has been always there to listen and give advice to me and also to my family for their continuous support during my entire life.

## Contents

Chapter 1: General Introduction .....	1
<b>1.1 Motivation of the Present Study .....</b>	<b>1</b>
<b>1.2 Application of Sand jets and Particle Clouds .....</b>	<b>2</b>
<b>1.3 Overview of the Present Study .....</b>	<b>4</b>
<b>1.4 Novelty of the Study .....</b>	<b>4</b>
Chapter 2: Literature Review .....	6
<b>2.1 Single-Phase Flow .....</b>	<b>6</b>
<b>2.2. Two-Phase Flow .....</b>	<b>15</b>
Chapter 3: Experimental Study of Sand Jets and Particle Clouds in Water .....	27
<b>3.1 Introduction .....</b>	<b>27</b>
<b>3.2 Theory and Background .....</b>	<b>30</b>
<b>3.3 Experimental Design and Data Analysis .....</b>	<b>34</b>
<b>3.4 Experimental Results .....</b>	<b>36</b>
3.4.1 General Evolution of Sand Jet Front .....	36
3.4.2 Effect of particle size .....	48
3.4.3 Particle Cloud Concentration .....	52
3.4.4 Effect of impact velocity: .....	56
<b>3.5 Summary and conclusion .....</b>	<b>63</b>
<b>3.6 Acknowledgement .....</b>	<b>64</b>
<b>3.7 Notation .....</b>	<b>65</b>
Chapter 4: Experimental Study of Oblique Particle Clouds in Water .....	67
<b>4.1 Introduction .....</b>	<b>67</b>
<b>4.2 Theory and Background .....</b>	<b>70</b>
<b>4.3 Experimental Setup .....</b>	<b>74</b>
<b>4.4 Experimental Results .....</b>	<b>77</b>
4.4.1 General Evolution of Sand Jet Front .....	77
4.4.2 Effect of Particle Size .....	82
4.4.3 Effect of Drop Angle .....	86
4.4.4 Effect of Drop Height .....	88
4.4.5 Entrainment Coefficient of Particle Clouds .....	91

4.4.6 Drag Coefficient of Particle Clouds .....	93
<b>4.5 Summary and Conclusion .....</b>	<b>97</b>
<b>4.6 Notation .....</b>	<b>99</b>
Chapter 5: General Conclusions and Recommendations for Future Research .....	101
<b>5.1 General Conclusions .....</b>	<b>101</b>
<b>5.2 Future Research Studies.....</b>	<b>105</b>

## List of Figures

Figure 1.1 Construction of Palm Jumeirah (Photo by Stive RKH).....	2
Figure 1.2: Discharge of slurry into Tailing Storage Facility.....	3
Figure 3.1 Schematic of the experimental setup and coordinate system. ....	36
Figure 3.3: Evolution of transient sand jets for particle size of $D_{50}=0.389$ mm at different non-dimensional time $t^*$ considering the effect of $L_o/d_o$ ratio: a) $L_o/d_o = 5$ , b) $L_o/d_o = 1.8$ , c) $L_o/d_o = 0.8$ .....	40
Figure 3.4: Effect of $L_o/d_o$ ratio on the normalized depth $x/L_i$ along normalized time $t/T$ : a) $D_{50}=0.196$ mm, b) $D_{50}=0.389$ mm, c) $D_{50}=0.507$ mm.....	42
Figure 3.5: Effect of $L_o/d_o$ ratio on the normalized velocity $u_f/u_\infty$ along the normalized depth $x/d$ : a) $D_{50}=0.196$ mm, b) $D_{50}=0.389$ mm, c) $D_{50}=0.507$ mm.....	45
Figure 3.6: Effect of $L_o/d_o$ ratio on the normalized width $b/d_o$ along the normalized depth $t/T$ : a) $D_{50}=0.196$ mm, b) $D_{50}=0.389$ mm, c) $D_{50}=0.507$ mm.....	47
Figure 3.7: Effect of particle size at different $t^*=t/T$ : a) A15, $D_{50} = 0.718$ mm, b) A7, $D_{50} = 0.389$ mm, c) A14, $D_{50} = 0.1375$ mm. ....	49
Figure 3.8: Effect of particle size on normalized velocity $u_f/u_\infty$ along normalized depth $x/d_o$ . ....	51
Figure 3.9: Effect of particle size on width: a) Normalized width $b/d_o$ along normalized depth $x/d_o$ , b) Normalized width $b/d_o$ along normalized time $t/T$ .....	52
Figure 3.10: Concentration comparison for sand jets and particle clouds. a) Particle clouds for small and large particle sizes ( $D_{50}=0.196$ and $0.507$ mm) b) The line is correspond to sand jets (Hall et al., 2010) .....	54
Figure 3.11: Variation of normalized volume $V/b^3$ with normalized time $t^*$ . a) $D_{50}=0.196$ mm, b) $D_{50}=0.389$ mm, c) $D_{50}=0.507$ mm. ....	55
Figure 3.12: Effect of drop height on normalized width $b/d_o$ along normalized depth $x/d_o$ for small particle size, $D_{50}=0.196$ mm. a) $L_o/d_o =1.5$ , b) $L_o/d_o =4.9$ , c) $L_o/d_o =5.8$ , d) $L_o/d_o =19.6$ ....	58
Figure 3.13: Effect of drop height on normalized width $b/d_o$ along normalized depth $x/d_o$ for medium particle size, $D_{50}=0.389$ mm. a) $L_o/d_o =0.8$ , b) $L_o/d_o =1.8$ , c) $L_o/d_o =5.0$ , d) $L_o/d_o =15$ . .	60
Figure 3.14: Effect of drop height at different $x/d_o$ for particle size of $D_{50}=0.389$ mm. a) Test No. A5, $H=0$ m, b) Test No. B11, $H=1.3$ m. ....	61
Figure 3.15: Effect of drop height on normalized width $b/d_o$ along normalized depth $x/d_o$ for large particle size, $D_{50}=0.507$ mm. a) $L_o/d_o =4.9$ b) $L_o/d_o =19.6$ . ....	62
No table of figures entries found. Figure 4.1.: Schematic of entrainment in vertical particle clouds and experimental setup a) Entrainment in initial phase b) Entrainment in thermal phase c) Schematic of the experimental setup. ....	77
Figure 4.2: Evolution of oblique particle cloud for particle size of $0.389$ mm at different normalized time $t/T$ considering the effect of aspect ratio. a) Test No. A2, $L_o/d_o = 4$ , b) Test No. A4, $L_o/d_o = 11$ .....	79
Figure 4.3: Effect of aspect ratio on normalized vertical velocity $u_y/u_\infty$ of oblique particle cloud with initial oblique angle of $60^\circ$ . a) $D_{50}=0.389$ mm, b) $D_{50}=0.507$ mm. ....	81

Figure 4.4: Effect of aspect ratio on trajectory results of oblique particle cloud with initial oblique angle of $60^\circ$ . a) Particle size of 0.389 mm b) Particle size of 0.507 mm .....	82
Figure 4.5: Effect of particle size at different normalized time $t/T$ for oblique particle cloud with initial oblique angle of $45^\circ$ and aspect ratio of 4. a) A11, $D50=0.507\text{mm}$ , b) A13, $D50=0.275\text{mm}$ , c) A14, $D50=0.196\text{mm}$ .....	83
Figure 4.6: Effect of particle size on trajectory results of oblique particle cloud with initial oblique angle of $60^\circ$ .....	84
Figure 4.7: Effect of particle size on normalized velocity of oblique particle cloud $u_y / u_\infty$ along normalized depth $y/d_o$ for drop angle of 60 degree.4.4.3 Effect of Oblique Angle .....	85
Figure 4.8: Effect of initial oblique angle for medium particle size (i.e. $D50=0.275\text{mm}$ ) at different normalized time $t/T$ . a) A18, $\alpha=15^\circ$ , b) A2, $\alpha=60^\circ$ .....	86
Figure 4.9: Effect of initial oblique angle on trajectory of particle cloud. a) $L_o/d_o = 7.5$ , $D50=0.507\text{ mm}$ , b) $L_o/d_o = 1.2$ , $D50=0.389\text{ mm}$ , c) $L_o/d_o = 4$ , $D50=0.507\text{ mm}$ , d) $L_o/d_o = 4$ , $D50=0.196\text{ mm}$ .....	88
Figure 4.10: Effect of height on trajectory of oblique particle cloud for particle size of 0.389 mm and oblique angle of $60^\circ$ . a) $L_o/d_o = 1.2$ , b) $L_o/d_o = 7.5$ , c) $L_o/d_o = 11$ , d) $L_o/d_o = 15$ .....	90
Figure 4.11: Effect of height at different normalized time $t/T$ for oblique particle cloud with initial oblique angle of $60^\circ$ and $L_o/d_o$ ratio of 15. a) A26, $H=0.6\text{ m}$ , b) A30, $H=1\text{ m}$ .....	91
Figure 4.12: Effect of particle size on entrainment coefficient of vertical particle cloud .....	93
Figure 4.13: Variation of the drag coefficient of particle cloud along the particle Reynolds number, .....	95
Figure 4.14: Effect of aspect ratio and particle size on drag coefficient of particle cloud. a) Variation of drag coefficient along normalized depth $y/d_o$ for different aspect ratio b) Effect of particle size on drag coefficient for small aspect ratio of 1.54.5 Summary and Conclusion.....	96

## List of Tables

### **Chapter 3:** Experimental Study of Sand Jets and Particle Clouds in Water

Table 3.1: Experimental details of particle clouds in water..... 38

Table 3.2: Coefficient of equations (16), (18) and (19)..... 44

### **Chapter 4:** Experimental Study of Oblique Particle Clouds in Water

Table 4.1: Experimental details of oblique particle clouds in water..... 76

## **Chapter 1: General Introduction**

### **1.1 Motivation of the Present Study**

Oil sand mines are found in several countries such as Venezuela, United States, Russia, and Canada. Alberta province has one of the largest crude oil reserve in the world (Energy, An Overview, 2009). Oil sands are a mixture of sand, clay, and water that are saturated with a dense viscous form of petroleum called bitumen. Once the oil sand is excavated, it goes to the extraction process to remove the sand and other particles. The bitumen (or heavy oil) is used as a source of energy. The mixture of water, residual bitumen, sands, and clay particles is called tailings. When these tailings are pumped into tailing ponds, the sand particles settle on the bottom and some of the water rises to the top. The middle layer is a mixture of about 70% water and 30% clay particles, which is known as mature fine tailings (MFT). These very small particles are not heavy enough to settle on the bottom of the pond and will be suspended in the water media for many decades to form a solid surface.

Therefore, reducing the amount of fluid in fine tailing ponds has become one of the biggest challenges for the oil industry. According to Alberta's regulations of Alberta department of energy (1995), the oil sand operators must reclaim tailing ponds to its original landscapes. One of the effective methods of reclaiming tailing ponds is to discharge new slurries into the pond to accelerate the settling of fine particles. In this method, the volume of fine tailings will be reduced.

The settlement of sand in the pond is influenced by many factors. In this research focuses on study the effect of controlling factors on the behavior of sand particle clouds in water media.

## 1.2 Application of Sand jets and Particle Clouds

Particle clouds are commonly observed when a finite amount of particles is released into the water media. Particle-laden jets are formed when a continuous source of particles are released into the water. Sand jets and particle clouds can be found in many engineering applications such as marine bed capping, artificial island formation, dredged material disposal and disposal of slurry into a tailing storage facility. Artificial island formation is the construction of manmade islands that is performed by pumping sand into the desired location until enough sand is accumulated to the desired locations (Figure 1.1). Several considerations must be taken into account in the design of an artificial island such as water depth, wave characteristics, existing infrastructure and sources of materials to be used.



**Figure 1.1** Construction of Palm Jumeirah (Photo by Steve RKH)

Marine bed capping is a technique where clean sand is used to cover contaminated soil to isolate the contaminants from the environment and reduce the spreading of these contaminants

into the environment. The process of marine bed capping involves the installation of a geomembrane followed by sand being placed and spread over the contaminated area until the cap reaches a certain thickness (Sharma & Reddy, 2004).

In a variety of mining operations, only a small portion of the mined material is actually of interest, and the remaining portion being a waste to be handled and removed. Generally, water is introduced during extraction process. The leftover slurry of ground rock and effluent material can vary greatly in density and composition. The slurry is then pumped to a Tailing Storage Facility (TSF) (Figure 1.2). Upon reaching the TSF, the slurry is discharged. The TSF may be underground but generally is man-made, above ground dam facility. The incoming slurry will be discharged into the already placed slurry as a jet. Over time, the slurry mix will begin to separate, while the liquid component becoming less dense and beginning to return to the uncontaminated water. The solid material will continue to settle out and collect within the TSF. The TSF will be kept in use and will expand during the life of the mining operation.



**Figure 1.2:** Discharge of slurry into Tailing Storage Facility

### **1.3 Overview of the Present Study**

Two-phase solid-liquid jets have many engineering applications such as industrial discharge, dredging, and marine bed capping (Bush et al. 2003, Azimi et al. 2012a). Several experimental studies have been conducted to consider the behavior of two-phase jets including Noh and Fernando (1993), Bush et al. (2003), Cai et al. (2010), Hall et al. (2010), Azimi et al. (2012a). Solid-liquid jets can be classified into sand jets for a continuous source of sand and particle clouds for a finite amount of sand at the nozzle. This study focuses on the effect of controlling parameters on particle clouds behavior such as sand particle size ( $D_{50}$ ), nozzle diameter ( $d_o$ ), release height ( $H$ ), initial oblique angle and aspect ratio  $L_o/d_o$  which  $L_o$  is the length of the sample.

This thesis is organized into 5 chapters. In chapter 2, a literature review concerning the present study is discussed. In chapter 3, the experimental study of the sand jet and particle cloud is described including the experimental setup and procedures, experimental results for considering the effect of  $L_o/d_o$ , sand particle size, and impact velocity on particle clouds behavior. In chapter 4, experimental study of oblique particle clouds in water media is discussed which includes experimental setup, effects of aspect ratio, sand particle size, drop angle, and drop height on the behavior of oblique particle clouds. Summary and conclusion of this thesis are presented in chapter 5.

### **1.4 Novelty of the Study**

To the author's knowledge, limited attention was made to consider the effects of initial parameters such as mass of sand particles, particle size, nozzle diameter, oblique drop angle and falling height on the formation and spreading of particle clouds in the water media. In the literature, the behavior of particle cloud has been studied recently (section 2.2). However, most

of the investigation have been based on a constant or limited mass of particles. Azimi et al. (2013) studied the effect of particle size and nozzle diameter on the behavior of sand jets. In this thesis, an effort has been made to cover a different range of sand mass to form both sand jets and particle clouds. Experimental study of Bond and Johari (2005) on single phase thermal shows that  $L_o/d_o$  ratio plays an important role in spreading of buoyant thermals. In this study, the effect of mass on the behavior of particle clouds is presented in the form of aspect ratio (or  $L_o/d_o$  ratio) to consider both effects of mass of particles and nozzle diameter. The initial angle of the particle cloud at release time can also be an important factor that can change the trajectory of particle clouds. In the literature, most of the studies on particle clouds are based on the vertical release mechanism which makes it easy to predict the final position where the clouds will settle. However, any change in releasing angle of sand particles can change the trajectory of the particle clouds. In this study, the simultaneous effect initial release angle, particle size, and particles mass on the trajectory of particle cloud have been studied.

Recent investigations (Qu et al., 2011, 2013) also indicated that the fall height can change the initial momentum of the two-phase jets. Zhao et al. (2012) studied the effect of release height on particle clouds; however, they consider a constant mass with a limited release height ranged from 0.02 m to 0.10 m which may not consider the real effect of drop height. In this study, a large range of drop height was considered ranged from zero to 1 m to completely cover the effect of release height on dynamics of particle clouds. Drag coefficient and entrainment coefficient are other important parameters in describing the characteristic of particle clouds. In this study, equations are developed to present the effect of particle size, and aspect ratio  $L_o/d_o$  on the drag coefficient and entrainment coefficient of particle clouds.

## Chapter 2: Literature Review

### 2.1 Single-Phase Flow

Single-phase flow was studied widely over the years. Pantzloff and Lueptow (1999) studied the effects of transient positively and negatively buoyant turbulent round jets. Experiments were completed in a flat bottomed cylindrical tank with a diameter of 0.295 m and a height of 0.87 m. An upward pointing nozzle with a diameter of 0.508cm and 2:1 contraction ratio was located in the center of the bottom of the tank. The Reynolds number of the jet ranged from 2500-21000. Particle image velocimetry (PIV) was used to investigate jet flow. Florescent dye was added to the jet liquid for visualization. A 10 W argon laser was used for lighting. Different flow structures were observed in the tank depending on momentum and buoyancy of the jet. For the positively buoyant jet, the flow was driven by the buoyancy and the jet reached to the surface.

The negatively buoyant jets were found to have two different scenarios for low and high Reynolds number. For Reynolds number  $2500 < Re < 15000$ , a turbulent fountain was found to occur. The fountain height depends on the initial upward momentum and the opposing downward negative buoyancy force. In the next step, the jet falls back to itself which decrease the maximum height. It was found that the penetration height fluctuating around a mean value of 70% of the maximum height of penetration. For larger Reynolds number, the fountain was not formed. Instead, a weak circulation region was formed from the top of the tank to the bottom. Effects of initial geometry on the development of thermal were studied by Bond and Johari (2005). The experiments were conducted in a glass tank with length and width of 0.33 m and 66 m of height. The experiments were performed using a negatively buoyant fluid released into a

uniform density environment. The ambient fluid was a mixture of glycerol and water while the buoyant fluid was a solution of potassium dihydrogen phosphate in water. The buoyant fluid was held in a cylindrical acrylic tube, sealed by latex membranes on the top and bottom that would burst when subject to heating. Four cylindrical tubes were used in such experiments, with lengths ( $L_0$ ) ranging from 38 to 80 mm, and diameters ( $d_0$ ) of 19 and 9.5 mm, giving four aspect ratios ( $L_0/d_0$ ) of 2, 4, 6, and 8. Cylinders were placed a depth of  $5d_0$  below the free surface to minimize any free surface interactions where  $d_0$  is the diameter of the nozzle. The region of the tube exit to approximately  $11D$  is imaged in these experiments. A set of five runs was conducted for each case. A digital camera was used to capture images of the experiments for the analysis purpose.

They also conducted a separate set of experiments using particle imaging velocimetry (PIV) technique. The vorticity fields computed from the PIV data were used to examine the structure of the flow fields. Using the vorticity field in the first frame, corresponding to the time when the buoyant fluid had completely drained from the tube, it is indicated that the fluid had formed into a compact vortex ring. This ring expanded radially as it traveled downstream resembling a thermal with the majority of the vorticity residing in a ring-like structure. It was also found that the evolution of the buoyant fluid could be divided into two phases, initial acceleration phase and a subsequent deceleration flow phase with thermal like qualities. Nearly all of the released fluids ended up in a single thermal like structure. In the initial phase, the buoyant fluid accelerated out of the discharge tube and the boundary layer on the tube wall began to roll up. The initial phase usually lasted  $1-2T$ , where  $T$  is the time for the complete drainage of the tube. The length and time scales in the initial phase were found to be dependent on the initial

geometry. For the larger aspect ratios, the flow in the near field was found to consist of a vertical structure followed by a trailing column.

In the thermal phase, the buoyant fluid mixed with sufficient ambient fluid and decelerated. It was noted that  $Z_t$ , increases with the initial buoyant fluid volume to the power of  $1/3$  where  $Z_t$  is the distance to reach the thermal phase. Moreover, the flow was found to be in a constant circulation. The time to reach constant circulation was approximately  $6-7T_o$  where  $T_o$  is the time of the initial phase. It was concluded that the flow characteristics in the second phase were independent of initial geometry.

Mohseni and Gharib (1998) considered an analytical model for predicting the universal time scale for the formation of vortex rings generated through impulse started jets. They used the following equations for estimating circulation, impulse and kinetic energy per unit density for the slug of fluid with a length of  $L_o$ , diameter of  $d_o$ , and uniform velocity of  $U_p$ .

$$\Gamma = \frac{1}{2} L_o U_p \quad (2.1)$$

$$I = \frac{1}{4} \pi d_o^2 \rho_p L_o U_p \quad (2.2)$$

$$E = \frac{1}{8} \pi d_o^2 \rho_p L_o U_p^2 \quad (2.3)$$

They formed non-dimensional energy and circulation using the following equations.

$$E_{nd} = E / \Gamma^{3/2} I^{1/2} \quad (2.4)$$

$$\Gamma_{nd} = \Gamma / I^{1/3} U_p^{2/3} \quad (2.5)$$

Through dimensional analysis they determine that  $L_o/d_o$  is dependent upon the non-dimensional energy,  $E_{nd}$  and circulation  $\Gamma_{nd}$ .

They also predicted that  $\Gamma_{nd}$  is in the range of 1.77 to 2.07, indicating that steady vortex rings with a higher value of  $\Gamma_{nd}$  is not possible.

The near field development of buoyant vortex ring was studied experimentally by Bond and Johari (2010). The experiments were conducted in a tank with cross-sectional dimensions of 0.33m and the height of 0.66 m using a negatively buoyant fluid with a density difference of 4.7% released into a uniform density environment. The vortex ring fluid was held in a cylindrical tube with diameter of  $d_o=19$  mm and  $L_o/d_o$  ratio of 2. For the buoyancy vortex ring experiments, the container was placed at least  $5d_o$  below the free surface. The result of the buoyant ring was compared with non-buoyant ring with the same Reynolds number of  $\sim 5000$ . To generate the momentum driven non-buoyant vortex ring, the container was positioned on the free surface and filled with the same fluid as the tank fluid to allow the gravity to drive the flow. For the buoyant vortex ring, they observed a vortex ring with a large diameter compared with the non-buoyant ring. For the buoyant ring, they found a constant circulation while for the non-buoyant ring, the circulation started to decrease after it travels about  $3d_o$  from the generator. They also observed that the non-buoyant ring converts to a thick core ring right after the ring formation, while the buoyant ring should travel  $6d_o$  to form a thin core ring. Formation and evolution of the vortex ring at a shock tube was studied by Arakeri et al. (2004). In their research, early evolution of the vortex ring was examined. Three different shock Mack number of  $M=1.1, 1.2$  &  $1.3$  were used in their experiments. Mack number represent the ratio of the shock speed and ambient speed of sound ( $M=u/c$ ). At the end of the ring formation, it was observed that its translation speed is  $0.7u_b$ ; however, the vortex diameter was different for three cases even after the formation is complete where  $u_b$  is the fluid velocity behind shock as it exits the tube. Moreover, in their experiments, the pinch off was occurred at  $L/d$  ratio of 2.5 for all the three experiments where  $L$  is the length of ejected fluid.

An experimental investigation into the pinch off process of a starting buoyant plume was performed by Pottebaum & Gharib (2004). The pinch off is considered when the vortex ring becomes separated from the trailing part of the plume. They considered the non-dimensional time as

$$\tau_1 = \frac{t}{\tau} \quad (2.6)$$

where  $\tau$  is the characteristic time scale for vortex ring (Lundgren et al., 1992). The characteristics time scale can be expressed as

$$\tau = \left[ \frac{R_o \rho_p}{g(\rho_p - \rho_w)} \right]^{0.5} \quad (2.7)$$

where  $R_o$  is the equivalent radius of particle cloud if its shape simplified to a hemisphere (Shusser and Gharib, 2000b). The buoyant plume was produced by the use of an electrical heater located at the bottom of a temperature-controlled tank. The tank consisted of a 133 mm square inner region filled to a depth of 216 mm with a 15% glycerol solution. The background temperature of the experiments was 25.8°C. Images were captured using a 3CCD color video camera placed approximately 2 m from the tank. The experiments showed that the cap and stem are initially connected however; they eventually separate into a vortex ring and trailing plume with a region of ambient fluid in-between. The pinch-off was determined to occur between the non-dimensional times of 4.4 and 4.9.

Penetration of negatively buoyant jet in the miscible fluid was studied by Philippe et al. (2005). The laminar liquid jet with a density of  $\rho$  was negatively injected with a constant flow rate from the nozzle into a miscible liquid of the density of  $\rho + \Delta\rho$ . The injection was done with the syringe pump from a large storage tank. The flow rate was varied from 0.002 cm<sup>3</sup>/s to about 20 cm<sup>3</sup>/s with nozzle diameter varied from 0.254 mm up to 4.83 mm and a nozzle length of 20,

30 and 64 mm. After releasing the liquid jet from the nozzle, it penetrates in the tank; however, it slows down due to the opposing buoyancy force. In this phase of motion, the jet consists of a thin body with a large head similar to thermal rising plumes. After a few seconds, the jet reaches a steady state with a constant penetration depth. In the last step, the jet rises back to the surface. They found that the behavior of the liquid jet depends on relative difference density between inner liquid and outer liquid  $\Delta\rho/\rho$ , injection flow rate and internal diameter of the nozzle. They observed that any increase in each of  $\Delta\rho/\rho$  and nozzle diameter causes a decrease in penetration depth; however, penetration depth increases with increasing the flow rate.

The experimental study of forced plume produced by a constant flux of buoyant fluid was performed by Rogers et al. (2009). The focus of the study was in the starting plumes when the ascending head exists. A glass tank with length and width of 0.13 m and height of 0.50 m was used for the experiment. In the center of the tank floor, a vertical glass tube was built. For injecting the fluid, a syringe pump was connected to the bottom end of the outlet pipe. The syringe was filled with a slightly less dense fluid than the ambient fluid. They classified the plume head by Richardson number which is the ratio of buoyancy forces to inertial effects. For  $Ri > 1$  a confined plume was observed which can retain a mushroom shape with stable vortex ring while rising in the tank. However, for  $Ri < 1$ , it was found that the vortex ring only exists for a short time before dispersing.

The structure of water and fuel interface caused by the impingement of water jet was studied by Friedman and Katz (1999). A tank with the dimension of 0.65x0.65x1 m was used for the experiments. The fuel layer floats on the top of the heavier water layer and was bounded by a plate to adjust the fuel layer height. Water jet exits from an adjustable pipe at the bottom of the tank. For most of the experiments, the flow has a turbulent velocity profile based on the Re

(30,000 < Re < 1000). Four different flow regimes were observed based on the aspect ratio ( $AR$ ) which is the ratio of deformation height and water jet diameter ( $AR = h_1/D_i$ ) and also Richardson number at interface  $Ri_i$ . The interface Richardson number can be defined as follows.

$$Ri_i = \frac{D_i(\rho_{water} - \rho_{oil})g}{\rho_{water}u_i^2} \quad (2.8)$$

where  $D_i$  and  $u_i$  are the water jet diameter and velocity at the interface. For  $Ri_i > 15$ , a smooth stable deformation at the interface occurred. In this regime, no mixing was observed. As the velocity increased ( $15 > Ri_i > 1.1$ ), an increase was observed in the depth of interfacial deformation. It also caused a flow separation at the edge of deformation and formed an unsteady, closed separation bubble. The next regime was resulted due to  $Ri_i < 1.1$  and aspect ratio  $AR < l_1/D_i$  ( $l_1$  is the fuel layer thickness). In this regime, the side of interfacial deformation became vertical with an unstable penetrated layer and a little water mixing was observed. For the aspect ratio  $AR > l_1/D_i$ , the momentum is sufficient enough to cause mixing of fuel and water. In this regime, the water jet penetrates into the fuel surface and breaks into small droplets that rain down.

Turner (1986) assumed that the ambient fluid which enters into a plume is proportional to the velocity of centerline plume ( $u_e = \alpha u_p$ ). Scase et al. (2007) described the mixing process in plumes by tracking the evolution of both ambient fluid and plume. Due to the buoyancy force, the plume fluid rises upward and due to the entrainment, it spreads outward. To provide the fluid for entrainment purpose, the ambient fluid flows horizontally inward the plume. Near the center of the plume (i.e.  $r/b = 0$  where  $r$  is the distance from the center and  $b$  is the half width of the plume), the total radial flow is outward and dominated by the behavior of the plume fluid. In the far field (i.e.  $r/b = \infty$ ), the radial flow is dominated by the horizontal inward flow of the ambient fluid. For the top-hat profile plumes, the total velocity of the fluid can be find using the following equation.

$$u = \left( \frac{-r}{2} \frac{du_p}{dz}, u_p \right) \quad \text{for } r < b \quad (2.9)$$

$$u = \left( \frac{u_e b}{r}, 0 \right) \quad \text{for } r \geq b \quad (2.10)$$

Where,  $u_p$  is the vertical velocity of the plume fluid,  $du_p/dz$  is the rate of change in plume velocity by a distance from the nozzle, and  $u_e = \alpha.u_p$  is the entrainment velocity.

The behavior of starting buoyant jet with different formation number was studied by Wang et al. (2009). A numerical model was developed to examine the formation dynamics of a starting buoyant jet. The numerical model was verified with the experimental data of a pure jet. Their computational domain had dimensions of  $0.3 \times 0.3 \times 0.8 \text{ m}^3$ . The starting buoyant jet was released downward with the velocity of  $u_o$  into the ambient fluid. The nozzle diameter used in their model had a diameter of 50 mm. The buoyant fluid was heavier than the ambient fluid with a relative density difference of  $\Delta\rho/\rho_o$ . From Fitcher et al. (1979), the Richardson number was defined as  $(\pi/4)^{1/4} (g'd_o/u_o^2)^{1/2}$ . Formation number is the  $L/d_o$  ratio equivalent to the critical value of formation time where the trailing part remains behind the leading vortex ring. Gharib et al. (1998) determined the formation number of a starting jet by defining it based on the circulation of the starting vortex attaining a maximum. In Wang et al. model (2009), the circulation continues to increase even after the pinch off, which was due to the buoyancy of the plume fluid. They observed that the circulation of the starting vortex increases while the formation process fed by the trailing part. Then a step jump in circulation will happen when the pinch off occurs. After the pinch off, the vortex ring becomes separated from the trailing part. Because of losing the supply of vortex ring from the trailing part, the circulation increase slows down to a magnitude corresponding the buoyancy of the vortex itself. They identified the formation number based on the step jump that was observed in the circulation of the vortex ring. Based on

the numerical results for two source condition of  $Re=2000$  and  $2500$ , it was observed that the buoyant formation number will increase by increasing the Richardson number.

Transient behavior of starting buoyant jet was studied by Wang et al. (2011). The computational domain of their study was a rectangular volume with dimensions of  $6d \times 6d \times 30d$ , where  $d$  is the dimension of the nozzle. During the computational runs, a buoyant jet with a heavier density compared to the ambient density is formed at the top of the domain from a circular nozzle with diameter of 5 cm. For validating purposes, they modeled a pure jet and a plume and compared the velocity and concentration decay rate with the experimental data of Wang et al (2002). The results were in a good agreement with the experimental data. They also used the model for simulating starting buoyant jets with a wide range of buoyancy effects from pure jet to plume. The same penetration rate was observed for all jet fronts for  $tu_o/d < 0.8$ . Afterward, for  $(tu_o/d > 0.8)$ , the penetration of the pure jet was linear while any increase in buoyancy caused a faster penetration. The development of penetration rate was divided into three phases of overlapped phase, acceleration phase and a final phase with a decrease in penetration rate. In the overlapped phase, the buoyancy is not effective enough to accelerate the penetration. In the acceleration phase, the buoyancy force is dominant compared to momentum which cause a different penetration rate for different buoyancy flux. They also found that the penetration distance can be resolved as the sum of the separate effects of initial momentum and buoyancy. Finally, in the last phase, due to the high entrainment of ambient fluid, the total penetration rate decreases. They finally came up with an equation for PFD (period of flow development) region which the flow behavior is affected by the source condition.

$$\frac{x}{d} = 0.1 \frac{B_0}{Q_0 d} t^2 + 0.47 \frac{M_0^{3/2}}{Q_0^2} t \quad (2.11)$$

where,  $Q_o=1/4\pi d^2 U_o$ ,  $M_o=1/4\pi d^2 U_o^2$  and  $B_o=1/4\pi g(\Delta\rho_o/\rho_o)d^2 U_o$  are initial volume flux, momentum flux, and buoyancy flux.

## 2.2. Two-Phase Flow

There are three ways to study and predict the behavior of multiphase flows including experimental, laboratory model and computational. This study focuses mainly on the experimental analysis of sand-jets in water media. In this section, an overview of two-phase flow is presented that covers main researches that have been done in the literature. An experimental study of the particle laden jet in the air with rather coarse particles ranged from 0.17 mm to 1.4 mm with the density of 1020 kg/m<sup>3</sup> was done by Tsuji et al (1988). They normalized the distance and velocity of particles by the nozzle diameter and initial velocity; and compared the air velocity for different particle sizes and observed that the smaller the particle sizes, the larger the effect of the particles on air velocity. They also compared two different conditions of rough and smooth wall for the releasing particles and pointed that the rough pipe can result in extensive particle diffusion on leaving the particles from the nozzle because of the irregular motion of large particles in the pipe. Swamee et al. (1991) studied the drag coefficient of nonspherical particles and obtained empirical equations for the drag coefficient of nonspherical particles with natural and mechanical origin (i.e. crushed particles). The following are equations for natural and crushed particles respectively.

$$C_{DNa} = 0.84 \left[ \frac{33.78}{(1 + 4.5\beta^{0.35})^{0.7} \text{Re}^{0.56}} + \left( \frac{\text{Re}}{\text{Re} + 700 + 1000\beta} \right)^{0.28} \frac{1}{(\beta^4 + 20\beta^{20})^{0.175}} \right]^{1.428} \quad (2.12)$$

$$C_{DCr} = 0.84 \left[ \frac{48.5}{(1 + 4.5\beta^{0.35})^{0.8} \text{Re}^{0.64}} + \left( \frac{\text{Re}}{\text{Re} + 100 + 1000\beta} \right)^{0.32} \frac{1}{(\beta^{18} + 1.05\beta^{0.8})} \right]^{1.25} \quad (2.13)$$

where,  $\beta=c'/(a'b')^{0.5}$  is the shape factor of a nonspherical particle,  $a'$ ,  $b'$  and  $c'$  are the lengths of three principal axes of the particle in decreasing order of magnitude.

Sheen et al. (1994) studied the effect of particle size on the two-phase solid-gas jets. They used polystyrene with the particle sizes of 0.210, 0.460, and 0.780 mm and density of 1020 kg/m<sup>3</sup>. The  $L/d_o$  ratio of the pipe they used was 135 (length of 2 m with a diameter of 0.015 m). Reynolds number of their experiments was  $2 \times 10^4$  based on the fluid-phase centerline velocity at the nozzle exit  $u_o=20$  m/s and the pipe diameter. They found that for the larger particle sizes, the decreasing rate of the axial velocity of the fluid-phase is larger. Moreover, in two-phase flow, the spreading rate of the fluid phase along the radial direction was observed to be smaller than that of a single-phase flow. Particle velocity fluctuation of non-Brownian spheres was studied by Nicolai et al. (1995). The velocity fluctuation can result in a randomly fluctuating motion of the particle and found a decrease in self-diffusivity for the large concentration of sedimenting spheres because the particle is locked into a settling cluster of other particles. Ham and Homsy (1988) observed a large particle velocity fluctuation up to 46% of the mean in their experimental study of the vertical velocity of a marked particle in a quiescent sedimenting suspension.

Luketina and Wilkinson (1998) performed an experimental study in understanding the two-phase characteristics of the particle clouds. They pointed out that the behavior of particle clouds depends on the properties of individual particles, initial density of particles at the release tube, and also properties of the fluid. The transition to swarm phase for particle clouds occurs at the particle settling velocity. They also found a relationship for describing the particle cloud's behavior,  $x=t^{1/2}$ . Ruggaber et al. (2000) studied the growth rate, velocity, and circulation of the particle clouds. They used glass beads with the density of 2.5 g/cm<sup>3</sup> which formed particle

clouds with initial aspect ratios ranged from 0.5 to 2.6 and introduced a time scale called release time which is the time required for the particles to exit the cylinder. In the thermal phase, it was observed that the cloud's radius is proportional to depth  $r=\alpha x$  where  $x$  is the distance from the nozzle and  $\alpha$  is the entrainment coefficient. It was also found that the radius versus depth plots decreases with depth and have two varying slopes which show two different entrainment coefficients in upper and lower part of the cloud. The intersection of the two slopes was called the transition of thermal phase to circulating thermal. The entrainment coefficient of the first slope which is in thermal phase ranged from 0.18 to 0.31 and the second slopes had entrainment coefficient in the range of 0.08 to 0.24.

The presence of particle phase in the turbulence of fluid flows known as the turbulent modulation was studied by Crowe (2000). He correlated laboratory experiments with different flow structures. A trend was found between the turbulence modulation and normalized length scale of  $d_o/L_e$ , where  $d_o$  is the particle size and  $L_e=0.039x$  is the length scale of the most energetic eddy in a single phase flow (Wyganski and Fiedler, 1969). He found that large particles increase the turbulence while small particles attenuate it. Sheen et al. (1994) used polystyrene with the particle sizes of 0.210, 0.460, and 0.780 mm and found that the turbulence intensity of the gas-phase in the two-phase flow is lower than single phase flow in the far field. The turbulence energy will transfer from eddies to particles which cause a reduction in turbulent intensity of the gas-phase.

Characterization of plunging liquid jets was studied by Qu et al. (2011). The experiments were done in a 0.3m  $\times$  0.3m  $\times$  0.5m water tank with water level of 0.28m. The water was pumped vertically into the water tank in the direction of gravity through a 0.55m long pipe with the diameter of 6 mm. Experiments were performed for different nozzle heights and volumetric

flow rates with the initial water velocity  $V_o$  at the nozzle in the range of 1m/s and 3.5m/s. For the measurement purpose, a high-speed camera was used to capture images of the effect of water jet in the water. Water jet velocity  $V_j$  at the liquid surface was calculated using free fall of water after leaving the nozzle using the following equation with the range between 1 m/s to 4 m/s.

$$V_j = \sqrt{V_o^2 + 2gL_i} \quad (2.14)$$

where  $L_j$  is the falling length from the nozzle tips to water surface and  $g$  is the gravitational acceleration. Increasing the nozzle jet velocity for a given nozzle size caused jet-interface instabilities and lead to entering more air bubbles beneath the water surface. By the presence of bubbles, the momentum of water jet diffused and caused a reduction in penetration depth which is the lowest point of the plume. This phenomenon was called jet-interface instability phenomenon. The combination of larger flow rate and jet-interface instability phenomenon can also cause larger air bubbles and as a result, a shorter penetration depth. Numerical analysis was performed and compared with experimental results (Qu et al., 2011). For penetration depth, the simulation method was in a good agreement with the experimental values. The penetration depth was also compared to empirical relationship of Bin (1984):

$$h_p = 2.1V_j^{0.775}d_o^{0.67} \quad (2.15)$$

where  $h_p$  is the penetration depth,  $V_j$  is the jet velocity at the water surface and  $d_o$  is nozzle diameter. Bin's relationship revealed a different behavior with experimental and simulation results which could be due to neglecting the jet free surface interaction in Bin's expression.

In plunging liquid jets, the flow structure consists of two distinct regions. The first region is diffusion cone moving downward induced by liquid jet and the second region is a swarm of rising bubbles which surround the liquid jet (Chanson, 1997). Qu et al. (2011), didn't measure

the water velocity and air concentration; Instead, the velocity analysis was performed by using the numerical model and comparing the result with semi-empirical correlation. The velocity distribution for a round turbulent single-phase jet can be found by the following semi-analytical correlation (Chanson, 2004):

$$\frac{V}{V_j} = \frac{5.745}{x/d_o} \left( \frac{1}{1 + 0.125(18.5 \frac{r}{x})^2} \right) \quad (2.16)$$

where  $x$  is the distance from the liquid surface and  $r$  is the distance of the velocity point and centerline. The general shape of velocity distribution was Gaussian. The centerline velocity in the numerical model was observed greater than semi-analytical correlation. On the other hand, numerical model had lower velocities away from centerline compared to semi-analytical correlation. The reason was the nature of the correlation which is valid for liquid-liquid jet flow and do not consider the effect of drag/buoyancy of entraining gas in the impinging jet.

Experimental characterization of air-entrainment in a plunging jet was studied by Qu et al. (2013). By conducting experiments was conducted in a 0.3m rectangular tank with a depth of 0.5m. During the experiment, the height of tank was maintained constant at the level of 0.43m. A digital camera was used to capture images of the experiments for the analysis purposes. They used different initial velocities (between 0.4 to 3 m/s) with different falling length  $L$ , ranging from 0.01 to 0.66m. Using the following equation, the impact velocity was found to be between 0.66 and 3.59 m/s. By using flow visualization, they obtained a flowmap regimes-entrainment depending on jet falling length  $L$  and impact velocity  $V_j$ . The flow was divided into four classes of no entrainment, incipient entrainment, intermittent entrainment and continuous entrainment. As a result, the  $L_i$  increased, continuous entrainment became the dominant mode. The velocity distribution for two different flow conditions of submerged jet and the impinging jet was also

considered. For the submerged jet, the water was injected below the surface and for the impinging jet, a height of  $2D$  was considered for the jet where  $D$  is the diameter of the nozzle. Considering the instantaneous velocity, the core of the jet had the highest velocity for both cases. However, for the impinging jet, the values of instantaneous velocity were higher with more velocity fluctuation due to the presence of instabilities at free surface. Mean jet velocity from the water surface to the width of 25mm of the tank was also considered. The maximum velocity of the impinging jet was 20% higher than the maximum velocity of submerged jet which is related to the free jet falling length.

Neto et al. (2008) studied the injection of water with different nozzle from the bottom of a glass tank with width and length of 1.2 m and a height of 0.8 m which was filled with water to the height of 0.76 m. The volumetric air flow of 33.3 and 50 cm<sup>3</sup>/s was discharged through different nozzles (single and multiple orifice nozzles and a porous airstone) and for measuring the bubble characteristic such as void fraction ( $\alpha$ ), bubble frequency ( $f_b$ ) and bubble velocity ( $u_b$ ), a double-tip optical fiber probe was used. For calculating specific interfacial ( $a$ ) and bubble mean Sauter diameter ( $d_b$ ) the following equations were used (Toombes and Chanson, 2005).

$$a = 4f_b / u_b \quad (2.17)$$

$$d_b = 6\alpha / a \quad (2.18)$$

They found that while changing the nozzle, bubble velocity remains almost constant. Comparing porous airstone instead of nozzles with large orifices, bubble size decreased and interfacial area increased. They also observed that bubble slip velocity was higher than terminal bubble velocity (Clift et al., 1978) which is due to the effect of trailing bubble that makes the bubble travel faster than the similar isolated bubble. Radial distribution of bubble characteristics was also studied in their research. The result revealed that mean Sauter diameter and velocity

distribution follow a straight line, while specific interfacial area distribution is more like a Gaussian curve.

The dynamics of particle clouds released into the water with ambient currents was studied by Gensheimer (2010). Three regimes of behavior depending to the current's strength was reported includes weak, transitional or strong current. In the weak ambient currents, particle clouds are advected downstream with a velocity equal to the ambient current, but the behavior and structure are similar to a cloud in a quiescent condition. The transitional currents are distinguished by a delay in the formation of the vortex ring. In the strong current, no vortex ring can be formed and the coherency of the particle cloud can be destroyed. The magnitude of the two thresholds depends mainly on the particle size. For example for glass bead with the median diameter of 0.725 mm, the ambient current weak threshold was +18 cm/s and for glass bead with the median diameter of 0.256 mm it was 12 cm/s. As a result, it was observed that any increase in particle size, can increase the weak threshold and also an increase in the range of strong thresholds. Gensheimer et al. (2012) found that up to 30% of the mass formed a trailing stem and was not incorporated into the cloud. The amount of trailing stem which was called the loss of sediment during the descent and was observed to increase sharply with the current speed.

Pignatell et al. (2011) studied the dynamic of particle clouds of glass spheres with different densities of 1.1, 2.4 and 4 g/cm<sup>3</sup> in a viscous fluid. They identified seven quantities that describe the properties of particle clouds in a fluid under gravity. The cloud can be described by its radius and number of particles, the fluid by the viscosity and density, and particles by density and diameter. They observed that the particle cloud tends to flatten first and form a ring shape. Then the ring shape becomes wider and finally as the cloud travels further, it breaks up into two droplets. An experimental study of sand jet front in water was studied by Azimi et al. (2011).

The experiments were conducted in a 1.33 m square tank. The tank was filled with tap water and held at a constant depth of 0.92 m. To complete the experiments a sand hopper was held vertically above the tank. The release height was no more than 5 mm above the water surface to minimize the initial momentum of the jet. A CCD camera was used to capture images of the particles for analysis and a 6W Argon-Ion laser and optics was used to generate a light sheet to illuminate the flow. Two series of experiments were conducted to study the effect of nozzle diameter (Series A) and particle size (Series B). For Series A, four nozzle sizes were used with nominal diameters of 2, 3, 4.75, and 10 mm to study the effect of nozzle size. Fine blasting sand particles with a  $D_{50}$  of 206  $\mu\text{m}$  and density of  $\rho_p = 2540 \text{ kg/m}^3$  were used in these experiments. The sand particle sizes were considered uniform. For Series B, sand particles with a density of  $\rho_p = 2540 \text{ kg/m}^3$  passed through a series of sieves ranging from 125 to 589  $\mu\text{m}$  and 8 classes were identified. The frontal shape of the jet was classified according to their  $Re_p$ . They found that for  $Re_p < 10$  jet acts as particle thermal, for  $Re_p \sim 10$ , particles form a bowl shape and finally for  $Re_p > 10$ , a narrow frontal head was observed due to the faster rate of the jet penetration in water. The analysis of the frontal velocity of the sand jets showed that larger particles produced higher frontal velocities. This velocity was found to be a function of nozzle diameter and particle size. They also observed that the velocity ratio ( $u_f/u_{co}$ ) drops continuously after releasing from the nozzle and reaches a plateau at  $x/d \sim 200$  which is called particle cloud fall velocity  $u_{fco}$ . For small particle sizes, the jet front terminal velocity was as large as 5 times of the individual settling velocity. The effect of particles on the frontal velocity of turbulent jets was found to be negligible close to the nozzle. However, along with the jet axis, it was found that when the larger particle sizes were used, the particle cloud settling velocity became larger.

Hall et al. (2010) studied the behavior of sand and slurry jets in water. Experiments were conducted in a rectangular glass tank filled with tap water with 1.25 m width, 2.5 m length, and 1.2 m depth. For the experiments involving sand jets, a conical hopper and plug was used, located at 75 mm above the water surface. For the sand jet, Silica sand particles with a  $D_{50}$  of 0.206 mm were funneled into the hopper and then released into the water. For the slurry jet experiments, silica sand with a  $D_{50}$  of 0.206 mm was mixed with tap water to form a slurry jet with an initial sand concentration of 0.055-0.124 and was fed into the water with a vertical pipe which was located 5 mm below the water level, at the center of the tank. A novel fiber optic probe was used to make simultaneous measurements of the sand particle velocities and concentrations. For both sand and slurry jets, it was found that the velocity and concentration profile fitted a Gaussian profile. The centerline sand concentration decay like a single phase plumes using a  $-5/3$  power relation. For the centerline particle velocity profile of the sand and slurry jets, it was observed to decay with a  $-1/3$  power relation and finally reaches a plateau region where the velocity remains roughly constant. They also observed that the velocity of both sand and slurry jets will increase with increasing the initial sand concentration. A spreading rate of 0.088 and 0.102 was found for sand concentration and sand velocity of the sand jet; however, for the slurry jets, it was concluded that the spreading rate depends mostly on the Froude number. Moreover, the spreading rate of the velocity was often larger than that of the concentration.

Cai et al. (2010) studied the behavior of sand jets in the air. Dry sand was released from a conical hopper and the sand was maintained over a depth more than 0.4 m above the bottom of the hopper during all the experiments. They approximated the initial sand jet velocity as  $0.68\sqrt{gd}$  where  $d$  is the nozzle diameter. In all experiments, the front velocity increased

continuously with distance from the nozzle. The particle size did not affect the speed of the front jet. It was also reported that the velocity of the jet front was related to the travel distance  $x$  using the following equation.

$$V^2 - V_0^2 = 2gx \quad (2.19)$$

A uniform velocity distribution was observed for the sand jet because diameter of the sand jet didn't spread due to interaction with the air. For the steady state velocity, it was found that the sand follow the same trend as the frontal velocity. Moreover, the diameter of the sand jet decreased while traveling in the jet direction until it reaches to a constant at about  $120d$  from the nozzle. Study of sand jets in a viscoplastic fluid was done by Cai et al. (2012). They performed several experiments by releasing sand jet into viscoplastic fluid. For less viscous gel, they found that when the inertial force dominates the viscous force ( $Re_p > 1$ ), the cylindrical sand jet mixes with viscous fluid; otherwise, the cylindrical shape of the sand jets is maintained while the sands travel in the viscous fluid. Moreover, for the fluid with high viscosity, they observed that the sand jet settles in the form of drops.

Experimental study of dense suspension jets in a miscible fluid was studied by Nicolas (2002). The suspension reservoir was a cylindrical glass tube which was held fully submerged in the tank. The tubes diameters were ranging from 4 mm to 8 mm with 0.20 m length. Seven different materials with four different liquids were used during the experiments. Four different jet regimes were observed. The ratio of gravity force to the viscous force  $M_p$ , particle Reynolds number  $Re_p$  and the ratio of particle inertia to viscous force (i.e. Stokes number) were used as non-dimensional parameters for classifying the flow behavior. For  $M_p < 1$  (viscous force is dominant), it was observed that the jet remained cylindrical and stable. For  $M_p > 1$  and  $Re_p < 1$ , an unstable jet with blob formation was formed.  $Re_p > 1$  resulted in an unstable jet with spiral

movement. Finally, atomization behavior was observed when the particle inertia was large compared to viscous force ( $Stk > 1$ ).

Zhao et al. (2012) studied the behavior of particle cloud at different release-height from the water surface. A constant of 8.4 g of dry glass beads with the density of  $2.5 \text{ g/cm}^3$  and the median diameter of 0.51 mm was released through a cylindrical container with the diameter of 20 mm. The  $L/d_o$  ratio of their experiments was 0.5 and the release-height ranged from 20 mm to 100 mm. Three phases of initial acceleration phase, thermal-like phase, and dispersive phase was observed in their experiments. They found that increasing the release-height makes the initial acceleration phase shorter. However, the growth rate in thermal-like phase is independent of the air release height. The lateral spread of sediment cloud and the depth penetration was studied experimentally by Lai et al. (2013). Both phases of sediment and entrained fluid were tracked in their investigation. They performed their experiments in a glass tank with the cross section of  $0.85 \text{ m} \times 2.82 \text{ m}$  and depth of 1.0 m. Three particle sizes of 0.725 mm, 0.513 mm, and 0.256 mm with the mass of 3 g in a cylindrical container with diameter of 9 mm was used in their experiments. A CCD camera with frequency of 15Hz was used to capture images of entrained fluid and another camera for capturing the images of sediment particle by fitting a 532 nm band pass filter. For all particle sizes, the experiments were repeated 10 times, 5 times for the upper level ( $x=0$  to 30 cm) and 5 times for the lower level ( $x=0$  to 30 cm). They found that in the beginning of the experiment, the particles remained with the entrained fluid and the cloud travels like a coherent mass resembling a thermal. Then, the particles settle out in the cloud which increases the particle concentration at the bottom of the thermal. Finally, the separation of entrained fluid and particles occurs and particles descend at their own particle settling velocity. The entrained fluid also descends but with a velocity lower than the particles. Entrained fluid

took two to three times longer than the particles to reach the bottom of the tank. Wang et al. (2015) extrapolate small-scale lab experiments or numerical models to the field operation. It was found that if the cloud number of two cases is equal, the major particle cloud dynamics are in accordance with the same behavior. The initial particle cloud number can be find using the following equation (Rahimipour and Wilkinson, 1992).

$$N_c = \frac{u_\infty R_o}{\sqrt{B_o / \rho_f}} \quad (2.20)$$

where  $B_o = m\Delta\rho/\rho_f g$  is the initial buoyancy of the particle cloud,  $\rho_f$  is the density of fluid and  $R_o$  is the initial radius of particle cloud.

## Chapter 3: Experimental Study of Sand Jets and Particle Clouds in Water

### 3.1 Introduction

Two-phase jets such as solid-liquid jets have many applications in industries and natural processes and can be found in wastewater discharge, dredging, and marine bed capping. Many research studies have been devoted to investigate the dynamics of solid-liquid jets (Parthasarathy and Faeth, 1987; Muste et al., 1998; Bush et al., 2003; Azimi et al., 2012a, 2014, 2015). Based on the initial conditions, solid-liquid jets can be classified into sand jets and particle clouds. Sand jets are formed by a continuous discharge of sand particles whereas particle clouds are formed by releasing a finite amount of sand into ambient water. In sand jets and particle clouds, the interaction between two phases (i.e., sand and water) and particle to particle interactions considerably affect particle dynamics such as mean velocity, solid-phase concentration distribution and turbulent fluctuations (Sheen et al., 1994; Muste et al., 1998; Bush et al., 2003; Hall et al., 2010).

The dynamics of dilute sand jets in water with low volumetric sand concentrations ( $c_o=0.1\%–2.4\%$ ) was investigated by Jiang et al. (2005) and found that the mean sediment velocity can be described as a combination of fluid velocity and particle terminal settling velocity  $u_\infty$ . The structure of particle laden jets with an initial particle volume fractions of 2.4% and 4.8% were studied by Parthasarathy and Faeth (1987). Solid glass sphere with a uniform particle size of 0.505 mm were injected into water to form particle laden jets. Time-averaged velocities and turbulence intensities of both phases were measured close to the nozzle at three cross sections of  $x/d_o=8, 16, \text{ and } 40$ , where  $x$  is the axial distance from nozzle and  $d_o$  is the nozzle diameter. Effects of nozzle size and initial jet velocity on the mean sand velocity and sand

concentration were studied for sand jet ( $c_o=60\%$ ) and slurry jets ( $c_o=5.5\%–12.4\%$ ) in water (Hall et al., 2010). Initial sand velocities were limited to a range of 1.00 to 2.29 m/s. A self-similar Gaussian profile for both sand velocity and sand concentration were observed. It was found that the centerline particle velocity dropped rapidly with a rate of  $-1/3$  and reached a plateau for  $x/d_o>64$ .

Effects of sand particle size and nozzle diameter on the dynamics of sand jets front was studied (Azimi et al., 2012a). Four nozzle sizes with different diameters of 2, 3, 4.75 and 10 mm and eight sand size classes ranged from 0.125 to 0.589 mm were used. It was found that the velocity of sand jet front was 5 times larger than the settling velocity of individual particle of the same size. Moreover, sand jets with larger particles have higher frontal velocities and they reached a plateau earlier than sand jets with smaller sand particles. It was reported that particle size plays an important role in dynamics of particles and sand jets front. The frontal shape of sand jets were classified into three categories of thermal, bowl-shaped and narrow frontal head depending on the particle Reynolds number  $Re_p=\rho_w u_{\infty} D_{50}/\mu$  where  $\rho_w$  is the density of water,  $D_{50}$  is the mean sand particle size and  $\mu$  is the dynamic viscosity of the ambient fluid. It was also found that  $Re_p=10$  is the threshold for classification of the bowl-shaped and narrow frontal head regimes.

Particle clouds can be formed when a finite amount of sand released into ambient water. Many experimental studies have been carried out to investigate the hydrodynamics of particle clouds in uniform and stratified ambient water (Noh and Fernando, 1993; Noh, 2000; Rahimipour and Wilkinson, 1992; Bush et al., 2003). Three different phases of motion were observed that influence the spreading of particle clouds in water namely as acceleration phase, thermal like phase and the disperse phase (Rahimipour and Wilkinson, 1992). Bush et al. (2003)

used normalized buoyancy  $F_B/x^2 u_\infty^2$  as the controlling parameter to classify two-phase particle clouds into thermal and swarm regimes where  $F_B=(\pi d_o^2/4)L_o c_o g(\rho_p - \rho_w)/\rho_w$  is the buoyancy force,  $L_o$  is the equivalent length of sand column,  $c_o$  is the initial sand concentration (i.e.,  $c_o=0.6$ ),  $g$  is the acceleration due to gravity, and  $\rho_p$  is the density of sand particles, respectively. They found that particle clouds settle as a thermal if  $F_B/x^2 u_\infty^2$  becomes greater than 0.1. For  $F_B/x^2 u_\infty^2 < 0.1$ , particles descended as swarm with a settling velocity close to  $u_\infty$ . Bond and Johari (2005) studied the effects of initial geometry on development of single-phase buoyant thermals. They found significant correlations between the dynamics clouds such as spreading rate and  $L_o/d_o$ . Their experimental results covered a narrow ranges of  $L_o/d_o$  ratios ranging from 2 to 8 and their experimental data were measured in the near field (i.e.,  $x/d_o < 11$ ). Effects of impact velocity  $u_i$  on the dynamics of two-phase jets were investigated for downward gas-liquid jets using different drop heights  $H$  (Qu et al., 2011, 2013). Different fall-heights ranging from 0.01 m to 0.25 m were used to form different impact velocities  $u_i$  ranging from 0.66 m/s to 3.59 m/s. Bernoulli's equation was employed to estimate the impact velocity as  $u_i=(u_o^2+2gH)^{1/2}$ . The flow was divided into four classes of no entrainment, incipient entrainment, intermittent entrainment and continuous entrainment. Variations of the kinetic energy and the magnitude of circulation in particle cloud as it descends in the ambient water can be used to identify the mixing strength and to predict the pinch off occurrence of vortex ring in one phase flow (Pottebaum and Gharib, 2004; Shusser and Gharib 2000a, b; Gharib et al., 1998).

Particle cloud can be formed by releasing a certain mass of particles through a nozzle. However, sand jet can be also formed if same amount of mass passing through a smaller nozzle. Therefore, depends on the particles mass and nozzle size, it is possible to form either particle clouds or sand jets. Formation of particle cloud and sand jet from identical masses of particles

can be analyzed using  $L_o/d_o$ . Relatively wide ranges of  $L_o/d_o$  ( $0.8 < L_o/d_o < 40.1$ ) are employed in this study. In addition, the effect of impact velocity on the dynamics of particle clouds and sand jets in water was systematically studied. Since only gravitational force and nozzle size control the impact velocity of particles, impact velocity can be altered by increasing the drop height. This thesis aims at investigating the effects of  $L_o/d_o$  and impact velocity on the formation of particle clouds and sand jets front. Previous experimental studies (Azimi et al., 2012a, b, 2015) indicated the importance of particle size on the dynamics of particle cloud and sand jets. Therefore, effects of  $L_o/d_o$  and initial sand velocity on formation of particle clouds and sand jets are investigated for three particle size groups of small ( $D_{50} \leq 0.196$  mm), medium ( $D_{50} = 0.389$  mm) and Large ( $D_{50} \geq 0.507$  mm). This thesis is organized as follows; in section 3.2, the background of particle clouds dynamics including dimensional analysis is described to present the controlling parameters on sand jets and particle clouds. In section 3.3, experimental setup and procedures are described. Section 3.4 shows the experimental results and discuss the effects of  $L_o/d_o$ , sand particle size, and impact velocity and finally in section 3.5, summary and conclusions are presented.

### 3.2 Theory and Background

Motion of particle clouds containing uniform particle sizes is controlled by the particle size  $D_{50}$ , dynamic viscosity of the ambient fluid  $\mu$ , mass of particles  $m$ , and the initial boundary conditions such as nozzle diameter and impact velocity. Noh and Fernando (1993) showed that the frontal width and velocity of particle clouds can be formulated as

$$w, u_f = f_1(d_o, m, D_{50}, \mu, x, g') \quad (3.1)$$

where  $g' = g(\rho_p - \rho_w)$  is the reduced gravity,  $\rho_p$  and  $\rho_w$  are the densities of sand particles and water, respectively. The evolution of thermal depends on the buoyancy force of a particle cloud (i.e.,

$F_B = V_o g'$ ) where  $V_o$  is the volume of a group of particles and it can be expressed for particle cloud released from a nozzle as

$$F_B = \left( \frac{\pi d_o^2}{4} \right) L_o c_o g' \quad (3.2)$$

where  $c_o$  is the initial volumetric sand concentration with a value of 0.6 for un-compacted uniform sand particles. Bush et al. (2003) found that the frontal velocity of turbulent thermal is a function of  $F_B$ , terminal settling velocity of particles  $u_\infty$  and  $x$  with the scaling relationship as

$$u_f \sim F_B^{1/2} x^{-1} u_\infty^2 \quad (3.3)$$

where  $u_\infty$  is a function of particle size and it can be predicted using Haywood tables (Holdich, 2002). It is important to estimate other quantities of interest such as initial circulation  $\Gamma$ , initial energy  $E$  and impulse  $I$  to describe dynamics of sand jets and particle clouds in water. One of the primary measures of rotation in a fluid can be defined by circulation. Mohseni and Gharib (1998) defined the initial circulation, energy per unit density and impulse for tube-piston assemblies as

$$\Gamma = \frac{1}{2} L_o U_p \quad (3.4)$$

$$E = \frac{1}{8} \pi d_o^2 \rho_p L_o U_p^2 \quad (3.5)$$

$$I = \frac{1}{4} \pi d_o^2 \rho_p L_o U_p \quad (3.6)$$

where  $U_p$  is the piston velocity which is equivalent to the exit velocity (Bond and Johari, 2005). For gravity-driven flows, initial velocity is related to the gravitational acceleration and nozzle diameter. Cai et al. (2010) approximated the initial velocity of sand jets in the air using orifice equation as

$$u_o = c_1 \sqrt{g d_o} \quad (3.7)$$

where  $c_l$  is a constant with a value of 0.68 in the study of Cai et al. (2010) and 0.74 in the study conducted by Rao and Nott (2008). Expressions for initial circulation  $\Gamma$ , energy  $E$  and impulse  $I$  generated by sand particles can be correlated with  $L_o/d_o$  and nozzle size  $d_o$  if Eq. (3.7) being used to estimate the initial velocity of sand particles.

$$\Gamma = f_2(L_o / d_o, d_o^{3/2}) \quad (3.8)$$

$$E = f_3(L_o / d_o, d_o^4) \quad (3.9)$$

$$I = f_4(L_o / d_o, d_o^{7/2}) \quad (3.10)$$

It is worth noting that all correlations for  $\Gamma$ ,  $E$  and  $I$  are independent of  $c_l$ . A non-dimensional energy  $\alpha$  can be defined as a critical parameter to compare the initial energy with the energy required to establish a steady vortex ring (Gharib et al., 1998).

$$\alpha = \frac{E}{\sqrt{\rho \Gamma^3}} \quad (3.11)$$

Employing expressions for  $\Gamma$ ,  $E$  and  $I$  from Eqs. (3-10) to (3-11) gives

$$\alpha = k(L_o / d_o)^{-1} \quad (3.12)$$

where  $k$  is a constant (i.e.,  $k=(\pi/2)^{1/2}=1.253$ ). Equation (3.12) shows that in order to generate a steady vortex for  $L_o/d_o=1$ , the jet's energy should be 25.3% more than the initial energy generated by sand particles. This extra energy can be produced by increasing the initial velocity of sand jets and releasing sand particles from higher elevations. A steady vortex is generated if  $\alpha \leq 1$ . This can be formed in sand jets and particle clouds for  $L_o/d_o \geq 1.235$ . The initial circulation can be defined in non-dimensional form as

$$\gamma = \frac{\Gamma \tau}{R_o^2} \quad (3.13)$$

where  $R_o$  is the equivalent radius of particle cloud if its shape can be simplified to a hemisphere (Shusser and Gharib, 2000b) and  $\tau$  is the characteristic time scale for vortex ring (Lundgren et al., 1992). The characteristics time scale can be expressed as

$$\tau = \left[ \frac{R_o \rho_p}{g(\rho_p - \rho_w)} \right]^{-0.5} \quad (3.14)$$

By replacing Eqs. (3.4) and (3.14) into Eq. (3.13), the normalized circulation can be simplified to as

$$\gamma = f_5 (L_o / d_o)^{1/2} \quad (3.15)$$

Equation (3.15) shows that the non-dimensional circulation also correlates with  $L_o/d_o$ . Many researchers have studied the variations of sand concentration along the axis of multi-phase jets and plumes (Papanicolaou and List, 1988; Wang and Law, 2002). For single phase plumes, Papanicolaou and List (1988) suggested the following equation to obtain the centerline concentration with the normalized distance  $x/d_o$  as

$$\frac{c_m}{c_o} = \frac{9.3F^{2/3}}{\left( \frac{x}{d_o} \right)^{5/3}} \quad (3.16)$$

where  $F = u_o / (gd_o(\rho_p - \rho_w) / \rho_w)^{0.5}$  is the Froude number. Cai et al. (2010) consider the effect of sand concentration on sand jet in the air. They found that the normalized concentration decreases with  $x/d_o$  up to  $x/d_o=120$ . Hall et al. (2010) found experimentally that centerline concentration in sand jet in water decreases similar to single phase plume. Numerical analysis of sand jet in water conducted by Azimi et al. (2011) also showed a good agreement with experimental results (Hall et al., 2010). For continuous sand jets, the length scale of  $d_o F^{2/5}$  was used to normalize sand concentration variations (Hall et al., 2010). They proposed the following formulation for prediction of sand concentration.

$$\frac{c_m}{c_o} = \frac{12.83}{\left( \frac{x}{d_o F^{2/5}} \right)^{5/3} + 5.13} \quad (3.17)$$

### 3.3 Experimental Setup and Data Analysis

For considering the effects  $L_o/d_o$  ratio, impact velocity and particle size of particle clouds, laboratory experiments were conducted. Experiments were carried out in a rectangular glass tank with width and length of 0.40 m and depth of 1.0 m, respectively. The tank was filled with tap water and the water temperature was maintained at room temperature (i.e.,  $\approx 20^\circ\text{C}$ ). A steel frame was placed on top of the tank to secure the release tubes and brass nozzle inside the tube. A schematic of the experimental setup is shown in Fig. 3.1. Sand particles with a density of  $2540 \text{ kg/m}^3$  were used. The sand particles were classified using different sieves with sieve numbers ranged from #20 to #120 to form a narrow range of sand particles with median grain sizes of  $D_{50} = 0.1375, 0.196, 0.389, 0.507, \text{ and } 0.718 \text{ mm}$ . Particle sizes were classified into three categories based on the relationship between particle size and the size of the most energetic eddy in slurry jets (Azimi et al., 2012b). Two median particle sizes of 0.1375 mm and 0.196 mm represented small particle class,  $D_{50} = 0.389 \text{ mm}$  represented the medium particle class and  $D_{50} = 0.507 \text{ mm}$  and 0.718 mm represented the class of large particles.

A total of 36 experiments were conducted to study the dynamics of sand jets and particle clouds. 15 experiments were conducted with a relatively wide  $L_o/d_o$  to study the effect of normalized kinetic energy and circulation. In order to form a wide range of  $L_o/d_o$ , six sand masses of  $m = 1, 3, 6, 9, 12, \text{ and } 18 \text{ grams}$ , and five different nozzle diameters of  $d_o = 5, 8, 10, 12, \text{ and } 14 \text{ mm}$  were used. The selected parameters formed a wide range of  $L_o/d_o$  ranging from 0.8 to 40.1. The non-dimensional energies and the non-dimensional circulations were calculated using Eqs. (3.12) and (3.15) ranged from 0.03 to 1.5 and 0.65 to 4.56, respectively (see Table 3.1). Effects of the impact velocity on particle clouds were studied. To alter the impact velocity of sand particles, different heights of  $H = 0.1, 0.2, 0.3, 0.75 \text{ and } 1.3 \text{ m}$  were tested. Effects of drop heights on the impact velocity of sand particles are shown as  $u_i/u_o$  in Table 3.1. The impact

velocity can be calculated using Bernoulli's equation  $u_i=(u_o^2+2gH)^{1/2}$  and  $u_o$  can be estimated using orifice equation  $u_o=c_I(gd_o)^{1/2}$  with  $c_I=0.68$  (Cai et al., 2010). Three particle size ranges with the mean particle sizes of  $D_{50}=0.196$  mm, 0.389 mm and 0.507 mm were selected. In total, 21 experiments were carried out to study the effects of impact velocity and are denoted as series B in Table 3.1.

A high speed camera was used in conjunction with AVT Vimba Viewer v.1.1.3 software (Allied Vision Technologies GmbH, Germany). The camera was located perpendicular to the tank at a distance of 1.4 m. Images were recorded with a speed of 20 frames per seconds. In order to reduce air entrainment and bubble formation, nozzles were kept at most 5 mm above the water surface for the cases with  $H=0$ . Two light sources were perpendicularly placed beside the tank to remove the shadows of particles and to improve the quality of images. To increase the quality of images and to differentiate the particle cloud from the background flow, the color of images was inversed and then changed in to black and white. Horizontal and vertical rulers were used in the tank to detect any image distortion. Additionally, the rulers are used as the scales for calculating the displacement of particle clouds at different times. A top-hat concentration profile was assumed to estimate the variations of the averaged sand concentration along the  $x$  axis. At each specific time, the volume of particle cloud  $V$  was calculated by tracing the boundary of the cloud and revolving the boundary around the vertical axis.

The uncertainty in experimental data was verified through repeatability tests. Four experiments were repeated (i.e., Test No. A7,  $L_o/d_o=5$ ,  $D_{50}=0.389$  mm) to study the reliability of measurements. Variations of the frontal position  $x$ , width  $w$ , and frontal velocity  $u_f$  at different times were measured. The maximum uncertainties in measurements for the thermal cloud phase were  $\pm 3\%$ ,  $\pm 13\%$  and  $\pm 5\%$  for  $x$ ,  $w$ , and  $u_f$ , respectively. Relatively large uncertainty for  $w$  in

thermal phase may be due to formation of strong shear layer and turbulence close to the nozzle. The uncertainties of experiments reduced in particle swarm regime (i.e.,  $F_B/x^2 u_\infty^2 < 0.1$ ) to  $\pm 2.5\%$ ,  $\pm 3\%$  and  $\pm 4\%$  for  $x$ ,  $w$ , and  $u_f$ , respectively.

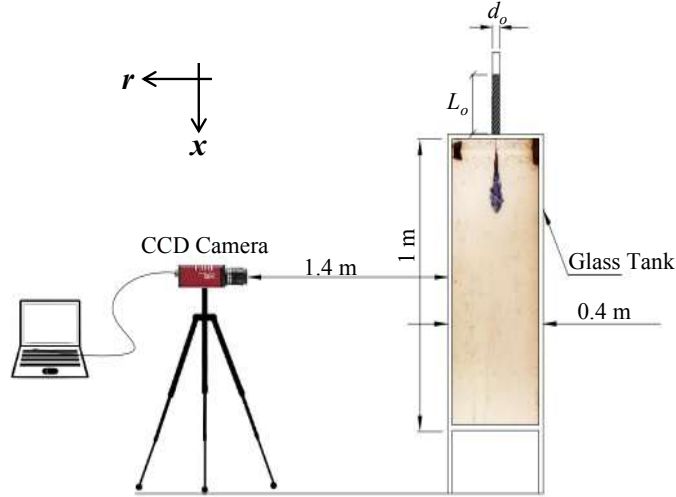


**Figure 3.1** Schematic of the experimental setup and coordinate system.

### 3.4 Experimental Results

#### 3.4.1 General Evolution of Sand Jet Front

Variations of the normalized frontal velocity of particle cloud with the normalized buoyancy for small particle size (i.e.,  $D_{50}=0.196$  mm) is shown in Fig. 3.2. Prediction lines for particle cloud with small  $L_o/d_o$  ratios ( $0.02 < L_o/d_o < 6$ ) and sand jet front ( $L_o/d_o \sim \infty$ ) were added for comparison. The solid line in Fig. 3.2 reflects the prediction line proposed by Azimi et al., (2012a) for continuous sand jets and the dashed line shows the prediction of Bush et al., (2003) for particle clouds with small  $L_o/d_o$  ratios. As can be seen for small particle sizes (i.e.,  $D_{50}=0.196$  mm) and for all  $L_o/d_o$  ratios tested in this study, particle clouds remain in the thermal phase. The terminal settling velocity is small for this particle size range ( $u_\infty=0.02$  m/s) and particles should pass a relatively long distance to reach terminal settling velocity  $u_\infty$ .

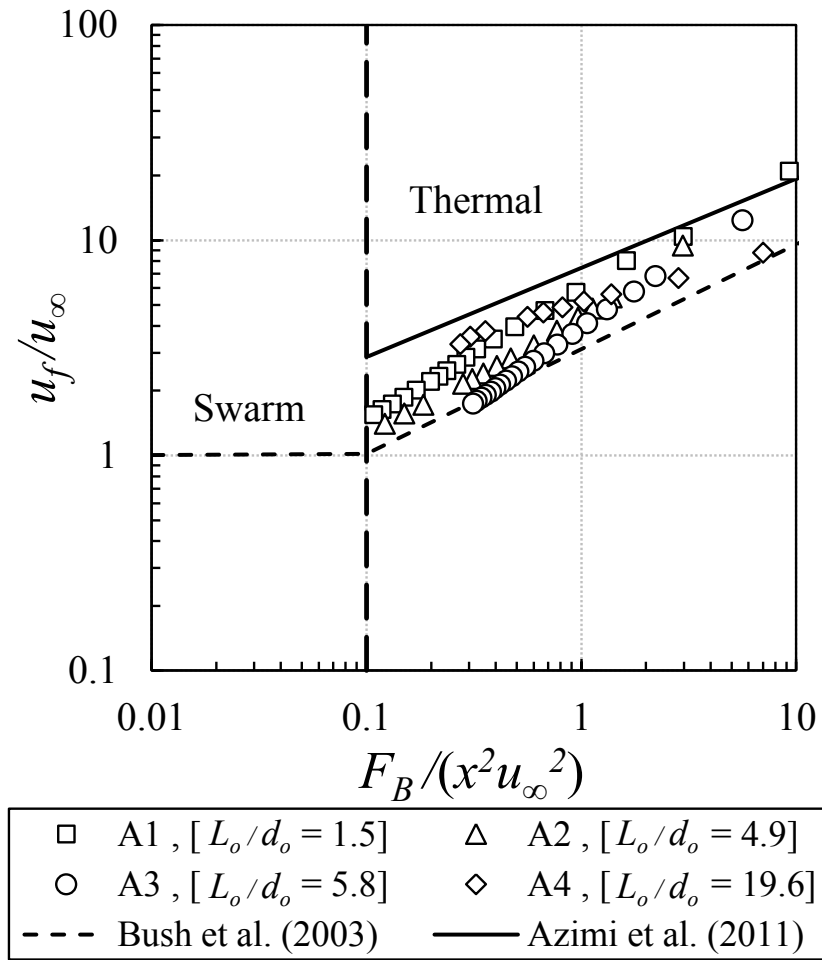


**Figure 3.2:** Correlation between the normalized frontal velocity and the normalized buoyancy force for particle size  $D_{50}=0.196$  mm.

**Table 3.1:** Experimental details of particle clouds in water.

Test No.	$D_{50}$ (mm)	$d_o$ (mm)	$m$ (g)	$u_{\infty}$ (m/s)	$H$ (m)	$L_o/d_o$	$Re_p$	$\alpha$	$\gamma$
A1	0.196	12	3	0.02	0.0	1.5	4.4	0.86	0.87
A2	0.196	8	3	0.02	0.0	4.9	4.4	0.26	1.59
A3	0.196	12	12	0.02	0.0	5.8	4.4	0.22	1.73
A4	0.196	8	12	0.02	0.0	19.6	4.4	0.06	3.19
A5	0.389	10	1	0.055	0.0	0.8	21.3	1.50	0.66
A6	0.389	14	6	0.055	0.0	1.8	21.3	0.69	0.97
A7	0.389	10	6	0.055	0.0	5.0	21.3	0.25	1.61
A8	0.389	10	18	0.055	0.0	15.0	21.3	0.08	2.79
A9	0.389	5	6	0.055	0.0	40.1	21.3	0.03	4.56
A10	0.507	12	3	0.075	0.0	1.5	37.6	0.86	0.87
A11	0.507	8	3	0.075	0.0	4.9	37.6	0.26	1.59
A12	0.507	12	12	0.075	0.0	5.8	37.6	0.22	1.73
A13	0.507	8	12	0.075	0.0	19.6	37.6	0.06	3.19
A14	0.1375	10	6	0.013	0.0	5.0	1.8	0.25	1.61
A15	0.718	10	6	0.089	0.0	5.0	48	0.25	1.61
B1	0.196	12	3	0.02	0.1	1.5	4.4	0.86	0.87
B2	0.196	12	3	0.02	1.3	1.5	4.4	0.86	0.87
B3	0.196	8	3	0.02	0.3	4.9	4.4	0.26	1.59
B4	0.196	8	3	0.02	1.3	4.9	4.4	0.26	1.59
B5	0.196	12	12	0.02	0.3	5.8	4.4	0.22	1.73
B6	0.196	12	12	0.02	1.3	5.8	4.4	0.22	1.73
B7	0.196	8	12	0.02	0.1	19.6	4.4	0.06	3.19
B8	0.196	8	12	0.02	0.3	19.6	4.4	0.06	3.19
B9	0.196	8	12	0.02	1.3	19.6	4.4	0.06	3.19
B10	0.389	10	1	0.055	0.2	0.8	21.3	1.50	0.66
B11	0.389	10	1	0.055	1.3	0.8	21.3	1.50	0.66
B12	0.389	14	6	0.055	0.75	1.8	21.3	0.69	0.97
B13	0.389	14	6	0.055	1.3	1.8	21.3	0.69	0.97
B14	0.389	10	6	0.055	1.3	5	21.3	0.25	1.61
B15	0.389	10	18	0.055	0.2	15	21.3	0.08	2.79
B16	0.389	10	18	0.055	0.75	15	21.3	0.08	2.79
B17	0.389	10	18	0.055	1.3	15	21.3	0.08	2.79
B18	0.507	8	3	0.075	0.3	4.9	37.6	0.26	1.59
B19	0.507	8	3	0.075	1.3	4.9	37.6	0.26	1.59
B20	0.507	8	12	0.075	0.3	19.6	37.6	0.06	3.19
B21	0.507	8	12	0.075	1.3	19.6	37.6	0.06	3.19

In order to study the evolution of particle clouds in stagnant water, a non-dimensional time scale  $t^* = t/T$  is proposed where  $T$  is the time when all the particles are in water. Fig. 3.3 shows the evolution of the particle clouds of medium size (i.e.,  $D_{50} = 0.389$  mm) at different non-dimensional times of 1, 5, 8.6 and 15. The evolution of particle clouds with  $L_o/d_o = 5, 3$  and 1.8 were shown in Figures 3.3a-3.3c, respectively. As can be seen from Fig. 3.3a (i.e.,  $L_o/d_o = 5$ ), particles travel a long distance from the nozzle ( $x = 0.67$  m) at  $t^* = 15$ , while the traveling distance for particle clouds with  $L_o/d_o = 3$  and 1.8 are 0.52 m and 0.28 m, respectively. As a result, increasing  $L_o/d_o$  ratio caused the particle cloud to progress a further distance in a given  $t^*$ . The ratio of  $L_o/d_o$  can be increased either by increasing the mass of sand particles  $m$  or decreasing the nozzle size  $d_o$ . Increasing mass of particles results in an increase of buoyancy force  $F_B$ . As buoyancy force  $F_B$  increases, sand particles tend to progress faster in the water.  $L_o/d_o$  can also be increased by decreasing nozzle size for a given mass. In this condition, since smaller interface area is subjected, sand particles can penetrate easier into the ambient water.

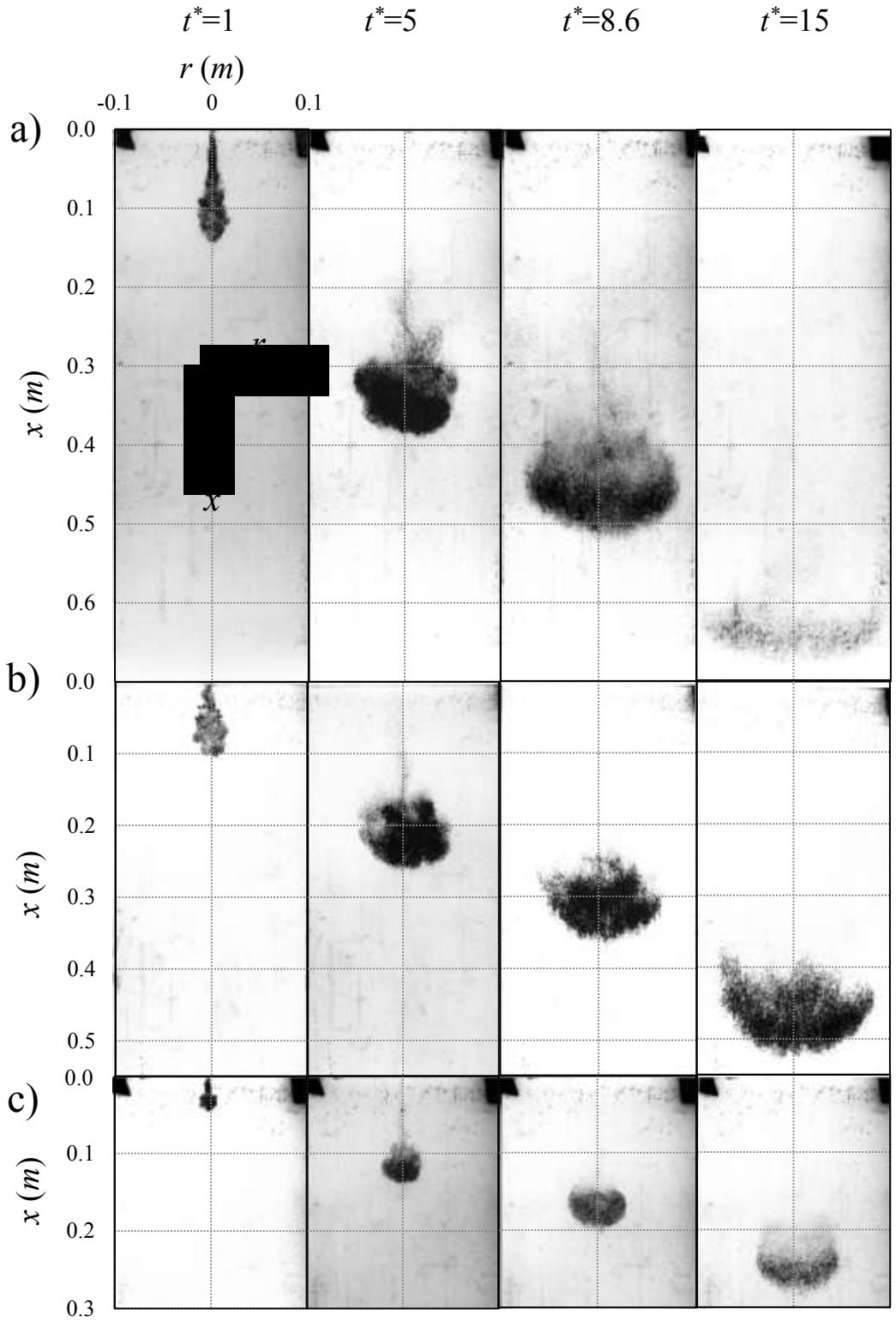


**Figure 3.3:** Evolution of transient sand jets for particle size of  $D_{50}=0.389$  mm at different non-dimensional time  $t^*$  considering the effect of  $L_0/d_0$  ratio: a)  $L_0/d_0 = 5$ , b)  $L_0/d_0 = 1.8$ , c)  $L_0/d_0 = 0.8$ .

Analysis of depth progression was carried out by comparing the variations of the normalized depth  $x/L_i$  with the normalized time  $t^*$  as shown in Fig. 3.4. In this figure,  $t^*=1$  indicates the time particle cloud requires to completely enters into the ambient water. Fig. 3.4a shows the depth progression data of particle cloud with small particles (i.e.,  $D_{50}=0.196$  mm). Two phases were observed named as initial and thermal phases. The initial phase starts from the onset of flow to  $t^*=1$ . In this regime, shear forces at the boundary of the jet develops instability and disperse particles as it descends. As the particles descend further, shear layer instabilities generate small eddies similar to buoyant thermals. In buoyant thermals, frontal velocity decreases with time while the size of thermal increases (Rahimipour and Wilkinson, 1992). Fig. 3.4b shows the depth progression of particle clouds with medium particle size (i.e.,  $D_{50}=0.389$  mm). For this particle size range, three phases of motion were observed. The swarm phase starts when the frontal velocity of particle could reaches the terminal settling velocity. Experimental observations indicate that the swarm phase for this particle size and  $L_0/d_0$  range starts from  $t^*=4.5$ . Fig. 3.4c shows the depth progression of large particle sizes (i.e.,  $D_{50}=0.507$  mm). Similar to the medium particle size range, three phases were observed. The swarm phase for  $D_{50}=0.507$  mm starts from  $t^*=2.5$ . As can be seen from Fig. 3.4, as particle sizes become larger, the thermal regime becomes narrower.

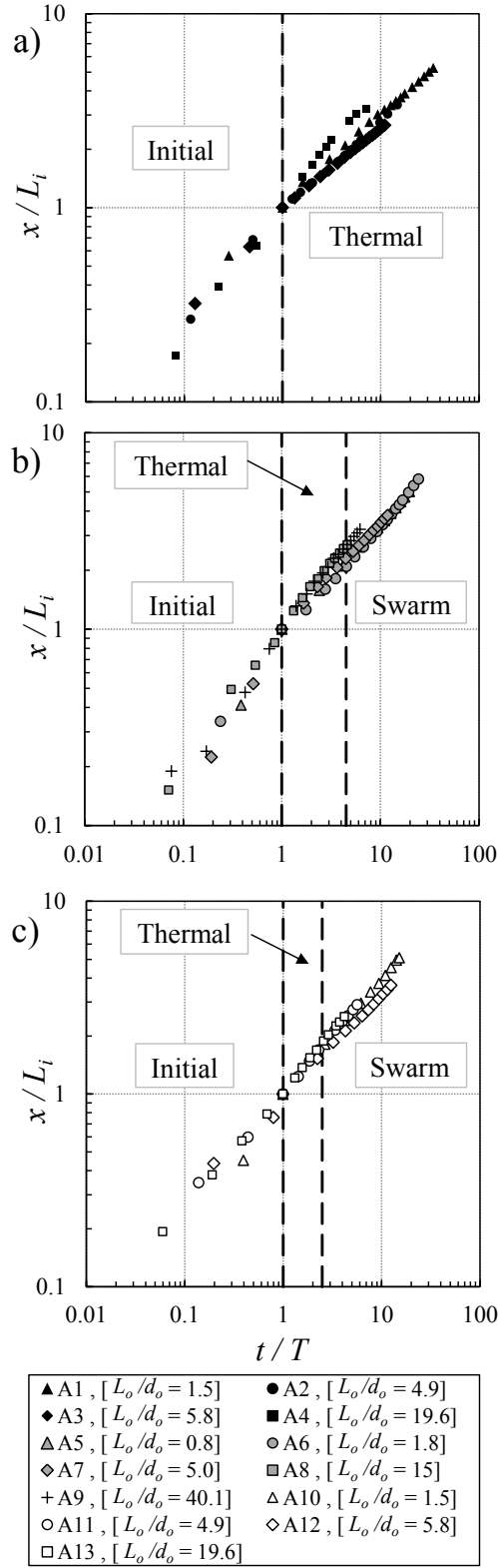


**Figure 3.4:** Effect of  $L_0/d_0$  ratio on the normalized depth  $x/L_i$  along normalized time  $t/T$ : a)  $D_{50}=0.196\text{mm}$ , b)  $D_{50}=0.389\text{mm}$ , c)  $D_{50}=0.507\text{mm}$ .

For thermal regime of particle cloud with small particle size, the superficial velocity was found to be close to the ambient water velocity. For larger particles, since they have larger particle Reynolds number  $Re_p$ , the grouping effect of particles becomes less effective and particles tend to drop individually (Azimi et al., 2012a). Therefore, relatively larger particles (i.e.,  $D_{50}=0.507$  mm) do not follow eddies generated by shear layer instabilities and this results in a shorter thermal regime for particle clouds with larger particles. Particle clouds with smaller particle size will eventually move into the swarm regime far from the nozzle. A power law correlation was found to be suitable for explaining the variations of the depth progression with time in all three phases of initial, thermal and swarm regions as  $x/d = a(t/T)^b$ , where  $a$  and  $b$  are constants. The constant  $a$  was found to be 17.72, 18.1 and 19.42 for the initial, thermal and swarm phases, respectively. The average exponent of the power law correlation  $b$  was found to be 0.65, 0.60 and 0.58 for the initial, thermal and swarm phases, respectively. For single-phase thermal regime, the average exponent of the proposed power law equation was reported 0.60 (Bond and Johari, 2005). For sand jet front, Azimi et al. (2012a) reported a power index range between 0.57-0.63 for different nozzle sizes of 2-10 mm. A correlation was found to predict the axial distance from the nozzle  $x$  for different  $L_o/d_o$  and particle sizes as

$$\frac{x}{d_o} = \varepsilon \left( \frac{t}{T} \left( \frac{L_o}{d_o} \right)^\varphi \right)^\gamma \quad (3.18)$$

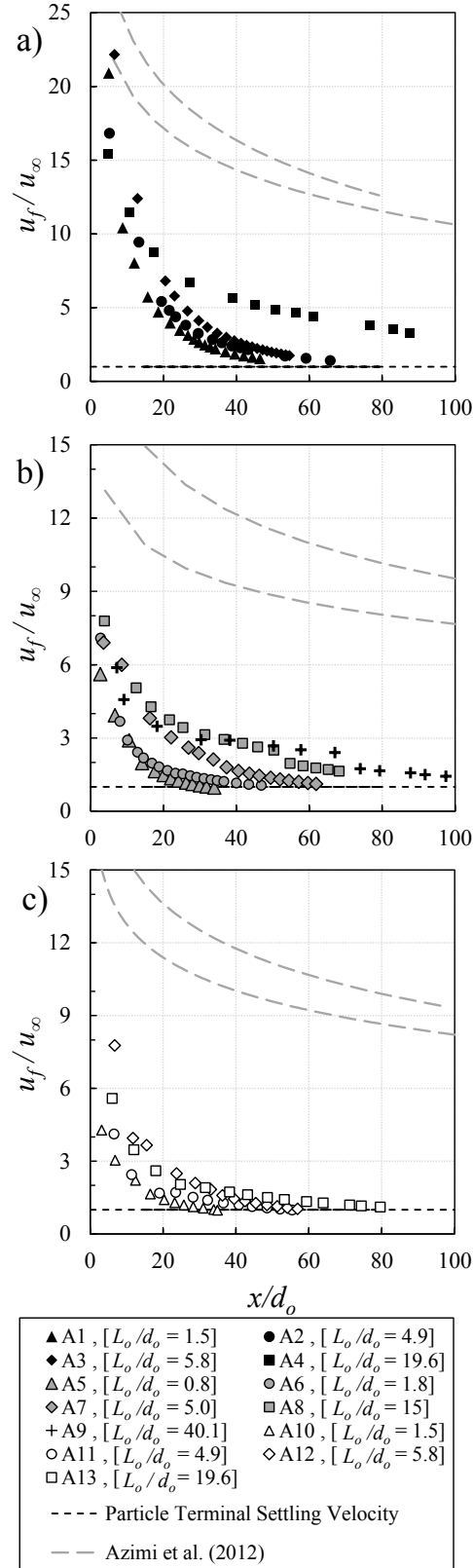
where  $\varepsilon$ ,  $\varphi$ , and  $\gamma$  are constant and can be found in Table 3.2.

**Table 3.2:** Coefficients of equations (3-16), (3-18) and (3-19) with R-squared values

<i>x</i>	$D_{50}$ (mm)	0.196	0.389	0.507
	$\varepsilon$	7.2	5.5	6.25
	$\gamma$	0.5	0.60	0.56
	$\varphi$	1	0.90	1
	$R^2$	0.96	0.97	0.94
$u_f$	$\theta$	68.2	9.4	9.9
	$\delta$	-0.97	-0.61	-0.68
	$\beta$	-0.25	-0.5	-0.4
	$R^2$	0.87	0.90	0.91
<i>b</i>	$\eta$	2.1	2.1	1.98
	$\lambda$	0.6	0.6	0.5
	$\kappa$	1	0.9	1.2
	$R^2$	0.87	0.90	0.91

Fig. 3.5 shows the variations of the normalized cloud width  $b/d_o$  with the normalized time  $t^* = t/T$  for small, medium and large particle sizes. Fig. 3.5a, shows the effect of  $L_o/d_o$  ratio on the cloud width for small particles (i.e.,  $D_{50}=0.196$  mm). As it can be seen, particle clouds with larger  $L_o/d_o$  (higher normalized circulation) expand faster than clouds with smaller  $L_o/d_o$ . Similar trend was observed for medium and large particle sizes (i.e.,  $D_{50}=0.389$  mm and 0.507 mm). A power law equation was proposed to estimate the normalized width for different  $L_o/d_o$  ratios as

$$\frac{b}{d_o} = \theta \left( \frac{t}{T} \left( \frac{L_o}{d_o} \right)^\beta \right)^\delta \quad (3.19)$$



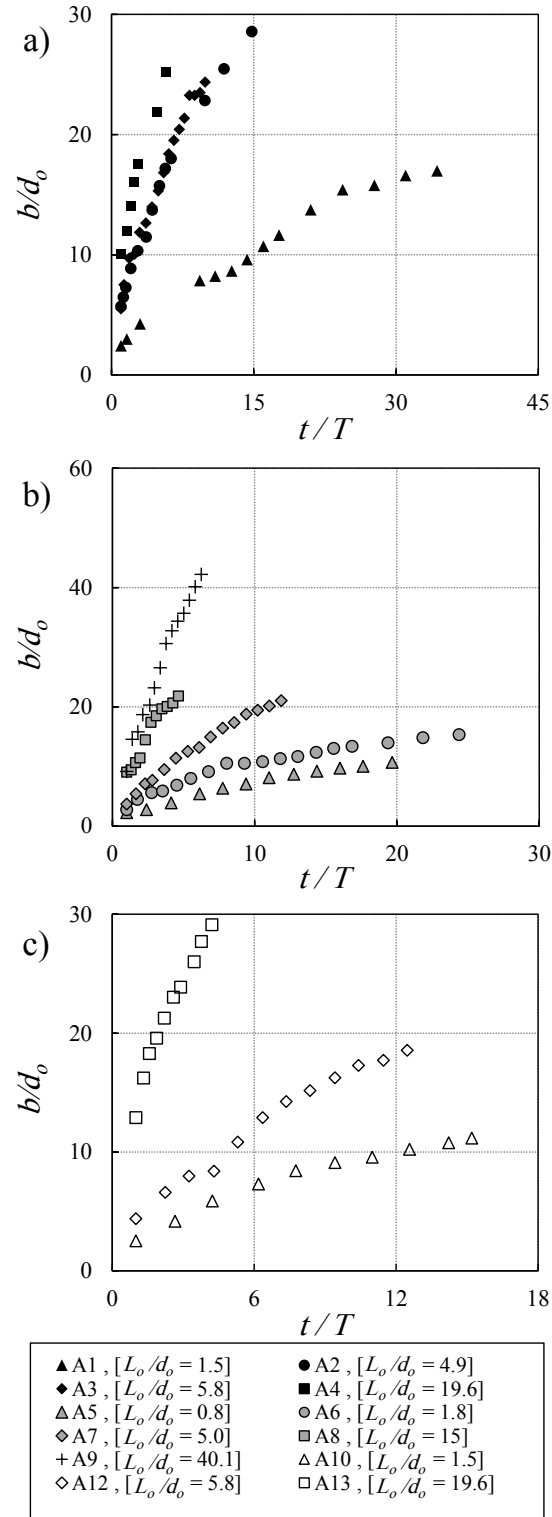
**Figure 3.5:** Effect of  $L_o/d_o$  ratio on the normalized velocity  $u_f/u_\infty$  along the normalized depth  $x/d_o$ : a)  $D_{50}=0.196$  mm, b)  $D_{50}=0.389$  mm, c)  $D_{50}=0.507$  mm.

Fig. 3.5 shows the variations of the normalized velocity  $u_f/u_\infty$  with  $x/d_o$  for small, medium and large particle sizes. Dashed curves in Fig. 3.5 indicate the predictions of the sand jet frontal velocity (i.e.,  $L_o/d_o \approx \infty$ ) with  $x/d_o$  from experimental study of Azimi et al. (2012a) for different particle size ranges.

$$\frac{u_f}{u_\infty} = -\frac{1}{4} \left( \frac{D}{d_o} \right)^{-0.75} \ln \left( \frac{x}{d_o} \right) + 3.8 \left( \frac{D}{d_o} \right)^{-0.55} \quad (3.20)$$

As can be seen from Fig. 3.5, frontal velocities of particle clouds are between the frontal velocity of continuous sand jets and terminal settling velocity. Effects of  $L_o/d_o$  on variations of  $u_f/u_\infty$  with  $x/d_o$ , for small particle sizes ( $D_{50}=0.196$  mm) in Fig. 3.5a. As can be seen, the frontal velocity of particle cloud increases with increasing  $L_o/d_o$ . Fig. 3.5b shows the effect of  $L_o/d_o$  ratio for medium particle sizes ( $D_{50}=0.389$  mm). It is clear that frontal velocity of small  $L_o/d_o$  ratios (i.e.,  $L_o/d_o=0.8$  and  $1.8$ ) reached  $u_\infty$  at  $x/d_o \approx 35$ , whereas for large  $L_o/d_o$  ratio (i.e.,  $L_o/d_o=40.1$ ),  $u_f$  reached  $u_\infty$  at  $x/d_o > 100$ . Fig. 3.5c shows the variation of  $u_f/u_\infty$  with  $x/d_o$  for large particle sizes ( $D_{50}=0.507$  mm). For small  $L_o/d_o$  ratios (i.e.,  $L_o/d_o=1.5$ ), frontal velocity reached  $u_\infty$  at  $x/d_o \approx 26$  whereas for large  $L_o/d_o$  (i.e.,  $L_o/d_o=19.6$ ) it reached at  $x/d_o \approx 70$ . Recent observations on sand and slurry jets (Azimi et al., 2012a, b) indicated that the grouping effect of particles became less significant for relatively large particle sizes ( $D_{50} > 0.389$  mm). Therefore, particles tend to descend individually and reach the plateau in relatively short distance compare to small particle sizes. Comparison of the variations of frontal velocity for different particle size ranges for  $x/d_o > 40$  indicates that the effect of  $L_o/d_o$  ratio becomes more pronounced for small particle sizes. A correlation was found to predict the frontal velocity of the particle clouds for different  $L_o/d_o$  and particle sizes as:

$$\frac{u_f}{u_\infty} = \eta \left( \frac{y}{d_o} \left( \frac{L_o}{d_o} \right)^\kappa \right)^\lambda \quad (3.21)$$



**Figure 3.6:** Effect of  $L_0/d_0$  ratio on the normalized width  $b/d_0$  along the normalized depth  $t/T$ : a)  $D_{50}=0.196$  mm, b)  $D_{50}=0.389$  mm, c)  $D_{50}=0.507$  mm.

### 3.4.2 Effect of particle size

To consider the effect of particle size, three tests were compared (A14, A7 and A15) with the same  $L_o/d_o$  ratio of 5. Particle sizes used in this section were  $D_{50}=0.1375$ ,  $0.389$  and  $0.718$  mm with the corresponding settling velocities of  $0.013$  m/s,  $0.055$  m/s and  $0.089$  m/s, respectively. The evolution of particle cloud with different particle sizes and  $t^*$  values of 1, 4.8, 8.6, and 13.8 was studied (see Fig. 3.7). It is worth noting that all particles released into water at  $t^*=1$ . Fig. 3.7a shows the evolution of particle cloud with large particle sizes ( $D_{50}=0.718$  mm). For relatively large particle sizes, particle cloud moved to the swarm phase at very short  $t^*$  (i.e.,  $t^*\sim 2.1$ ). As can be seen in Fig. 3.7, the initial length of the particle cloud in water  $L_i$  for small particle size was smaller than  $L_i$  for medium and large particle sizes. The initial width of particle cloud for small particle sizes was also found to be larger than clouds with medium and large particle sizes. Since the buoyancy force exerted from large particles is higher than the smaller particles, particle clouds with larger particle size descend at relatively higher frontal velocity. As a result, clouds made of larger particles tend to fall individually and they do not follow the generated vortices. Particle clouds can be classified into three different shapes based on particle size. An arc shaped can be developed for large particle sizes (Fig. 3.7a). For medium particle sizes a bowl shape can be formed and for smaller particle sizes, a semi-spherical shape can be formed. For the present range of  $L_o/d_o$ , a frontal head following with trailing part was observed for particle clouds with medium and small particle sizes (see Fig. 3.7b and 3.7c). It was observed that for clouds with small particles, the trailing part last longer ( $t^*\sim 13.8$ ) than clouds with large particles ( $t^*\sim 3.6$ ).

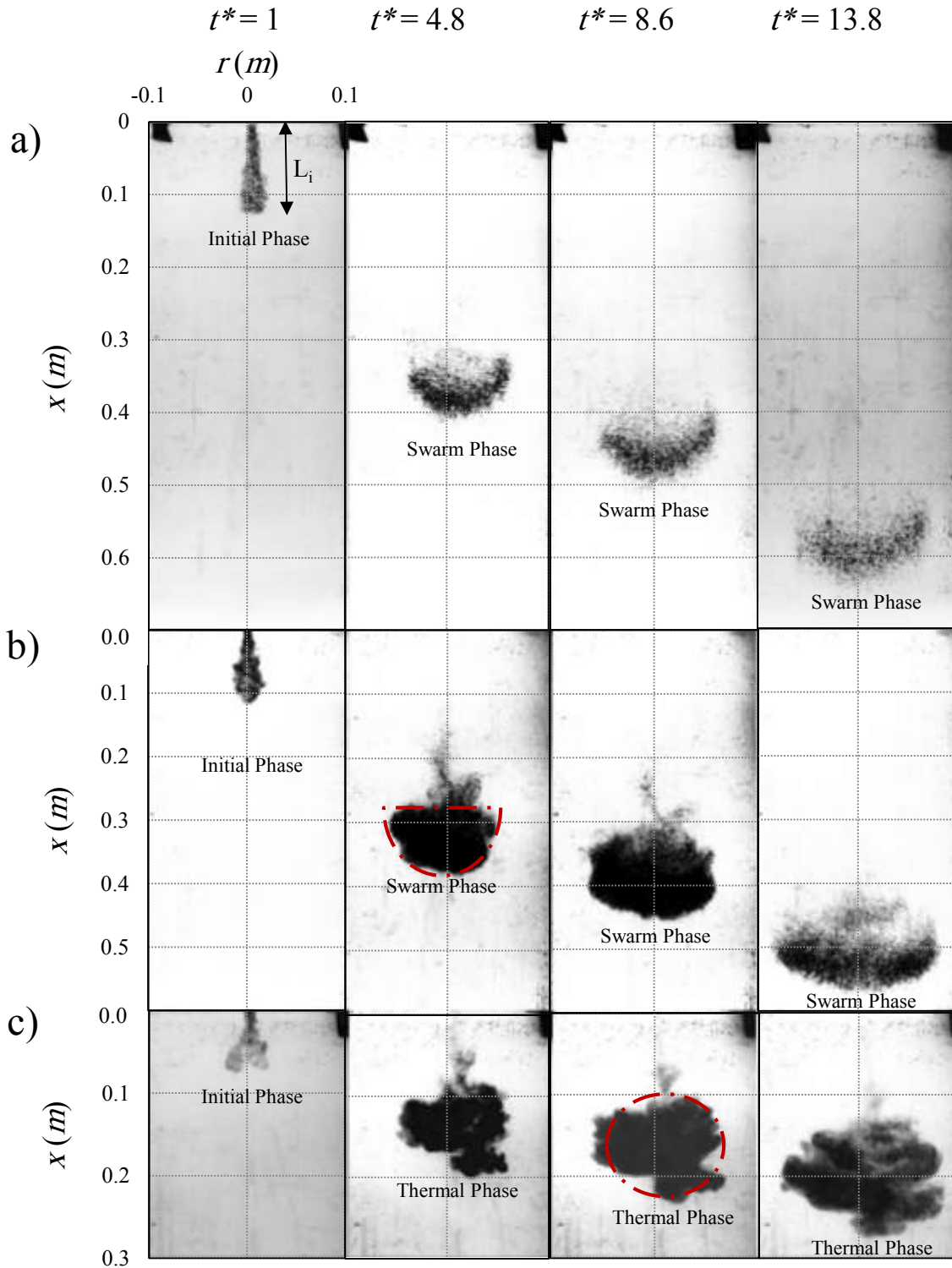


**Figure 3.7:** Effect of particle size at different  $t^*=t/T$ : a) A15,  $D_{50} = 0.718$  mm, b) A7,  $D_{50} = 0.389$  mm, c) A14,  $D_{50} = 0.1375$  mm.

Effect of particle size on the frontal velocity of sand particle cloud with  $L_o/d_o=5$  is shown in Fig. 3.8. Dashed curves in this figure reflect the prediction of frontal velocity of sand jet front in water for  $L_o/d_o \approx \infty$  (Azimi et al., 2012b). Particle clouds with smaller particle sizes have a larger normalized velocity ( $u_f/u_\infty$ ) since  $u_\infty$  are much smaller for clouds with small particle sizes. It is expected that the frontal velocity of particle clouds eventually reaches a plateau far from the nozzle (Noh and Fernando, 1993; Bush et al. 2003; Bond and Johari, 2005; Azimi et al., 2012b). Since small particles in particle clouds follow shear layer vortices and disperse, clouds with small particle sizes ( $D_{50}=0.1375$  mm) require a large distance from the nozzle to reach plateau.

Our observations indicate that clouds with large particle sizes ( $D_{50}=0.718$  mm) reach particle terminal settling velocity in relatively shorter distance from the nozzle ( $x/d_o \approx 25$ ). Since clouds with large particles move to the swarm phase faster, particles begin acting independently and approach particle terminal settling velocity in relatively shorter time and distance. As can be seen from Fig. 3.8, clouds with medium and small particle sizes (i.e.,  $D_{50}=0.389$  mm, 0.1375 mm) reached  $u_\infty$  at  $x/d_o \approx 50$  and 75, respectively whereas the frontal of sand jets reached the plateau at  $x/d_o > 125$  for particle sizes ranged from 0.196 mm to 0.507 mm and  $x/d_o > 200$  for particle sizes ranged from 0.1375 mm to 0.165 mm (Azimi et al., 2012b). Comparing between the results of frontal velocity for sand jets and particle clouds indicates that particle clouds have smaller normalized velocity. Experimental results for sand jets front shows that the frontal velocity was five times of the settling velocity at plateau (Azimi et al., 2012b) whereas for particle clouds, the frontal velocity in plateau region was equal to  $u_\infty$ . An empirical equation is proposed for  $L_o/d_o=5$  to consider the effect of particle size on the frontal velocity of particle clouds as:

$$\frac{u_f}{u_\infty} = 3.2 \left( \frac{x}{d_o} \left( \frac{D_{50}}{d_o} \right)^{0.9} \right)^{-0.77} \quad (3.22)$$

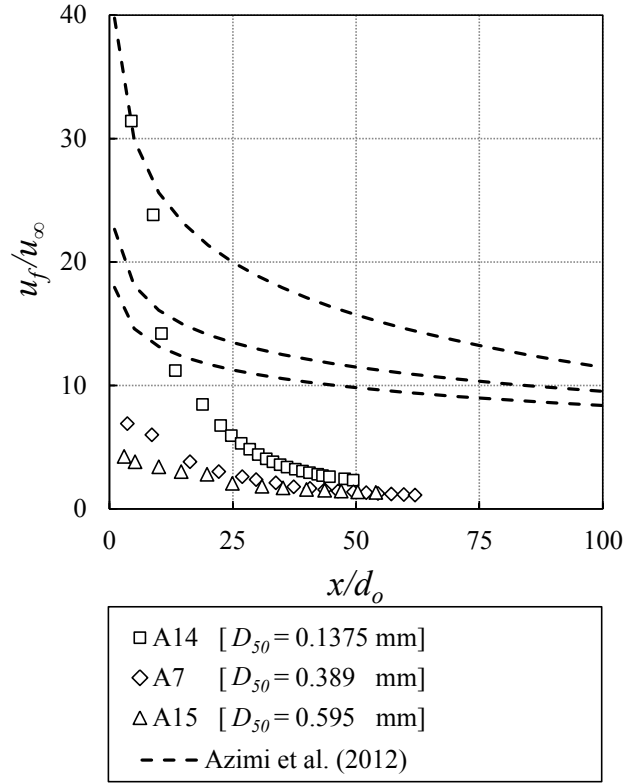


**Figure 3.8:** Effect of particle size on normalized velocity  $u_f/u_\infty$  along normalized depth  $x/d_o$ .

The coefficient of determination  $R^2$  for the correlation is 0.89. Fig. 3.9 shows the effects of particle size on the width of particle cloud with  $L_o/d_o=5$ . It was found that particle clouds with small particles (i.e.,  $D_{50}=0.1375$  mm) are wider than clouds with large particle sizes since the tendency of small particles to follow the shear layer vortices is higher. Fig. 3.9b shows the normalized width  $b/d_o$  with the normalized time  $t^*=t/T$ . As can be seen from Fig. 3.9b, particle size has no effect on the growth rate of particle cloud for  $0 < t^* < 10$ .

$$\frac{b}{d} = 0.04 \left( \frac{x}{d_o} \left( \frac{D_{50}}{d_o} \right)^{-0.5} \right)^{1.1} \quad (3.23)$$

The coefficient of determination  $R^2$  for the correlation is 0.97.

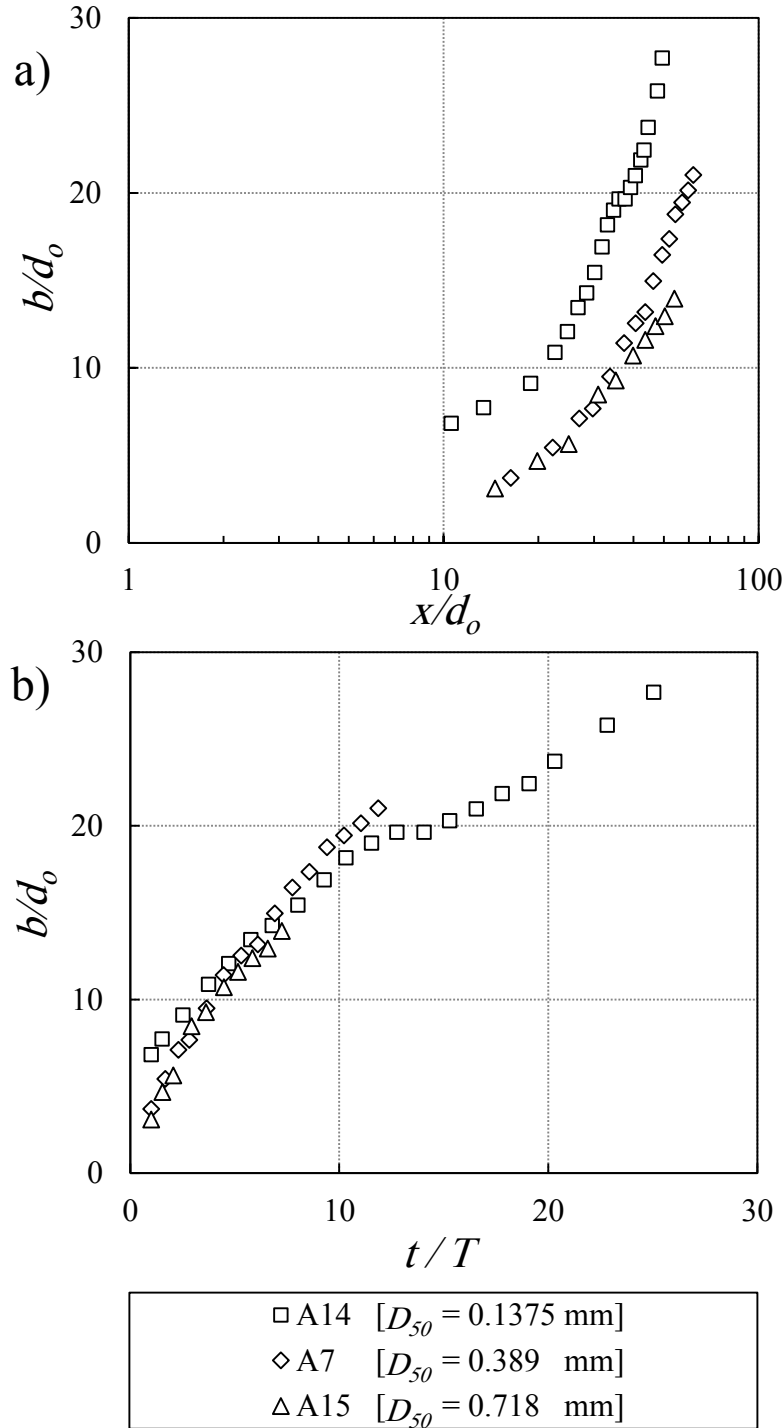


**Figure 3.9:** Effect of particle size on width: a) Normalized width  $b/d_o$  along normalized depth  $x/d_o$ , b) Normalized width  $b/d_o$  along normalized time  $t/T$ .

### 3.4.3 Particle Cloud Concentration

Assuming a relationship between the peak and average sand concentration in top-hat profiles (Lee and Chu, 2003), the averaged sand concentration  $c_{ave}$  can be converted to the peak

sand concentration  $c_m$  as  $c_m=1.4c_{ave}$ . Fig. 3.10 shows the variations of the normalized peak sand concentration  $c_m/c_o$  with the normalized depth  $x/(d_oF^{2/5})$  for particle clouds with small and large particle sizes (i.e.,  $D_{50}=0.196$  mm and 0.507 mm) and relatively wide ranges of  $L_o/d_o$  ratios of 1.5–19.6. Solid and open symbols show the concentration results of small ( $D_{50}=0.196$  mm) and large particle size ( $D_{50}=0.507$  mm), respectively. As can be seen, sand concentration for particle clouds decreased significantly after releasing particle from the nozzle and the normalized concentration reached to zero at around  $x/(d_oF^{2/5})=60$  for all  $L_o/d_o$  ratios used in this study. Results of sand concentration variations for continuous sand jets were added from experimental study of Hall et al. (2010). Fig. 3.10 clearly shows that spreading and dilution of particles in particle clouds were larger than sand jets. For instance, the normalized concentration dropped to 0.02 at normalized depth of 10 for particle clouds whereas for sand jets it occurred at  $x/(d_oF^{2/5})=60$ .

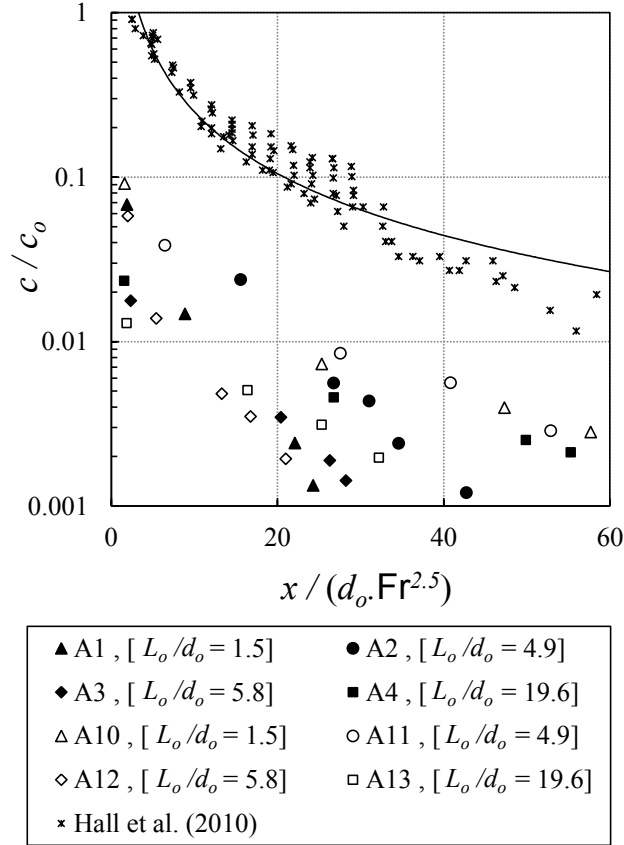


**Figure 3.10:** Concentration comparison for sand jets and particle clouds. a) Particle clouds for small and large particle sizes ( $D_{50}=0.196$  and  $0.507$  mm) b) The line is correspond to sand jets (Hall et al., 2010)

In order to investigate the effects of particle size on the shape of particle cloud, deviations of particle clouds from a spherical shape were studied. Volume of particle clouds  $V$  was normalized with the maximum width of the particle cloud  $V/b^3$  at each time. Variations of the normalized volume  $V/b^3$  with the normalized time  $t/T$  for different particle size ranges are shown in Fig. 3.11. The line corresponding to a sphere and a hemisphere (i.e.,  $\pi/6$  and  $\pi/12$ ) are added in Fig. 3.11. Fig. 3.11a shows the shape variations of particle cloud for small particle sizes ( $D_{50}=0.196$  mm). Spherical particle cloud with a tail can be observed if  $V > \pi b^3/6$ . As it can be seen from Fig. 3.11a, particle cloud has a trailing part for  $t/T < 5$ . The frontal head loses the tailing section and form a hemisphere for  $t/T \geq 10$  for all  $L_o/d_o$  ratios. For medium and large

particle sizes (i.e.,  $D_{50}=0.389$  mm and  $0.507$  mm), variations of the normalized volume with  $t/T$  shows a plateau occurred at  $t/T=7$  and  $4$ , respectively.

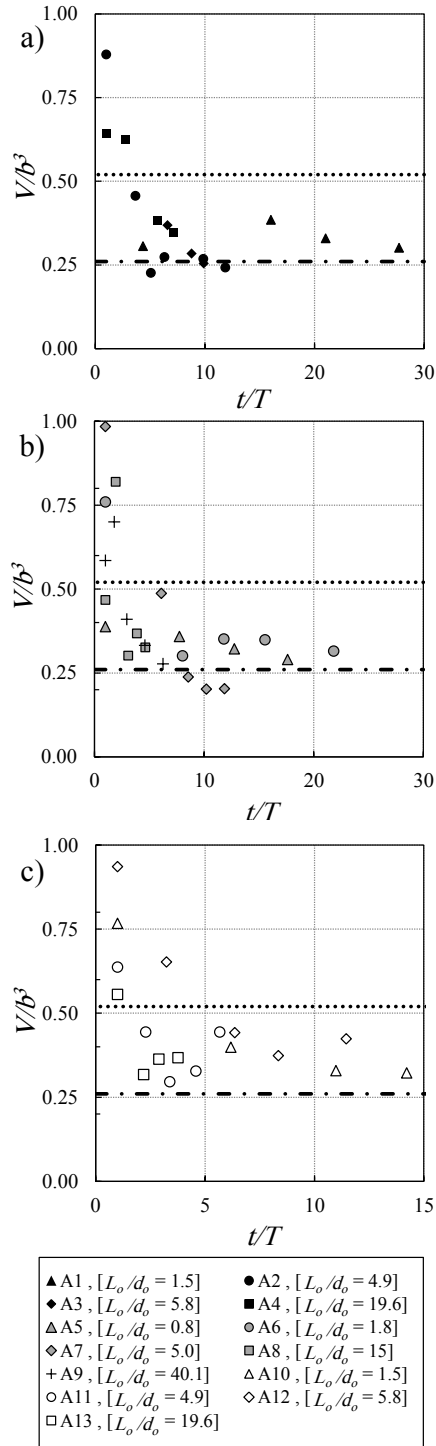


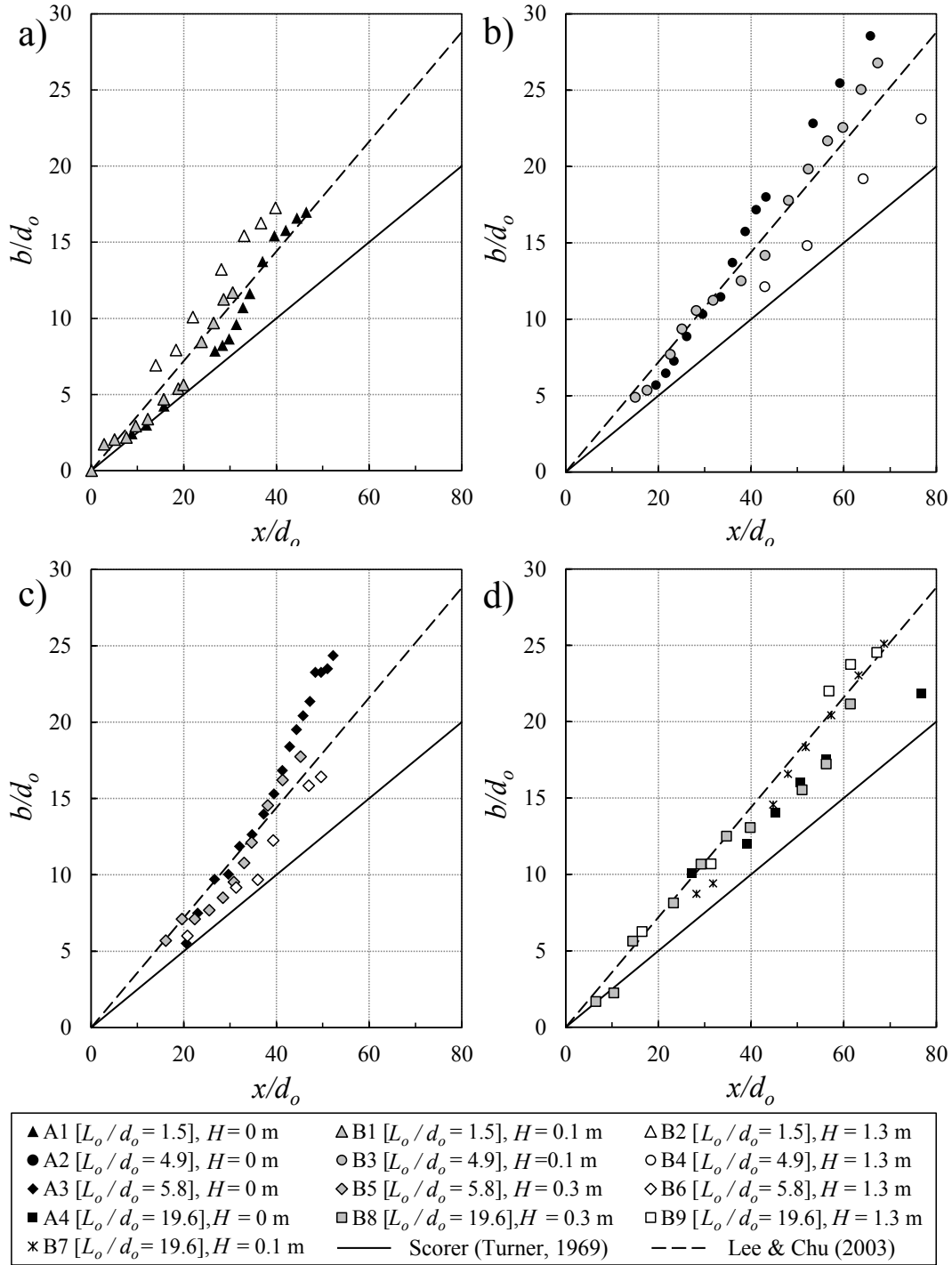
**Figure 3.11:** Variation of normalized volume  $V/b^3$  with normalized time  $t^*$ . a)  $D_{50}=0.196$  mm, b)  $D_{50}=0.389$  mm, c)  $D_{50}=0.507$  mm.

#### 3.4.4 Effect of impact velocity:

To consider the effect of impact velocity on the dynamics of sand jets and particle clouds, different heights of  $H=0.1, 0.2, 0.3, 0.75$  and  $1.3\text{m}$  were tested for three particle sizes ranges of small, medium and large particles (i.e.,  $D_{50}=0.196, 0.389$  and  $0.507\text{mm}$ ). Cai et al. (2010) consider the effect of released height on sand jets in air and found that the diameter of sand jets decreased with  $H$  and approached an asymptotic value at  $120d_o$ . Moreover, due to gravity force, sand jet frontal velocity accelerates with negligible air resistance. Our observations with the range of release heights indicate that  $H$  doesn't have significant impact on frontal velocity of particle cloud in water. Increasing the impact velocity causes instability at the water surface and enhances air entrainment in water (Qu et al., 2013). Instability of water surface consumes the excess momentum gained by the release height. Therefore, velocity of particles in the particle cloud suddenly changes once they hit the water surface. Moreover, the entrained air in water moves upward and decreases the velocity of the particle cloud. The combination of these two factors cancels the effect of release height on frontal velocity of particle cloud.

Fig. 3.12 shows the effect of impact velocity on the width of particle cloud  $b$  for small particle sizes ( $D_{50}=0.196\text{ mm}$ ) with different  $L_o/d_o$  ratios ranging from 1.5 to 19.6. Results were compared with predictions of a single-phase water jets in water (i.e., solid line) and a single-phase buoyant plume (i.e., dashed line). As can be seen from Fig. 3.12a, for  $L_o/d_o=1.5$ , the normalized width for all heights tested follow the prediction of single-phase buoyant plume and as the  $L_o/d_o$  increases (Fig. 3.12b, 12c and 12d), variations of the normalized width can be described by single-phase water jet model. However, for all  $L_o/d_o$  ratios with different initial velocities, the width of particle cloud is larger than the prediction of single-phase water jets in water. Fig. 3.12a demonstrates that particle clouds with higher impact velocity are wider and this effect became noticeable at  $x/d_o>20$ . For  $x/d_o=30$ , the normalized width of particle cloud for

$H=1.3\text{m}$  (Test No. B2) is almost 1.6 times of the same test releasing from zero height (Test No. A1). Spreading of particle clouds from higher  $H$  may be due to the effect of sand-air shear layer and deceleration of frontal cloud. For small  $L_o/d_o$ , effect of air-sand shear layer on spreading of sand particles becomes larger than the momentum gained by increasing the impact velocity (i.e., release height). As a result, for small  $L_o/d_o$ , when the release height increases, the cloud width increases as well.



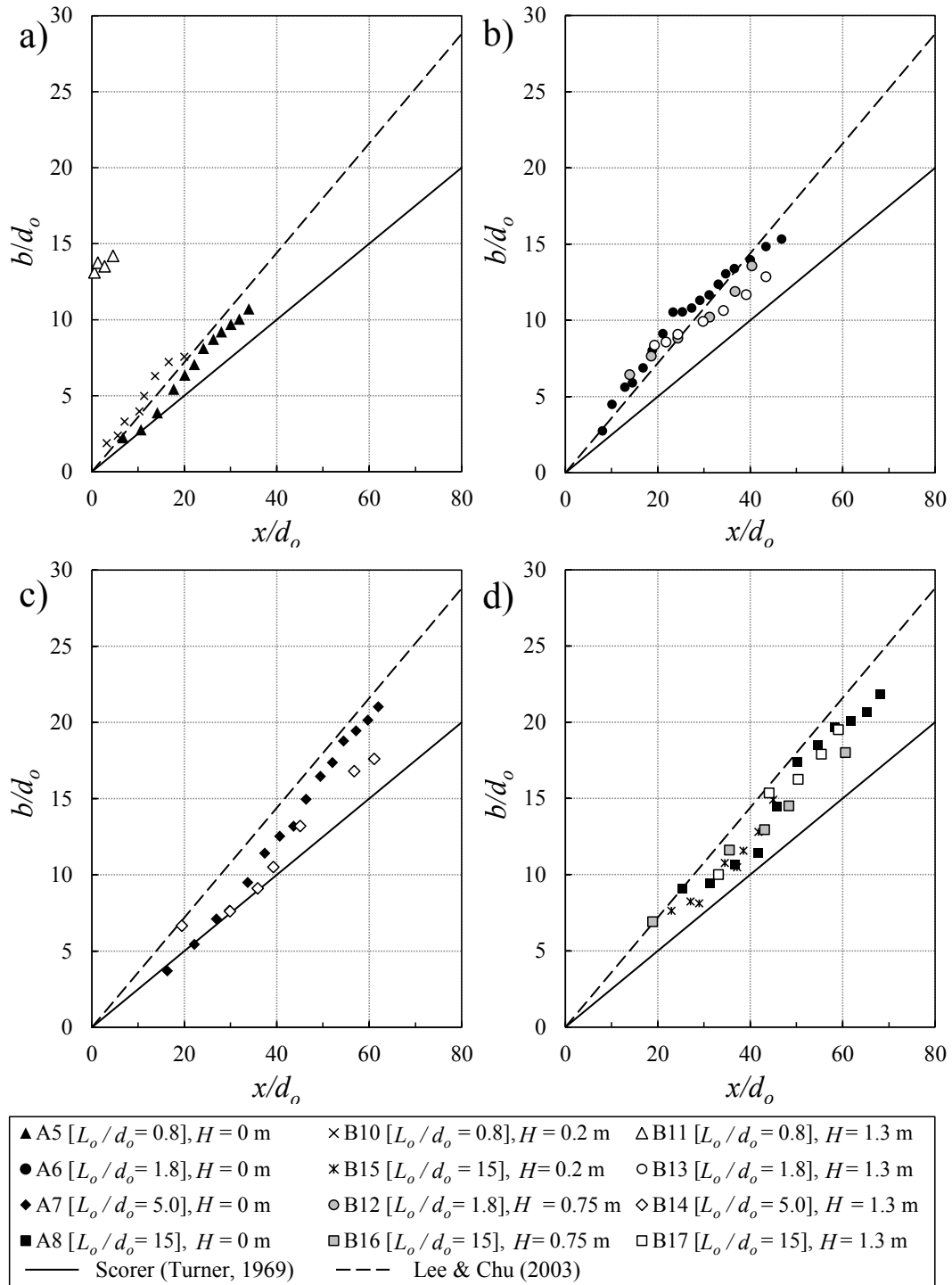
**Figure 3.12:** Effect of drop height on normalized width  $b/d_0$  along normalized depth  $x/d_0$  for small particle size,  $D_{50}=0.196$  mm. a)  $L_0/d_0 = 1.5$ , b)  $L_0/d_0 = 4.9$ , c)  $L_0/d_0 = 5.8$ , d)  $L_0/d_0 = 19.6$ .

Fig. 3.12b and 3.12c show the effects of  $H$  on  $b/d_0$  for small particle sizes and medium  $L_0/d_0$  (i.e.,  $L_0/d_0 = 4.9$  and  $5.8$ ). As it can be seen, release height has an adverse effect on cloud

width. Fig. 3.12b shows that for  $x/d_o=65$ , the normalized width of particle cloud with  $H=1.3$  m is 67% of the corresponding test for zero height. Similar results can be observed from Fig. 3.12c. For medium range of  $L_o/d_o$ , the momentum gained by higher impact velocity becomes larger than the air resistance. This causes particles to penetrate in water with a higher velocity and form particle clouds with smaller widths (see Fig. 3.14). Fig. 3.12d shows the effect of drop height on the spreading of particle clouds for small particle sizes and large  $L_o/d_o$  (i.e.,  $L_o/d_o=19.6$ ). As a result, for large  $L_o/d_o$  ratio,  $H$  doesn't have a significant effect on normalized width.

Effects of impact velocity on variations of cloud width with  $x/d_o$  for medium particle size of  $D_{50}=0.389$  mm is shown Fig. 3.13. Fig. 3.13a shows experimental results for small  $L_o/d_o$  ratios of 0.8. For small  $L_o/d_o$  (i.e.,  $L_o/d_o=0.8$ ), increasing the impact velocity forms wider particle clouds similar to small particle sizes (see Fig. 3.12a). This indicates that the sand-air shear layer overcomes the excess momentum due to higher impact velocity even for larger particle sizes. As it can be seen from Fig. 3.13a, at  $x/d_o=18$  the width of particle cloud releases from  $H=1.3$  m increases by 2.6 times of the same test with  $H=0$  m.

As  $L_o/d_o$  becomes larger, the excess momentum gain due to impact velocity overcomes the resistance from sand-air shear layer and causes narrower particle clouds. This imbalance clearly demonstrated in Figs. 3.13b and 3.13c. For  $L_o/d_o=1.8$  and  $x/d_o=35$ , as the release height increased from zero to 1.3 m, the normalized width decreased by 18%. For  $L_o/d_o=5$  (Fig. 3.13c) and at  $x/d_o=57$ , the width of particle cloud decreases by 14% due to the change in release height from zero to 1.3 m. No considerable changes were observed for  $L_o/d_o=15$ . Fig. 3.14 clearly shows the significant effect of the release height for small  $L_o/d_o$  ratios. Fig. 3.14b shows that the air resistance caused particles to spread in air before entering into the water whereas no particle spread in air occurred for similar test releasing at the surface (Fig. 3.14a).



**Figure 3.13:** Effect of drop height on normalized width  $b/d_o$  along normalized depth  $x/d_o$  for medium particle size,  $D_{50}=0.389$  mm. a)  $L_o/d_o=0.8$ , b)  $L_o/d_o=1.8$ , c)  $L_o/d_o=5.0$ , d)  $L_o/d_o=15$ .

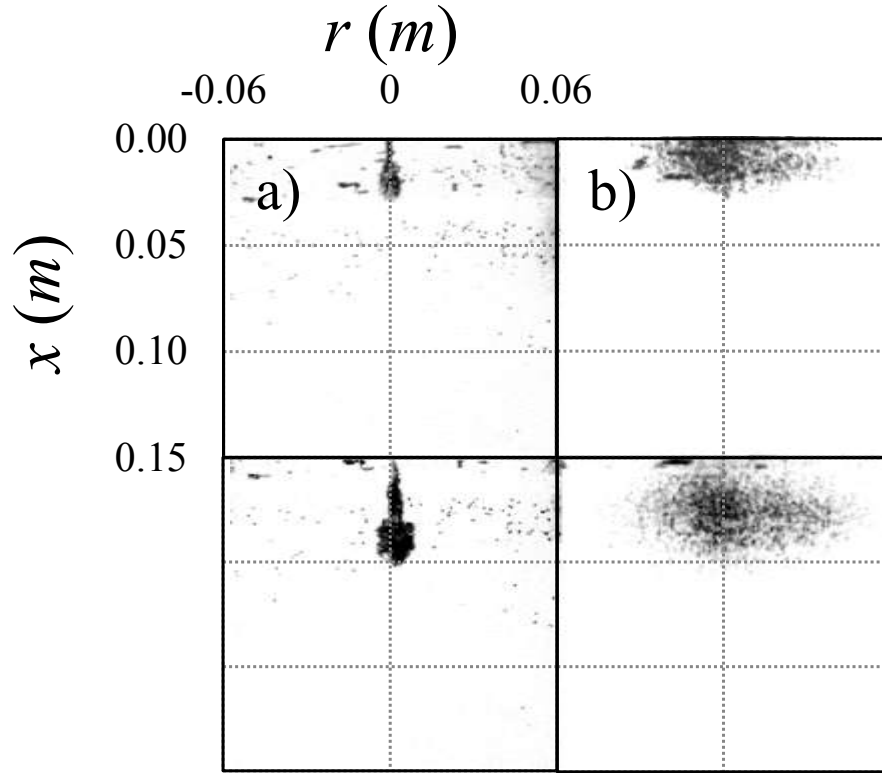


**Figure 3.14:** Effect of drop height at different  $x/d_o$  for particle size of  $D_{50}=0.389$  mm. a) Test No. A5,  $H=0$  m, b) Test No. B11,  $H=1.3$  m.

Effect of released height on variations of cloud width was studied for larger particle sizes with a mean particle size of  $D_{50}=0.507$  mm. Two  $L_o/d_o$  ratios of 4.9 and 19.6 were tested. Fig. 3.15a shows that the effect of impact velocity on variations of  $b/d_o$  with  $x/d_o$  for large particles was similar to small and medium particle sizes shown in Figs. 3.12b, 3.12c, 3.13b and 3.13c. Fig. 3.15b shows the effect of impact velocity on variations of the cloud width for  $L_o/d_o=19.6$ . It was found that the width of particle cloud decreases with increasing impact velocity. This can be due to the fact that larger particles (i.e.,  $D_{50}=0.507$  mm) has less tendency to be disturbed by sand-air shear layer and fall directly into the water and form particle cloud with smaller width. As can be seen in Fig. 3.15b, for  $x/d_o=65$ , the normalized width decreased by 20% for  $H=1.3$  m.

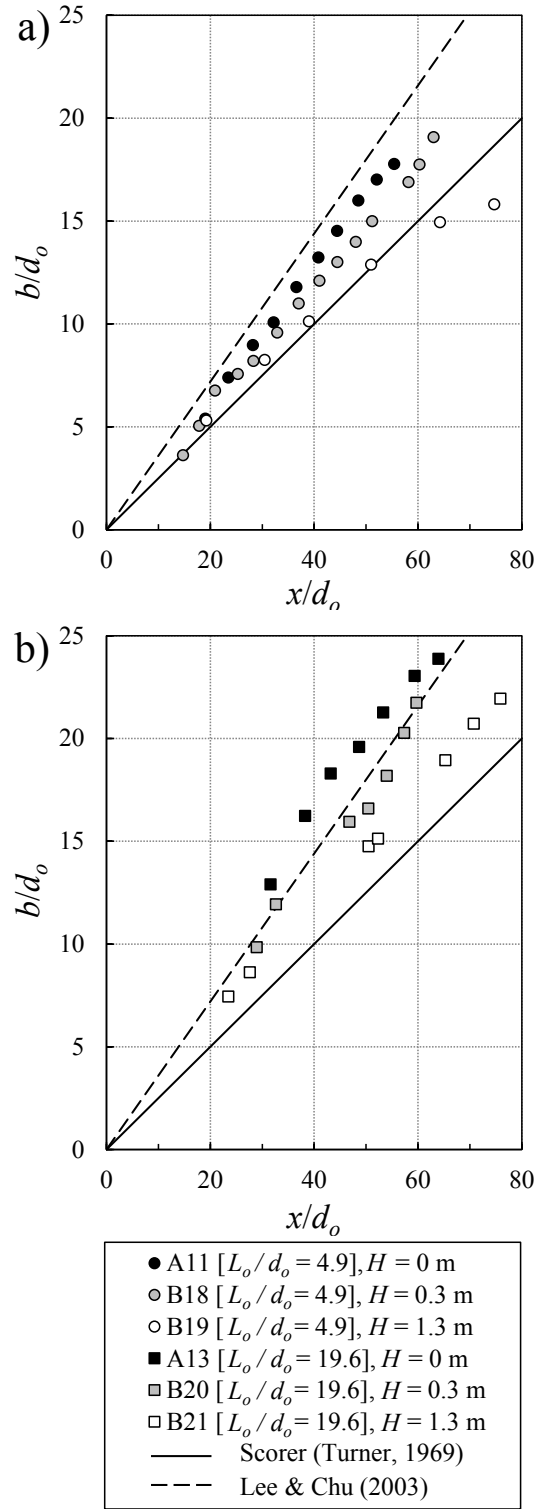


**Figure 3.15:** Effect of drop height on normalized width  $b/d_o$  along normalized depth  $x/d_o$  for large particle size,  $D_{50}=0.507$  mm. a)  $L_o/d_o = 4.9$  b)  $L_o/d_o = 19.6$ .

### 3.5 Summary and conclusion

Experiments were conducted to study the effect of  $L_o/d_o$  ratio, particle size and impact velocity on the dynamics of sand jets and particle clouds. Non-dimensional energy and circulation were modified using orifice equation to describe impact velocity of sand particles. It was found that both non-dimensional energy and circulation are a function of  $L_o/d_o$  indicating the importance of  $L_o/d_o$  on the dynamics of particles in water. Three phases of motion were considered for particle clouds evolution. For all  $L_o/d_o$  ratios in this study ( $0.8 \leq L_o/d_o \leq 19.6$ ), a power law equation was developed to correlate axial distance, cloud width and frontal velocity with time,  $D_{50}$  and  $L_o/d_o$ . It was found that particle clouds with higher  $L_o/d_o$ , spread faster than clouds with small  $L_o/d_o$ .

Different particle sizes ranged from 0.1375 mm to 0.718 mm were tested to investigate the effect of particle size on evolution of sand jets and particle clouds. It was observed that particle clouds with small particle sizes generate a longer tail in comparison with clouds made of large particles. Different shapes were observed for particle clouds with different particle sizes. A spherical shape was observed for clouds with small particle sizes. A bowl shape was formed for clouds with medium particle size ( $D_{50}=0.389$  mm) and an arc shape was formed for clouds with larger particles ( $D_{50}=0.595$  mm).

It was found that large particle sizes tend to act independently and also reach particle settling velocity in a short distance from the nozzle. While clouds made of small particle sizes, tend to mix with water and generate eddies which result in travelling a longer distance to reach the particle settling velocity. Wider clouds were generated with small particle sizes due to the tendency of small particles to follow eddies. Averaged concentration of particle clouds was calculated and results were converted to the peak concentration using top-hat hypothesis. It was observed that regardless of  $L_o/d_o$ , the peak concentration decreased in a very short distance close

to the nozzle indicating that particle clouds disperse 6 times faster than continuous sand jets. Volume of particle clouds was calculated and the results were normalized with the width of the cloud. The normalized volumes were compared with spherical and hemispherical shapes. The presence of a tail was observed for clouds with higher volume than a sphere. It was found that particle clouds with  $D_{50}=0.196$  mm have spherical shape for  $5 \leq t/T \leq 10$ .

Effects of initial sand velocity of the dynamics of particle clouds made of different particle sizes and different  $L_o/d_o$  were investigated by changing the drop height from zero to 1.3 m above the water surface. It was found that for small  $L_o/d_o$  ratios (i.e.,  $L_o/d_o \approx 1.5$ ), the air resistance cause the sand particles to disperse more and generate a wide cloud reaching the water surface. For  $L_o/d_o \approx 5$ , the momentum force produced by higher impact velocity became dominant. As a result, jets penetrate in water with a higher velocity and a smaller width. For  $L_o/d_o \approx 20$ , it was observed that the impact velocity has a negligible impact on the width of the cloud since width of the cloud was independent of the water surface instability consumes the excess momentum gained by the release height. Our observations with the range of release heights indicate that  $H$  doesn't have significant impact on frontal velocity of particle cloud in water.

### **3.6 Acknowledgement**

The work presented here was partially supported by the NSERC-Discovery grant No. 421785. We would like to thank undergraduate students (Jasdeep Dhillon, Mike Lee, Guillermo Martinez, and Benjamin Pomphrey) for their help to conduct part of laboratory experiments.

### 3.7 Notation

*The following symbols are used in this paper:*

$b$  = width of sand jet or particle cloud, m

$c_{ave}$  = averaged sand concentration, vol/vol

$c_m$  = peak sand concentration, vol/vol

$c_o$  = initial sand concentration, vol/vol

$d_o$  = nozzle size, mm

$D_{50}$  = mean particle size, mm

$E$  = Energy per unit density,  $\text{kg}\cdot\text{m}^2/\text{s}^2$

$F$  = Froude number

$F_B$  = buoyancy force, N

$g$  = acceleration due to gravity,  $\text{m}/\text{s}^2$

$g'$  = reduced gravity,  $\text{m}/\text{s}^2$

$m$  = sand mass, g

$H$  = release height, mm

$I$  = Impulse,  $\text{kg}\cdot\text{m}/\text{s}$

$L_o$  = length of sand occupied in a release tube, mm

$L_i$  = initial length of the jet when all particles are in the water, mm

$R_o$  = equivalent radius of parcel occupying a hemisphere in fluid, mm

$Re_p$  = particle Reynold's number

$t$  = time, s

$T$  = time at which sand has completely entered the water, s

$u_f$  = sand jet frontal velocity, m/s

$u_i$  = impact velocity at water surface, m/s

$u_o$  = initial velocity at the nozzle, m/s

$u_\infty$  = terminal settling velocity, m/s

$U_p$  = Piston velocity, m/s

$V$  = volume of Sand Jet,  $\text{mm}^3$

$V_o$  = initial volume of sand jet in tube,  $\text{mm}^3$

$x$  = distance from water surface to particle cloud front, mm

$\alpha$  = non-dimensional energy

$\gamma$  = non-dimensional circulation

$\mu$  = dynamic viscosity, kg/m.s

$\rho_p$  = density of sand particles, kg/m<sup>3</sup>

$\rho_w$  = density of sand particles, kg/m<sup>3</sup>

$\tau$  = characteristic time scale, s

$\Gamma$  = circulation, m<sup>2</sup>/s

## Chapter 4: Experimental Study of Oblique Particle Clouds in Water

### 4.1 Introduction

Solid-liquid flow has been widely used in many industries with engineering applications such as artificial island construction, marine bed capping, and waste disposal into lakes and rivers. In recent years, many studies have been done to investigate the behavior of two-phase flow (e.g. Azimi et al., 2011, 2012a, 2014, 2015; Bush et al., 2003; Cai et al., 2010; Hall et al., 2010; Jiang et al., 2005; Noh and Fernando, 1993; Qu et al., 2011, 2013; Rahimpour and Wilkinson, 1992). Single phase flows have been studied for several decades. Detailed information about single phase flow behavior can be found in several books (e.g., Fischer et al., 1979; Lee and Chu, 2003; Chin, 2012). Velocity, width, and buoyancy of plumes and thermals have been investigated by early studies of Turner (1969). The behavior of negatively buoyant round jet was studied by Pantzloff and Lueptow (1999), who reported three stages for the jet. First, the jet reached to its maximum height, then because of the downward backflow of the heavier fluid, the jet's penetration depth decreased and finally it fluctuated around 70% of the maximum penetration depth. Effect of initial geometry on buoyant thermal was studied by Bond and Johari (2005) using the non-dimensional parameter of aspect ratio  $L_o/d_o$  where  $L_o$  was the length of the container and  $d_o$  is the nozzle diameter. They divided the flow into two phases of initial acceleration phase for when the fluid continuously rises from the source and thermal like phase when the flow decelerate (Bond and Johari, 2005). For a starting buoyant plume, a pinch off was observed at the formation number between 4.4 to 4.9 where the formation number is equivalent to  $L/d_o$  ratio where  $L$  is the distance traveled by the piston, and  $d_o$  is cylinder diameter (Pottebaum and Gharib, 2004). Experimental studies have been performed to investigate the effect of drop angle on concentration profile of non-buoyant oblique jets released in moving

ambient (Wang and Kikkert, 2014). It was found that the concentration profile has two separate peaks for drop angle of  $90^\circ$  to  $50^\circ$ , while for drop angle of  $45^\circ$  to  $30^\circ$ , it has one peak and is not fitted with the single-Gaussian profile. For the drop angle less than  $30^\circ$ , the concentration profile was matched with the Gaussian profile. Limited attention was made to consider the effect of drop angle on the behavior of oblique particle cloud.

Particle clouds were classified into two regimes of thermal and swarm according to their normalized buoyancy  $F_B/\rho_w x^2 u_\infty^2$  where  $F_B = (\pi d_o^2/4)L_o c_o g(\rho_p - \rho_w)$  is the buoyancy force of the particle cloud,  $c_o$  is the initial sand concentration (i.e.,  $c_o=0.6$ ), and  $\rho_p$  and  $\rho_w$  are the densities of sand particles and water, respectively (Bush et al., 2003). Particle size  $D_{50}$  and nozzle diameter  $d_o$  were used as controlling parameters to consider the behavior of sand jets in water (Azimi et al., 2012a). For small particles, it was found that the jet front settling velocity is five times of the individual settling velocity. Moreover, the growth rate and width of the sand jets were reported to be smaller than the single-phase buoyant jets since the extra momentum generated by the particles. For the concentration and velocity profile of sand and slurry jets, a Gaussian profile was fitted to the experimental data. The centerline sand concentration decayed using a  $-5/3$  power relation for sand jets and slurry jets which is similar to single phase plume behavior. Experimental effect of drop height on the dynamics of two-phase gas-liquid jets was investigated by Qu et al. (2011). Experiments were performed at different volumetric flow rates with the initial water velocity at the nozzle  $v_o$  in the range of 1m/s to 3.5m/s. Water jet velocity at the liquid surface  $v_j$ , was calculated using free fall of water after leaving the nozzle using  $v_j = (v_o^2 + 2gH)$  where  $H$  is the drop height from the nozzle tips to the water surface. They found that increasing the  $v_j$  for a given nozzle size causes instabilities in the jet-interface and leads to an increase in air bubbles beneath the water surface and also a reduction in penetration depth which

is the lowest point of the plume. In previous chapter, it was observed that the behavior of particle clouds can be controlled by critical parameters such as mass  $m$ , nozzle diameter  $d_o$ , release height  $H$ , initial particle concentration  $c_o$ , and particle size  $D_{50}$ . The non-dimensional parameter of aspect ratio  $L_o/d_o$  was formed to consider the effect of nozzle diameter  $d_o$  and sand mass where  $L_o$  is the length of sand particles occupied in the pipe. It was also observed that increasing the aspect ratio, increases the circulation and results in a wider cloud. To the author's knowledge, the effect of drop angle on the behavior of the particle cloud was not considered in the literature.

In single phase flow, the entrainment velocity was assumed to be proportional to the centerline velocity via a coefficient called entrainment coefficient,  $\alpha_e$  (Morton et al., 1956). In plumes, momentum is transferred to the surrounding environment and causes an increase in diameter and entrainment and also a decrease in velocity. In plumes, the buoyant force helps to keep the motion while transferring the momentum (Moreira and Vilhena, 2009).

In single-phase flow, the width of jet grows linearly with distance from the nozzle, and the entrainment coefficient is constant along the jet axis (Fischer et al., 1979; Azimi et al., 2012b). Various experimental studies showed that the entrainment coefficient of single phase plumes is almost 50 percent larger than jets (Fischer et al., 1979; Papanicolaou & List, 1988). For thermal, since it has a higher rate of dilution, entrainment coefficient would also be larger compared to plumes (Turner, 1969).

In slurry jets, it was observed that the entrainment coefficient of slurry jets is smaller compared to single-phase water jets, because the velocity of slurry jets decays with a lower rate (Azimi et al., 2012b). Moreover, the width of slurry jets decreases with increasing the particle concentration which results in a decrease in the entrainment coefficient (Azimi et al., 2012b). In

this chapter, a relationship will be proposed for estimating the entrainment coefficient of particle cloud.

Relatively limited investigations have been devoted to study the behavior of oblique particle clouds in the water. The present research work is aimed mainly to explore the behavior of oblique particle cloud in water. Moreover, an attempt is made to correlate the entrainment coefficient and drag coefficient of particle clouds with controlling parameters such as aspect ratio and particle size.

This chapter is organized into 5 sections. Section 4.2 presents the dimensional analysis to find controlling parameters in oblique particle clouds. The experimental setup is described in section 4.3. In section 4.4, experimental results are discussed including the effects of aspect ratio, sand particle size, drop angle and height on oblique particle clouds, and also entrainment coefficient and drag coefficient of particle clouds. Summary and conclusion of the present study are presented in section 4.5.

## 4.2 Theory and Background

Parameters that may control the motion of oblique particle clouds are identified as

$$u_f = f_1(x, y, \alpha, H, d_o, c_o, m, D_{50}, \mu, g, \rho_s, \rho_w) \quad (4.1)$$

where  $x$  and  $y$  are the horizontal and vertical distance of cloud from nozzle respectively,  $\alpha$  is the initial drop angle,  $H$  is the release height,  $d_o$  is the nozzle diameter,  $c_o$  is the initial sand concentration in the pipe (i.e. 0.6),  $m$  is the mass of particles,  $D_{50}$  particle size,  $\mu$  dynamic viscosity of the ambient fluid,  $\rho_p$  and  $\rho_w$  are the densities of sand particles and water. In chapter 3, the effect of mass and particle size was expressed using aspect ratio  $L_o/d_o$  as a non-dimensional parameter where  $L_o$  is the length of sand particles occupied in the pipe. Effect of particle inertia over the ambient viscosity can be considered using particle Reynolds number,

$Re_p = \rho_w u_\infty D_{50} / \mu$ , where  $u_\infty$  is the particle settling velocity (Azimi et al., 2012a). Using Haywood tables, particle settling velocity can be predicted (Holdich, 2002). By considering a constant value for particle density and water density, equation (1) can be rewritten in non-dimensional form as

$$\frac{u_f}{u_\infty} = f_2 \left( \frac{x}{d_o}, \frac{y}{d_o}, \frac{L_o}{d_o}, \alpha, Re_p \right) \quad (4.2)$$

From chapter 3, depth, width, and velocity of particle cloud can be found using the following equations respectively.

$$\frac{y}{d_o} = \varepsilon \left( \frac{t}{T} \left( \frac{L_o}{d_o} \right)^\varphi \right)^\gamma \quad (4.3)$$

$$\frac{b}{d_o} = \theta \left( \frac{t}{T} \left( \frac{L_o}{d_o} \right)^\beta \right)^\delta \quad (4.4)$$

$$\frac{u_f}{u_\infty} = \eta \left( \frac{y}{d_o} \left( \frac{L_o}{d_o} \right)^\kappa \right)^\lambda \quad (4.5)$$

Where  $T$  is the initial phase time,  $\varepsilon$ ,  $\varphi$ ,  $\gamma$ ,  $\theta$ ,  $\beta$ ,  $\delta$ ,  $\eta$ ,  $\kappa$  and  $\lambda$  are the constants of the equations which reflect the effect of particle size and can be found in Table 3.1.

Turner (1969) assumed a spherical shape for estimating the volume of thermal. In particle clouds, this assumption doesn't seem to be precise as the cloud shape depends mostly on the travel time. Therefore, for a time greater than initial time, a function was developed to correlate the real shape of the particle cloud to the equivalent sphere shape with diameter  $b$ .

$$\psi(t) = 1.25 \left( \frac{t}{T} \right)^{-0.3} \quad (4.6)$$

Using this equation results in a coefficient larger than unit for initial time  $T$ , which means for  $t=T$ , the volume of cloud is larger than the equivalent sphere with diameter of  $b$  (Fig. 4.1.a).

As the cloud travels along the tank, this coefficient gradually becomes less than unit. Using Eq. (4-6), the volume of the vertical particle cloud can be estimated using the following equation:

$$V = \psi(t) \frac{\pi}{6} b^3 = 1.25 \left( \frac{t}{T} \right)^{-0.3} \left( \frac{\pi}{6} b^3 \right) \quad (4.7)$$

Substituting Eq. (4-4) into Eq. (4-7) results in the volume of the cloud as a function of time  $t$  and  $L_o/d_o$  ratio.

$$V = \left( 1.25 \left( \frac{t}{T} \right)^{-0.3} \left( \frac{\pi}{6} \theta^3 d_o^3 \left( \frac{t}{T} \left( \frac{L_o}{d_o} \right)^\beta \right)^{3\delta} \right) \right) \quad (4.8)$$

Taking the derivative of Eq. (4-8), the rate of the change of volume with respect to time can be found using the following equation.

$$\frac{dV}{dt} = \frac{1.25\pi\theta^3 d_o^3 (3\delta - 0.3)}{6T} \left( \frac{L_o}{d_o} \right)^{3\delta\beta} \left( \frac{t}{T} \right)^{3\delta-1.3} \quad (4.9)$$

In particle clouds, the rate of the change of volume with respect to time is equal to the amount of water that is added to the cloud by time ( $\Delta Q_e$ ).

$$\frac{dV}{dt} = \Delta Q_e = u_e A_s \quad (4.10)$$

where  $u_e$  is the water velocity entering the cloud and  $A_s$  is the surface area of the cloud.

The average entrained velocity of water  $u_e$  was assumed to be a linear function of frontal velocity,  $u_e = \alpha_e u_f$  where  $\alpha_e$  is the entrainment coefficient (Batchelor, 1954).

Turner (1969) assumed a spherical shape for calculating the surface area  $A_s$  in thermals. A function of time was estimated to correlate the surface area of the particle cloud to the equivalent sphere shape with diameter  $b$  and is valid for thermal and swarm phase ( $t/T > 1$ ).

$$\Omega(t) = 1.5 \left( \frac{t}{T} \right)^{-0.2} \quad (4.11)$$

Thus, the entrance surface area of the particle cloud can be calculated using the following equation.

$$A_s = \Omega(t)(\pi b^2) = 1.5 \left( \frac{t}{T} \right)^{-0.2} (\pi b^2) \quad (4.12)$$

Using Eq. (4-12), Eq. (4-10) can be rewritten as

$$\frac{dV}{dt} = (\alpha_e u_f) \left( 1.5 \left( \frac{t}{T} \right)^{-0.2} \pi b^2 \right) \quad (4.13)$$

Using Eq. (4-4), (4-5), (4-9) and (4-13),  $\alpha_e$  can be estimated by the following equation:

$$\alpha_e = \frac{1.25 \varepsilon^{-\lambda} \theta d_o (3\delta - 0.3)}{9T\eta u_\infty} \left( \frac{L_o}{d_o} \right)^{\delta\beta - \kappa\lambda - \lambda\gamma\varphi} \left( \frac{t}{T} \right)^{\delta - 1.1 - \lambda\gamma} \quad (4.14)$$

From Eq. (4-14), the entrainment coefficient is a function of the following parameters.

$$\alpha_e = f(d_o, D_{50}, \frac{L_o}{d_o}, \frac{t}{T}, T, u_\infty) \quad (4.15)$$

The average drag force  $\overline{F_D}$  acts in the surrounding fluid in particle clouds can be estimated by balancing the net force and momentum flux using Newton's second law.

$$F_B - \overline{F_D} = \frac{d(mu_f)}{dt} = \frac{d(\rho_s V_o u_f)}{dt} = \rho_s V_o \frac{du_f}{dt} \quad (4.16)$$

where  $V_o$  is the initial volume of sand particles in the pipe. The buoyancy force is known for each set of experiments and remains constant during the experiment.

$$F_B = \left( \frac{\pi d_o^2}{4} \right) L_o c_o g' \quad (4.17)$$

where  $g' = g\Delta\rho$  is the reduced gravity. Using Eq. (4-3) and (4-5), frontal velocity of particle clouds can be written as a function of time  $t$ .

$$u_f = u_\infty \eta \varepsilon^\lambda \left( \frac{t}{T} \right)^{\lambda\gamma} \left( \frac{L_o}{d_o} \right)^{\lambda(\kappa + \varphi\gamma)} \quad (4.18)$$

By taking the derivative of Eq. (4-18), the rate of change of frontal velocity with respect to time can be found using the following equation.

$$\frac{du_f}{dt} = \frac{\lambda\gamma u_\infty \eta \varepsilon^\lambda}{T} \left(\frac{t}{T}\right)^{\lambda\gamma-1} \left(\frac{L_o}{d_o}\right)^{\lambda(\kappa+\phi\gamma)} \quad (4.19)$$

Substituting Eq. (4-17) and (4-19) into Eq. (4-16), the average drag force can be obtained using the following equation.

$$\overline{F_D} = F_B - \rho_s V \frac{du_f}{dt} = \left(\frac{\pi d_o^2}{4}\right) L_o c_o g' - \rho_s V \frac{\lambda\gamma u_\infty \eta \varepsilon^\lambda}{T} \left(\frac{t}{T}\right)^{\lambda\gamma-1} \left(\frac{L_o}{d_o}\right)^{\lambda(\kappa+\phi\gamma)} \quad (4.20)$$

For computing the drag force of each individual particle in the cloud  $F_D$ , the average drag force can be divided by the number of particles in the cloud,  $N = V_o / (\pi/6 D_{50}^3)$ .

$$F_D = \frac{\overline{F_D}}{N} \quad (4.21)$$

If we assume all particles travel with frontal velocity  $u_f$ , drag force of each individual particle can be calculated using the following equation.

$$F_D = \frac{1}{2} \rho_w u_f^2 c_d A_p \quad (4.22)$$

Where  $A_p = \pi D_{50}^2 / 4$  is the projected frontal area of each particle. Using Eq. (4-5), (4-20), (4-21) and (4-22), the drag coefficient  $c_d$  of each particle in the cloud, can be calculated using the following equation.

$$c_d = \frac{2\overline{F_D}}{N \rho_w u_f^2 A_p} \quad (4.23)$$

### 4.3 Experimental Setup

Laboratory experiments were conducted to investigate the behavior of oblique particle cloud, by releasing sand particles into a rectangular glass tank with length, width and height of 1.65 m, 0.85 m, and 0.85 m respectively. The tank was filled with tap water at ambient temperature (i.e.,  $\approx 20^\circ\text{C}$ ). The oblique pipe was placed close to the water surface (i.e., 5 mm) to eliminate bubble formation and minimize the air entrainment. To accurately measure the displacement and width of the cloud and reduce the image distortion, horizontal and vertical

rulers were placed inside the tank. For considering the behavior of oblique particle clouds, a total of 30 experiments were conducted. For the effect of aspect ratio, a relatively wide  $L_o/d_o$  ratio ranging from 1.2 to 15 was chosen. The wide range of  $L_o/d_o$  ratio was formed by a nozzle with the diameter of  $d_o=15\text{mm}$  and five sand masses of  $m=5, 16.2, 30.4, 44.5$  and  $60.7$  grams. The effect of drop angle  $\alpha$  and release height  $H$  on the behavior of oblique particle clouds was studied using different initial oblique angle ranging from  $15^\circ$  to  $60^\circ$  and three different heights  $H$ , of  $0.25, 0.6$  and  $1$  m were used. The experimental runs details is given in Table 4.1.

A high-speed camera (Prosilica GT 1910c CCD) was utilized at a perpendicular distance of  $1.4$  m from the tank, and pictures were taken at a frame rate of  $20$  frames per second. A schematic of the experimental setup is shown in Fig. 4.1. The quality of images was enhanced using two light sources that were placed on either side of the camera facing inward into the tank. To improve differentiation of the cloud from the background of the tank, the color of images was inverted and changed to black and white. Sand particles with a density of  $2540 \text{ kg/m}^3$  were sieved using a sieve shaker with sieve numbers ranging from [#30–#80] (ASTM), with median grain sizes of  $D_{50}$  of  $0.196, 0.275, 0.3895, \text{ and } 0.507$  mm. The particles were divided into three classes based on their size,  $0.196$  mm represents small particles class,  $0.275\text{mm}$  and  $0.3895\text{mm}$  represent medium particle class, and  $0.507$  mm represents large particle class (Azimi et al., 2012b).

**Table 4.1:** Experimental details of oblique particle clouds in water.

Test No.	$D_{50}$ (mm)	$d_o$ (mm)	$m$ (g)	$\alpha$ (°)	$L_o/d_o$	$u_\infty$ (m/s)	$Re_p$	$H$ (m)
A1	0.389	15	5.0	60	1.2	0.055	21.3	0.25
A2	0.389	15	16.2	60	4.0	0.055	21.3	0.25
A3	0.389	15	30.4	60	7.5	0.055	21.3	0.25
A4	0.389	15	44.5	60	11.0	0.055	21.3	0.25
A5	0.389	15	60.7	60	15.0	0.055	21.3	0.25
A6	0.507	15	5.0	60	1.2	0.075	37.6	0.25
A7	0.507	15	16.2	60	4.0	0.075	37.6	0.25
A8	0.507	15	30.4	60	7.5	0.075	37.6	0.25
A9	0.507	15	44.5	60	11.0	0.075	37.6	0.25
A10	0.507	15	60.7	60	15.0	0.075	37.6	0.25
A11	0.507	15	16.2	45	4.0	0.075	37.6	0.25
A12	0.3895	15	16.2	45	4.0	0.055	21.3	0.25
A13	0.275	15	16.2	45	4.0	0.035	9.7	0.25
A14	0.196	15	16.2	45	4.0	0.020	4.4	0.25
A15	0.507	15	30.4	45	7.5	0.075	37.6	0.25
A16	0.389	15	5.0	15	1.2	0.055	21.3	0.25
A17	0.389	15	5.0	45	1.2	0.055	21.3	0.25
A18	0.389	15	16.2	15	4.0	0.055	21.3	0.25
A19	0.389	15	16.2	30	4.0	0.055	21.3	0.25
A20	0.196	15	16.2	15	4.0	0.020	4.4	0.25
A21	0.196	15	16.2	30	4.0	0.020	4.4	0.25
A22	0.196	15	16.2	60	4.0	0.020	4.4	0.25
A23	0.389	15	5.0	60	1.2	0.055	21.3	0.6
A24	0.389	15	30.4	60	7.5	0.055	21.3	0.6
A25	0.389	15	44.5	60	11.0	0.055	21.3	0.6
A26	0.389	15	60.7	60	15.0	0.055	21.3	0.6
A27	0.389	15	5.0	60	1.2	0.055	21.3	1
A28	0.389	15	30.4	60	7.5	0.055	21.3	1
A29	0.389	15	44.5	60	11.0	0.055	21.3	1
A30	0.389	15	60.7	60	15.0	0.055	21.3	1

One of the experiments was repeated six times to verify the uncertainty of the experimental data (i.e., Test No. A2,  $L_o/d_o=4$ ,  $D_{50}=0.389$  mm,  $\alpha=60^\circ$ ). Variation of frontal position of the particle cloud in the horizontal direction  $x$ , and vertical direction  $y$ , and frontal velocity in vertical direction  $u_y$ , at different time, were measured. For the initial phase, the maximum uncertainties of measurements for the oblique cloud were  $\pm 6.5\%$ ,  $\pm 9\%$  and  $\pm 8\%$  for  $y$ ,  $x$ , and  $u_y$ , respectively. For thermal phase, the maximum observed uncertainties were  $\pm 3\%$ ,  $\pm 9\%$  and  $\pm 7\%$  for  $y$ ,  $x$ , and  $u_y$ , respectively.

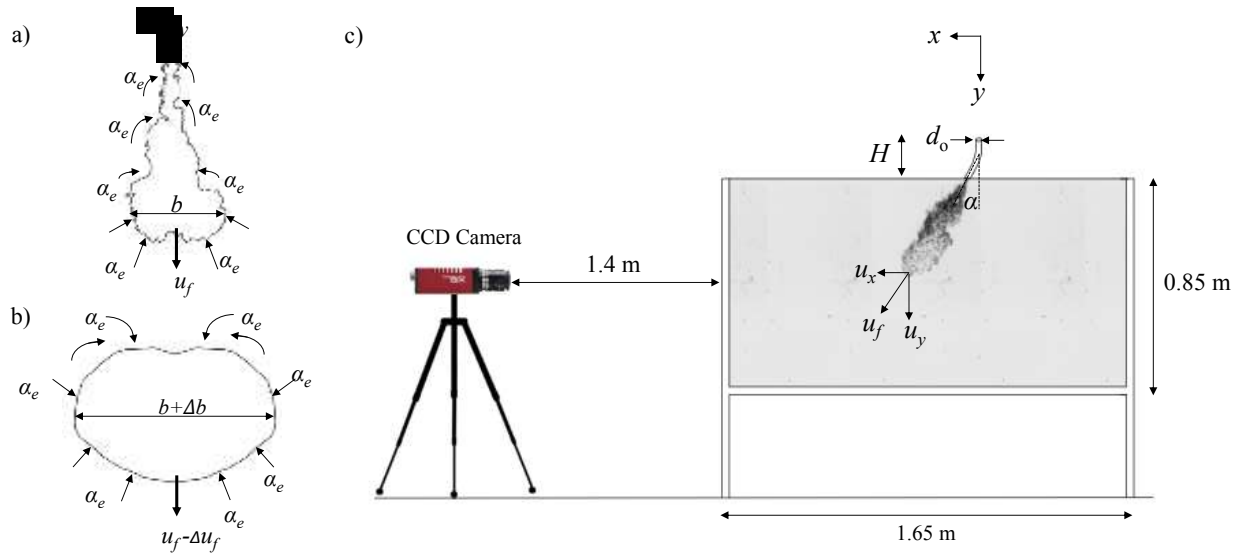


**Figure 4.1:** Schematic of entrainment in vertical particle clouds and experimental setup a) Entrainment in initial phase b) Entrainment in thermal phase c) Schematic of the experimental setup.

## 4.4 Experimental Results

### 4.4.1 General Evolution of Oblique Sand Jet Front

For considering the evolution of oblique particle cloud, three phases of motion includes initial, thermal and swarm phase observed during the experiments. The initial phase starts from the release time and continues until all the particles enter the water. In thermal phase, sand particles tend to follow the eddies generated by the turbulence which results in a considerable growth in the width during the thermal phase. In this phase of motion, the cloud's velocity

decreases until it reaches to the particle settling velocity which is the beginning of the swarm phase. In the swarm phase, all the particles settle with their settling velocity and the cloud's width still grows but with a low rate (Rahimipour and Wilkinson, 1992). The swarm phase is observed for experiments A1, A6, A23 and A27. For the rest of the tests, the tank's depth was not deep enough to record the data for the transition from the thermal to the swarm phase.

Fig. 4.2 shows the evolution of oblique particle clouds of medium size (i.e.,  $D_{50}=0.389$  mm) for two aspect ratios of 4 and 11 respectively (i.e. Fig. 4.2a and 4.2b). A non-dimensional time is proposed as the ratio of the actual time,  $t$  and the initial phase time,  $T$  (i.e.,  $t/T$ ). In both cases, the nozzle diameter  $d_o$  was constant; therefore, the aspect ratio was controlled by the different masses of particles released. As can be seen by comparing Fig. 4.2a and 4.2b, it can be seen that the shape of the particle cloud is influenced by the aspect ratio where a medium aspect ratio of four forms a spherical cloud at normalized time of 4 with a small tail (Fig. 4.2a), while a large aspect ratio of 11 forms a hemisphere with a large tail (Fig. 4.2b) at the same normalized time. Larger aspect ratios generate a greater momentum which leads the particle to move through the water at a higher speed. As can be seen from Fig. 4.2a, for medium aspect ratio (i.e.,  $L_o/d_o=4$ ), the travel distance of the cloud at  $t/T=4$  ( $x=0.34$  m) was significantly shorter than the travel distance of the larger aspect ratio ( $x=0.60$  m) from Fig. 4.2b at the same normalized time.

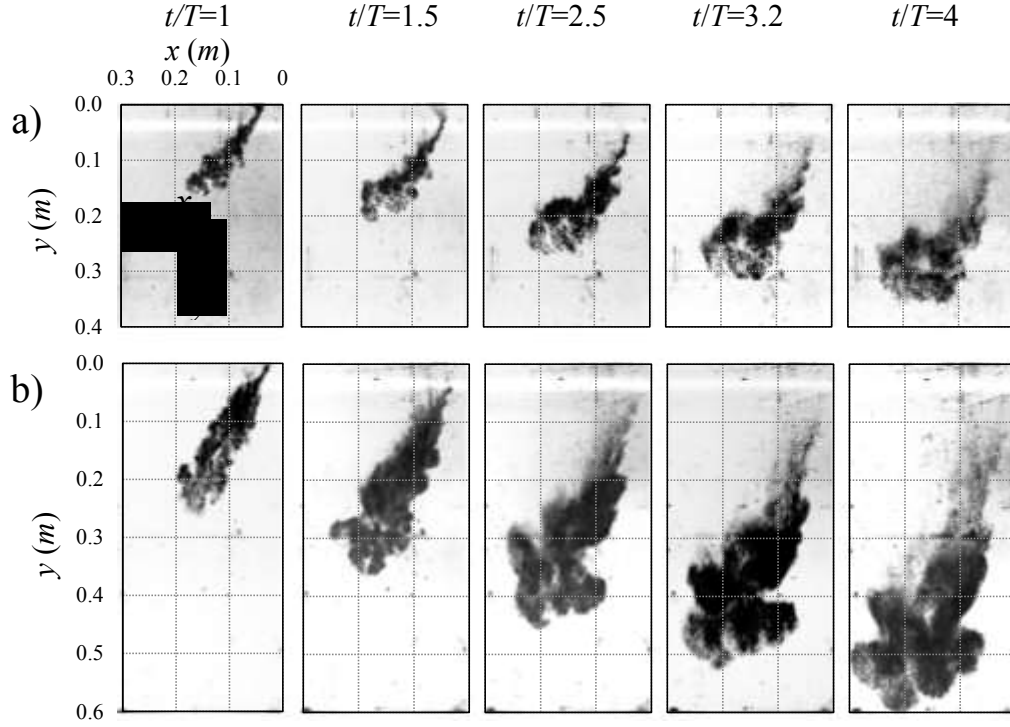


**Figure 4.2:** Evolution of particle cloud with oblique angle of  $60^\circ$  for particle size of 0.389 mm at different normalized time  $t/T$  considering the effect of aspect ratio. a) Test No. A2,  $L_o/d_o = 4$ , b) Test No. A4,  $L_o/d_o = 11$

Fig. 4.3 shows the effect of aspect ratio on the vertical velocity of oblique particle clouds. Variations of normalized vertical velocity  $u_y/u_\infty$  along normalized depth  $y/d_o$  for medium and large particle sizes (i.e.  $D_{50}=0.389$  mm and 0.507 mm) with a different aspect ratio of 1.2, 4, 7.5, 11 and 15 is shown in Fig. 4.3a and 3b respectively. From Fig. 4.3a, it can be observed that larger is the aspect ratio, the faster is the particle cloud travel in the vertical direction. For example, for  $y/d_o=20$ , it can be seen that the normalized vertical velocity for  $L_o/d_o=15$ , is almost four times of the  $u_y/u_\infty$  for  $L_o/d_o=1.2$ . The same result was also observed from Fig. 4.3b for large particle sizes (i.e.  $D_{50}= 0.507$  mm). As the cloud travels further in the tank,  $u_y/u_\infty$  decreases until the cloud moves from thermal phase to the swarm phase. From Fig. 4.3a, it can be observed that frontal vertical velocity of  $L_o/d_o = 1.2$ , reaches the swarm phase (i.e.,  $u_y=u_\infty$ ) at  $y/d_o \approx 28$ , whereas, for large aspect ratios (i.e.,  $L_o/d_o=11$  and 15), the cloud reaches swarm phase far from

the nozzle at  $y/d_o \gg 40$ . Therefore, for large aspect ratios ( $L_o/d_o > 11$ ), the cloud stays longer in thermal region. The same trend was also observed from Fig. 4.3b for large particle sizes.

For the maximum horizontal displacement of oblique particle cloud, it was observed that regardless of the aspect ratio and particle size, the cloud approaches its maximum horizontal displacement at approximately  $t/T=3$  for both the medium and large particle sizes. After this particular normalized time, the clouds only settle in the vertical direction. Fig. 4.4 considers the effect of aspect ratio on the trajectory of the oblique particle clouds with an initial angle of  $60^\circ$ . Variation of normalized horizontal displacement  $x/d_o$ , along normalized depth  $y/d_o$ , for medium and large particle sizes (i.e.  $D_{50}=0.389$  mm and 0.507 mm) are plotted in Fig. 4.4a and Fig. 4.4b respectively. From Fig 4a and 4b, for small aspect ratio (i.e.  $L_o/d_o=1.2$ ), less horizontal displacement was found compared to large aspect ratios. In other words, as  $L_o/d_o$  ratio increases, the maximum horizontal displacement will also increase. For example, the maximum horizontal displacement  $x_{max}/d_o$  for the aspect ratio of 4.0 is 1.20 times of aspect ratio of 1.2 for medium particles size (See Fig. 4.4a) and 1.7 times for large particle sizes (See Fig. 4.4b). The prediction line for the trajectory of large aspect ratio (i.e.  $L_o/d_o=11$ ) for test A4 and A9 was added to the Fig. 4.4b. As can be seen, the maximum horizontal displacement for the aspect ratio of 7.5 and 11 was not observed during the experiments due to the limited depth of the tank.

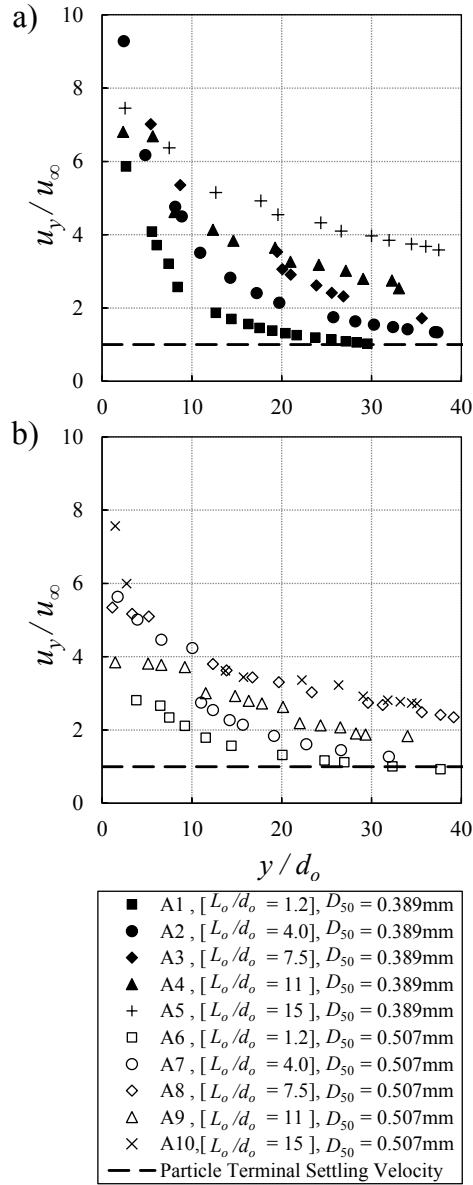


**Figure 4.3:** Effect of aspect ratio on normalized vertical velocity  $u_y/u_\infty$  of oblique particle cloud with initial oblique angle of  $60^\circ$ . a)  $D_{50}=0.389\text{mm}$ , b)  $D_{50}=0.507\text{mm}$ .

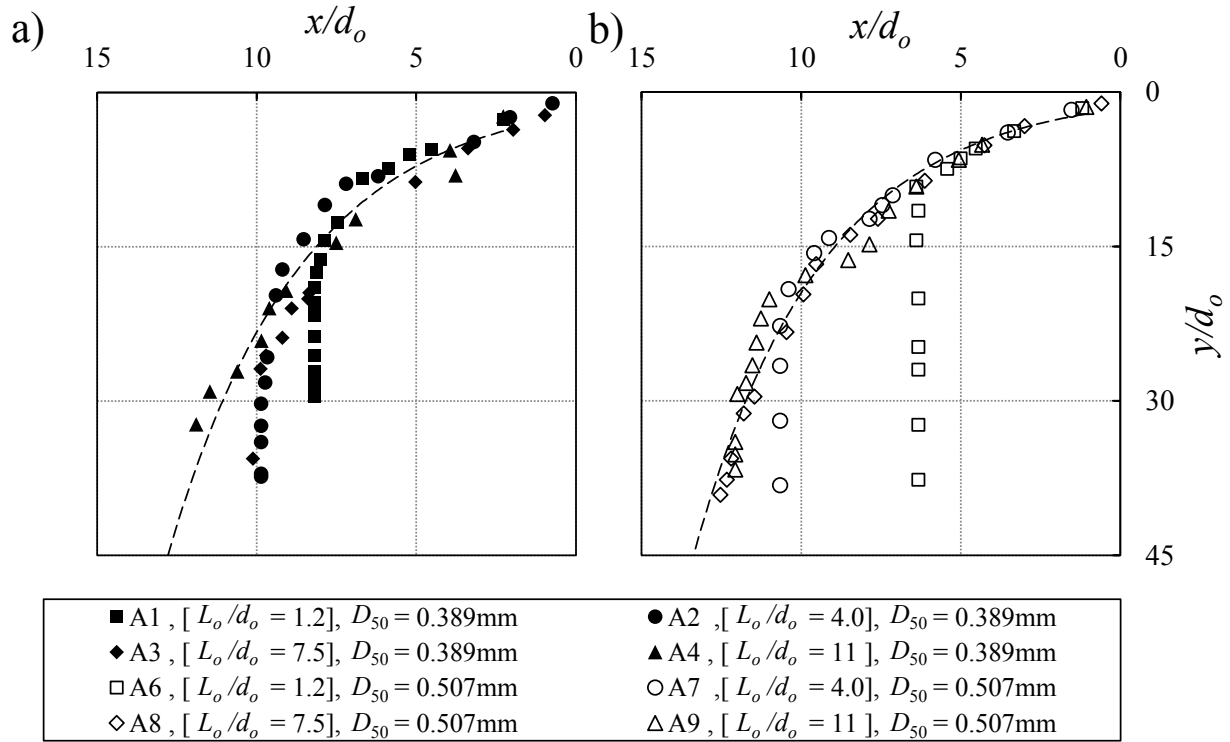


**Figure 4.4:** Effect of aspect ratio on trajectory results of oblique particle cloud with initial oblique angle of  $60^\circ$ . a) Particle size of 0.389 mm b) Particle size of 0.507 mm

#### 4.4.2 Effect of Particle Size

To study the effect of particle size on the behavior of oblique particle cloud, three different particle sizes of 0.196 mm, 0.389 mm and 0.507 mm with aspect ratios of 4 were conducted. Fig. 4.5 shows the evolution of oblique particle cloud for different particle sizes at different normalized time  $t/T$ . As can be seen from Fig. 4.5a, for large particle sizes (i.e.  $D_{50}=0.507$  mm) and  $t/T < 4$ , particle concentration distribution is almost uniform in the cloud. But, for  $t/T \geq 6.5$ , the concentration is high in bottom part of the cloud and low in the top part. It could be due to the existence of heavy particles in the cloud while the heavy particles tend to settle at the bottom of the cloud. Fig. 4.5b and 4.5c show the evolution of oblique particle cloud for medium (i.e.  $D_{50}=0.275$  mm) and small particle sizes (i.e.  $D_{50}=0.196$  mm). Comparing Fig. 4.5a,

4.5b and 4.5c at  $t/T=9$  it can be seen that the cloud passes the depth of 0.56 m for large particle sizes, 0.50 m for medium sizes and 0.48 m for small particle sizes. Therefore, the cloud with large particle sizes travels faster along the depth axis. Moreover, the trail part of the cloud with small particle size (Fig 4.5c,  $t/T=9$ ), last longer compared to large particle size (Fig 4.5a,  $t/T=9$ ).

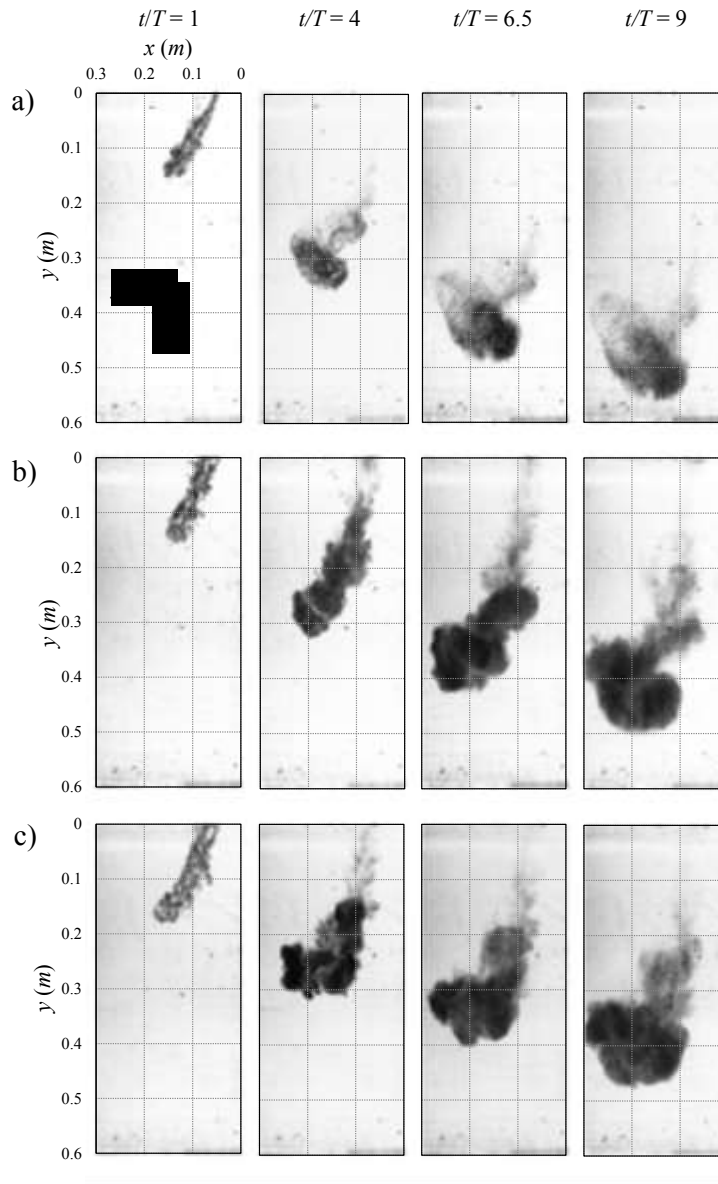


**Figure 4.5:** Effect of particle size at different normalized time  $t/T$  for oblique particle cloud with initial oblique angle of  $45^\circ$  and aspect ratio of 4. a) A11,  $D_{50}=0.507\text{mm}$ , b) A13,  $D_{50}=0.275\text{mm}$ , c) A14,  $D_{50}=0.196\text{mm}$

The effect of particle size on the trajectory of oblique particle clouds with the initial oblique angle of  $60^\circ$  is shown in Fig. 4.6. For all the three particle sizes of 0.196 mm, 0.389 mm and 0.507 mm, it was observed that the cloud reached its maximum horizontal displacement at  $t/T \approx 3$  regardless of the cloud's particle size. However, from Fig. 4.6, for the velocity comparison it was found that larger particle sizes travel longer in the horizontal direction. For example, the maximum horizontal displacement  $x_{max}$  for large and medium particles (i.e.  $D_{50} = 0.507$  and 0.389 mm) are almost 1.7 and 1.58 times of the  $x_{max}$  for small particle sizes respectively. Smaller particles tend to follow the eddies and mix with water which consumes some of the momentum to the mixing process and results in a less travel distance in the horizontal direction.

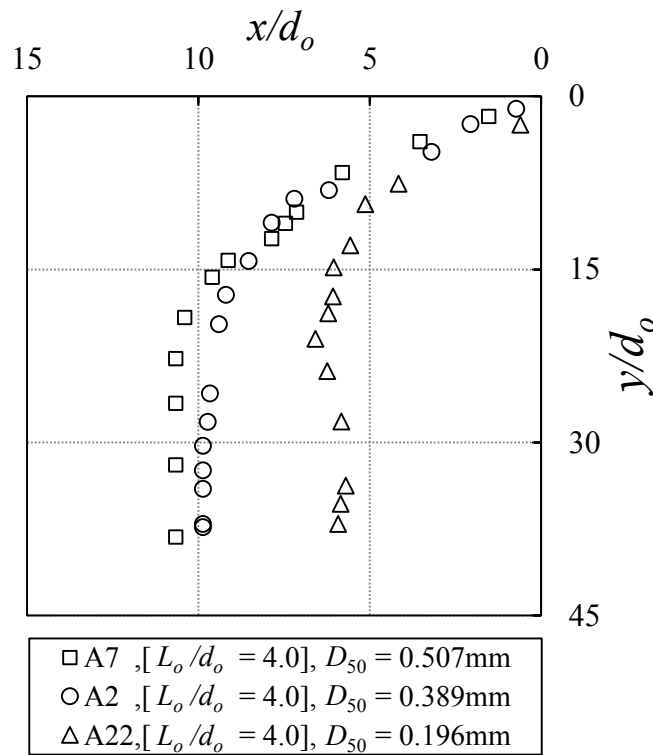


**Figure 4.6:** Effect of particle size on trajectory results of oblique particle cloud with initial oblique angle of  $60^\circ$ .

The effect that the particle size has on the velocity of oblique particle cloud is considered in Fig. 4.7. Although, large particle sizes (i.e.,  $D_{50} = 0.507$  mm) result in a higher frontal

velocity, clouds with smaller particle sizes have a larger normalized velocity ( $u_y/u_\infty$ ) since  $u_\infty$  is much smaller for clouds with small particle sizes. It is expected that the frontal velocity of particle clouds eventually reaches a plateau far from the nozzle (Noh and Fernando, 1993; Bush et al. 2003; Bond and Johari, 2005; Azimi et al., 2012). It was also observed that large particles reach their particle settling velocity or swarm phase earlier compared to small particle cloud. Dashed lines in Fig. 4.7 shows the prediction line for vertical particle cloud with  $D_{50} = 0.507$  mm and 0.196 mm (Equation 3.22). As can be seen, the normalized velocity of oblique particle cloud in the depth direction is lower than the velocity of vertical particle cloud (i.e.,  $\alpha=0$ ). Initial momentum in an oblique particle cloud is divided into the horizontal and vertical components. Therefore, some of the energy is used to generate horizontal displacement and as a result, the velocity in depth direction will decrease.

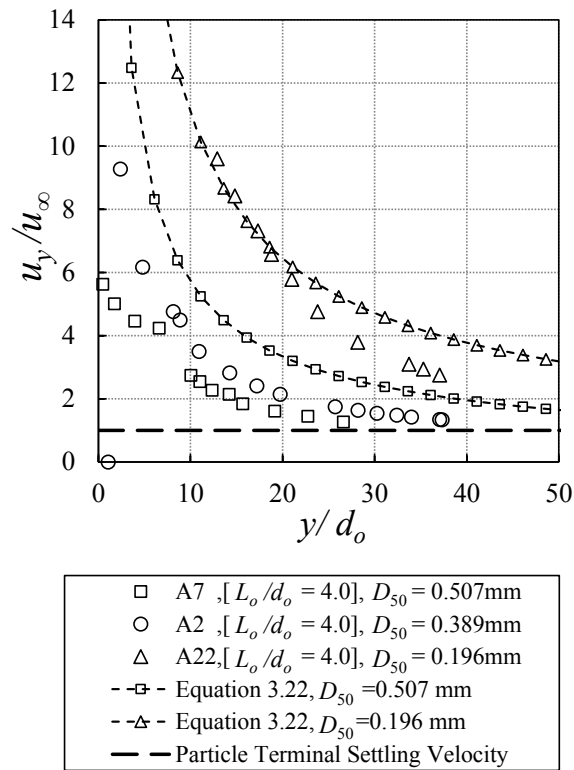


**Figure 4.7:** Effect of particle size on normalized velocity of oblique particle cloud  $u_y/u_\infty$  along normalized depth  $y/d_o$  for drop angle of 60 degree.

#### 4.4.3 Effect of Drop Angle

To study the effect of drop angle on behavior of oblique particle cloud, different angles of 15, 30, 45 and 60 degree were used for two particle sizes of 0.389 and 0.507mm. The evolution of oblique particle cloud for medium particle size (i.e.,  $D_{50} = 0.389$  mm) and oblique angles of 15, and 60 degrees at different normalized time of 1, 2.5, 5 and 8 is shown in Fig. 4.8. Comparing Fig. 4.8a and 8b for two different drop angle of 15 and 60 degrees, it can be seen that as the cloud releases by a higher angle, it travels longer in the vertical direction, but with a lower velocity in vertical direction  $u_y$ . For example, from Fig. 4.8a, at the normalized time of 8, the cloud travels to the point of  $x=0.18$  m and  $y = 0.55$  m in horizontal and vertical direction, while from figure 8b, for  $t/T=8$ , the cloud reached to  $x=0.29$  and  $y = 0.48$  m.

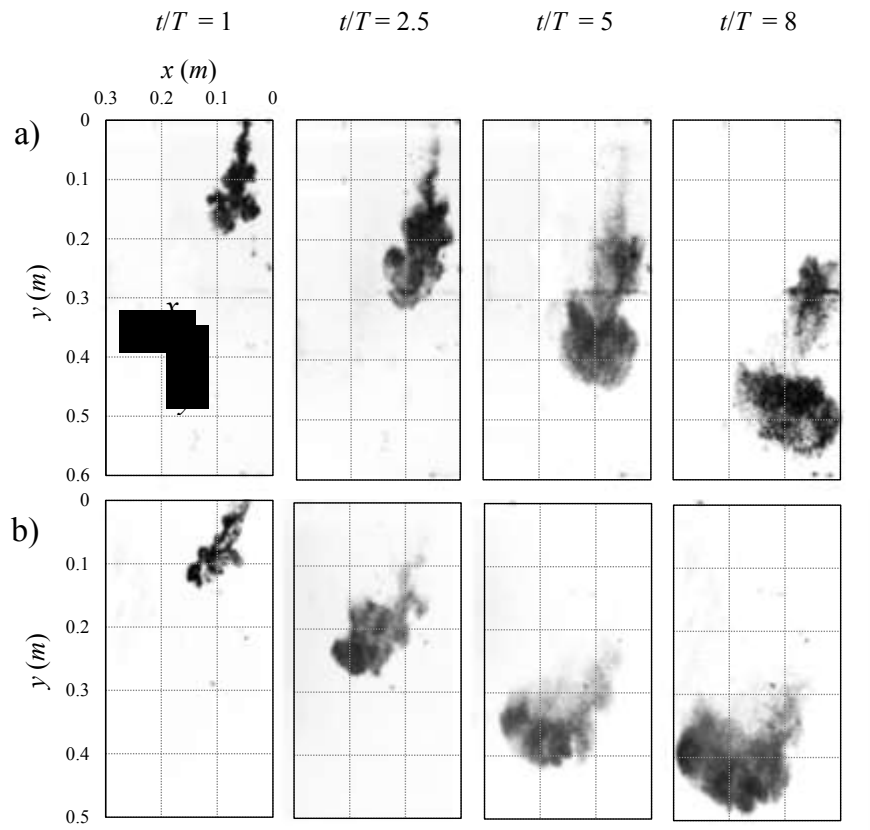


**Figure 4.8:** Effect of initial oblique angle for medium particle size (i.e.  $D_{50}=0.275$ mm) at different normalized time  $t/T$ . a)  $A_{18}$ ,  $\alpha=15^\circ$ , b)  $A_2$ ,  $\alpha=60^\circ$ .

Fig. 4.9 shows the effect of drop angle on the trajectory of oblique particle cloud. From the figure, it can be seen that the particle cloud with higher release angle travels longer in horizontal direction. Effect of drop angle for large particle size (i.e.  $D_{50}=0.507$  mm) and aspect ratio of 7.5 for two release angle of 45 and 60 degrees is plotted in Fig. 4.9a. Due to the limited depth of the tank, the maximum horizontal displacement was not observed during the experiment for aspect ratio of 7.5. Fig. 4.9b and 9c show the trajectory of oblique particle cloud for medium particle size (i.e.,  $D_{50}=0.389$  mm) and aspect ratio of 1.2 and 4. From Fig. 4.9b, it can be observed that for all oblique angles, the particle clouds reach to the maximum horizontal displacement. The  $x_{max}$  for oblique angle of 60 degrees is 1.15 and 3.2 of the clouds with drop angle of 45 and 15 degrees respectively (see Fig. 4.9b). For medium particle size and aspect ratio of 4 in Fig. 4.9c, it can be seen that the cloud with the oblique angle of 15 degrees, doesn't reach to the maximum horizontal displacement, while for oblique angles of 30, 45, and 60, the clouds reach to the  $x_{max}$ . Fig. 4.9d shows the trajectory of small particle size (i.e.  $D_{50}=0.196$  mm) with an aspect ratio of 4. From this figure, the  $x_{max}$  was not observed for any of the oblique angles which show the tendency of small particle sizes to follow the eddies.

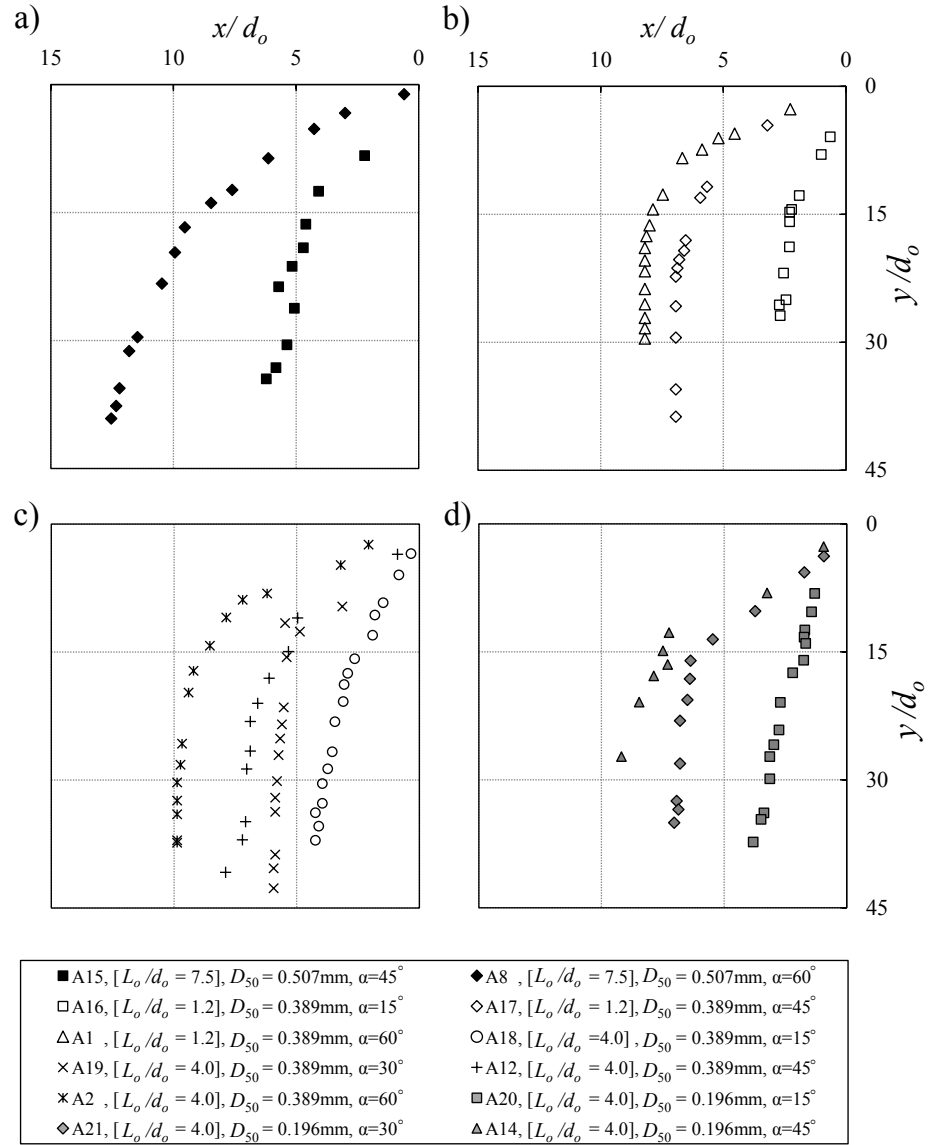


**Figure 4.9:** Effect of initial oblique angle on trajectory of particle cloud. a)  $L_o/d_o = 7.5$ ,  $D_{50}=0.507$  mm, b)  $L_o/d_o = 1.2$ ,  $D_{50}=0.389$  mm, c)  $L_o/d_o = 4$ ,  $D_{50}=0.507$  mm, d)  $L_o/d_o = 4$ ,  $D_{50}=0.196$  mm

#### 4.4.4 Effect of Drop Height

The effect of drop height on the trajectory of oblique particle cloud for medium particle size (i.e.  $D_{50} = 0.389$  mm) and release angle of 60 degrees, for different drop height  $H$ , of 0.25, 0.6, and 1 m can be seen in Fig. 4.10. From Fig. 4.10a, for small aspect ratio (i.e., 1.2), particle cloud travels less in the horizontal direction as the height increases. Increasing the height

increases the initial impact velocity from the Bernoulli equation  $v_j=(v_o^2+2gH)^{1/2}$ . However, for small  $L_o/d_o$  ratios, the particle segregation in the pipe is much greater than the extra momentum generated by the increase in the impact velocity. Due to the particle segregation of small  $L_o/d_o$  ratios, the group effect of the particles decreases while the drop height increases which leads to a reduction in horizontal travel distance. From Fig. 4.10a, it can be seen that the  $x_{max}$  for the drop height of 1 m, is 85% and 75% of the drop height of 0.6 and 1 m respectively. Fig. 4.10b shows the trajectory of oblique particle clouds while changing the height for medium aspect ratio (i.e 7.5). From this figure, particle cloud travels a longer distance in the horizontal direction as the height increases. The reason is that the momentum is dominant compared to the particles segregation. The same result was observed for large  $L_o/d_o$  ratios (i.e., 11 and 15) in Fig. 4.10c and 4.10d. The effect of the drop height for the aspect ratio of 15 and two different  $H$  of 0.6 and 1m at various  $t/T$  is shown in Fig 11a and 11b. It can be seen that for the aspect ratio of 15, the cloud travels faster in the x direction as the height increases. It can also be concluded that the oblique cloud with lower height (i.e. H=0.6 m) consist of two distinct section of front part and trail part (see Fig, 11a), while for  $H=1$  m, recognizing this two section is more complex.

Comparing Fig. 4.10b and 4.10d, it can be seen that as the  $L_o/d_o$  ratio increases, the effect of drop height or impact velocity on horizontal displacement will be more considerable. For example, from Fig. 4.10b, for aspect ratio of 7.5 the  $x_{max}$  for  $H=1$  m is 1.5 times greater than  $H=0.25$  m, while for aspect ratio of 15 in Fig. 4.10d, the  $x_{max}$  for  $H=1$  m is almost two times of the  $H=0.25$  m.

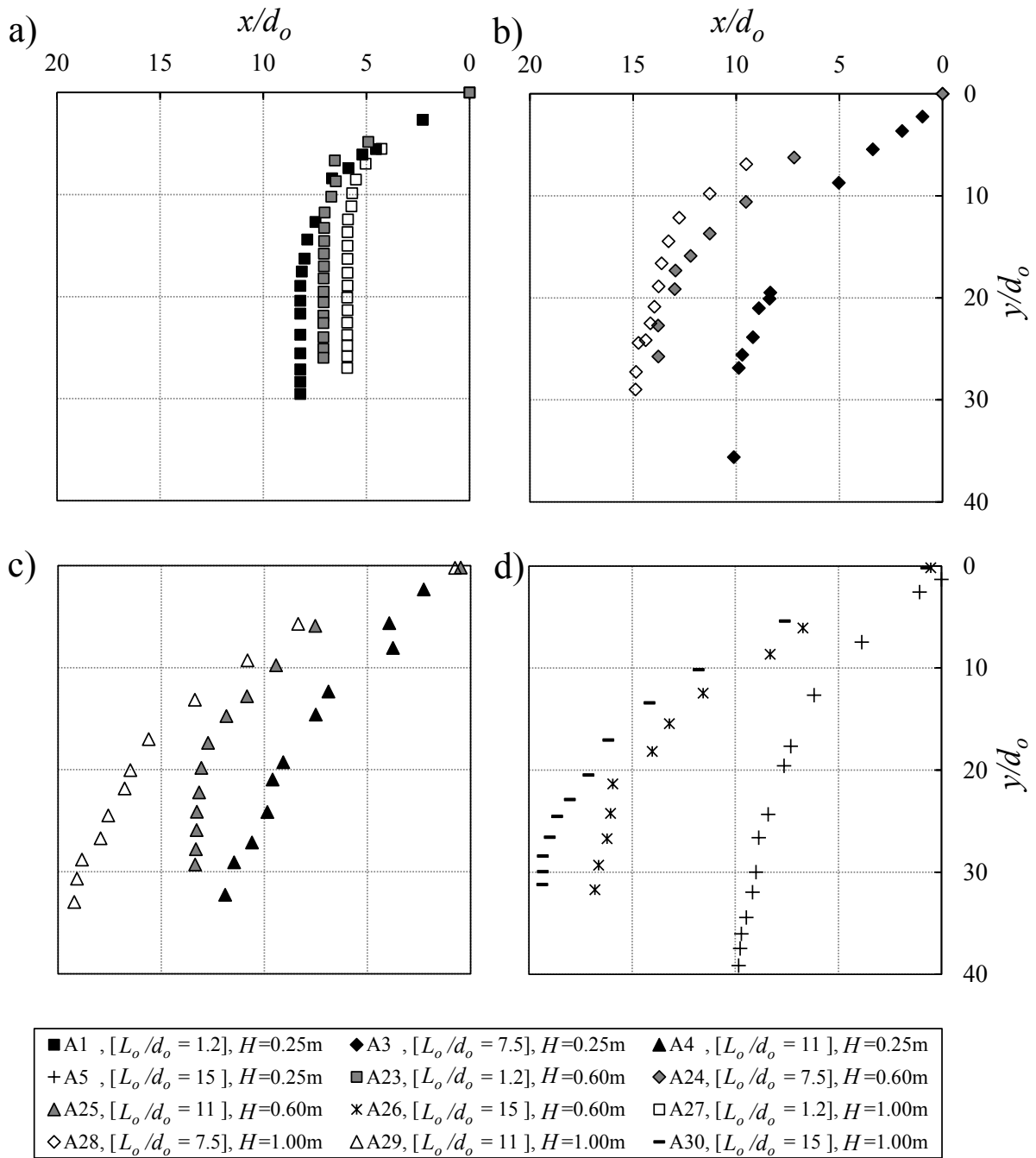


**Figure 4.10:** Effect of height on trajectory of oblique particle cloud for particle size of 0.389 mm and oblique angle of  $60^\circ$ . a)  $L_o/d_o=1.2$ , b)  $L_o/d_o=7.5$ , c)  $L_o/d_o=11$ , d)  $L_o/d_o=15$ .

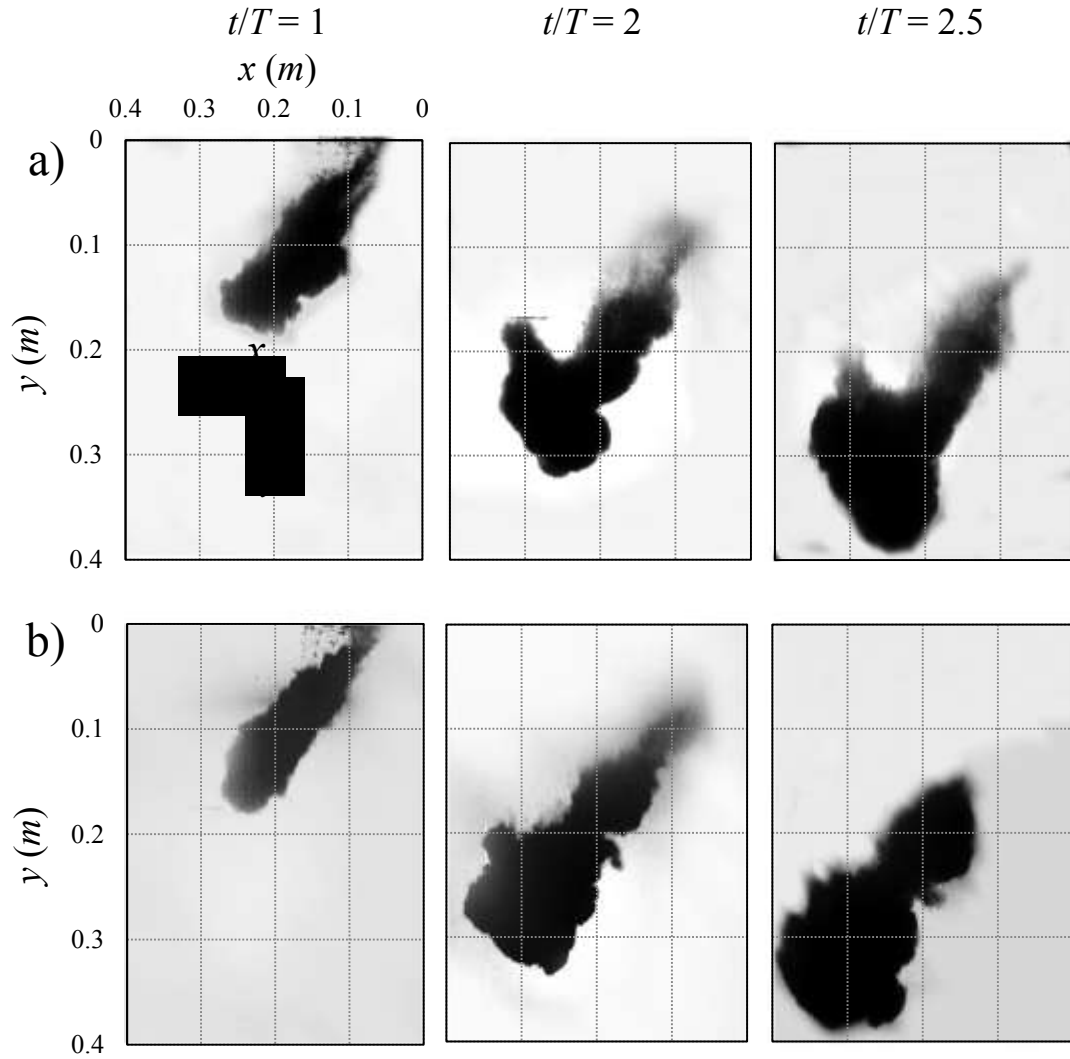


**Figure 4.11:** Effect of height at different normalized time  $t/T$  for oblique particle cloud with initial oblique angle of  $60^\circ$  and  $L_o/d_o$  ratio of 15. a) A26,  $H=0.6$  m, b) A30,  $H=1$  m.

#### 4.4.5 Entrainment Coefficient of Particle Clouds

Experimental studies reported a value between 0.1 to 0.16 for entrainment coefficient of plumes and 0.065 to 0.08 for entrainment coefficient of jets (Fischer et al., 1979; Papanicolaou & List, 1988). To consider the effect of particle size on vertical particle cloud ( $\alpha=0$ ), three different particles of 0.197, 0.389 and 0.507 mm with aspect ratio of 5 was used from the experiments of chapter 3. Azimi et al. (2012b) found that the entrainment coefficient of slurry jets is not constant

and it starts with a value of 0.06 and decreases with time and reaches a plateau with the value of 0.027. The effect of particle size on entrainment of particle cloud along normalized time can be seen in Fig. 4.12. Eq. 4.14 is used for predicting the entrainment coefficient of different particle sizes. For the comparison purpose, the entrainment coefficient of plumes and jets is added to the graphs by the dash lines with the constant values of 0.13 and 0.076 respectively (Apanicolaou & List, 1988). From the figure, it can be seen that the entrainment coefficient of small particle sizes is always greater than plumes and decreases with a very low rate. For medium and large particle sizes (i.e.  $D_{50}=0.389$  and  $0.507$  mm),  $\alpha_e$  decreases with time and varies in a range between the entrainment coefficient of plumes and jets. For the large particle size, the entrainment coefficient decreases and reaches the  $\alpha_e$  for jets at the normalized time of 5. From Fig. 4.12, it can be observed that at normalized time of 5, the entrainment of small particle sizes ( $D_{50}=0.196$  mm) is almost 1.4 and 2.1 times of medium and large particle sizes ( $D_{50}=0.389$  and  $0.507$  mm) respectively which shows the high tendency of small particles to mix with water.

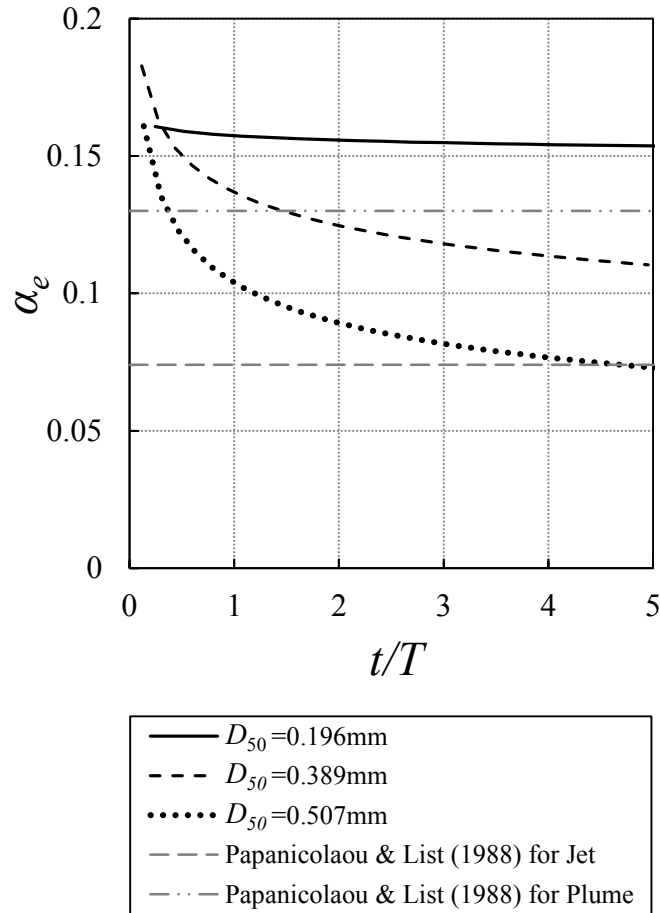


**Figure 4.12:** Effect of particle size on entrainment coefficient of vertical particle cloud

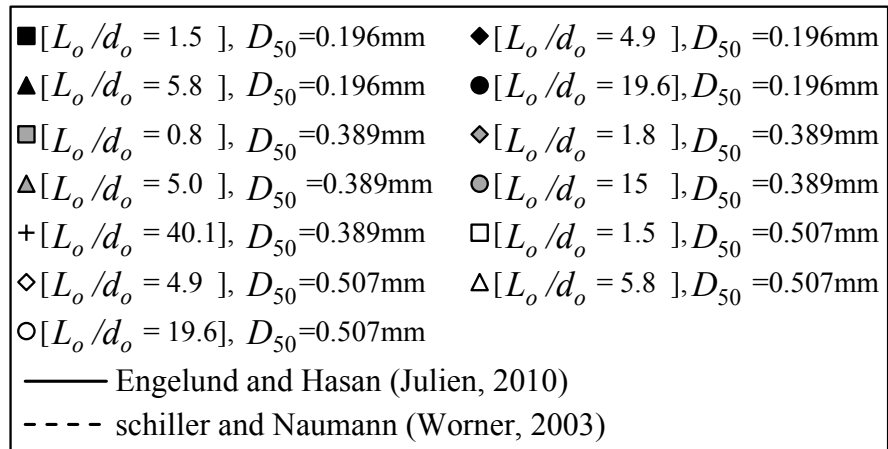
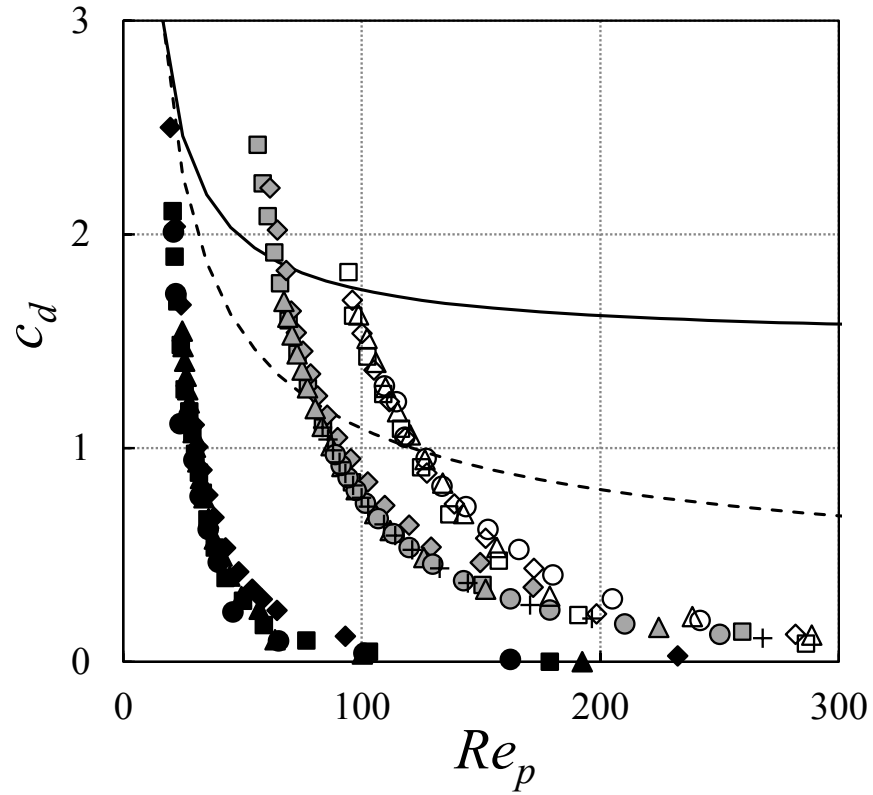
#### 4.4.6 Drag Coefficient of Particle Clouds

The classical drag coefficient was calculated from settling of a spherical particle in water. For the spherical shape, the drag coefficient can be obtained according to the research of Schiller and Naumann  $c_d=(24/Re_p)(1+0.15 Re_p^{0.687})$  (Wörner, 2003). From the experimental studies of Engelund and Hansen, the drag coefficient of sand and gravel can be obtained by  $c_d=(24/Re_p)+1.5$  (Julien, 2010). For considering the drag coefficient of particles in vertical particle clouds ( $\alpha=0$ ), Eq. (4.23) is used and the results for three particle size of 0.196, 0.389 and 0.507 mm with different aspect ratio ranging from 0.8 to 40.1 is plotted along particle Reynolds number in Fig. 4.13. For comparison, the prediction of  $c_d$  for spherical particle and sand is added to the figure. From the figure,  $c_d$  of particle cloud for all the range of  $Re_p$  is smaller than the

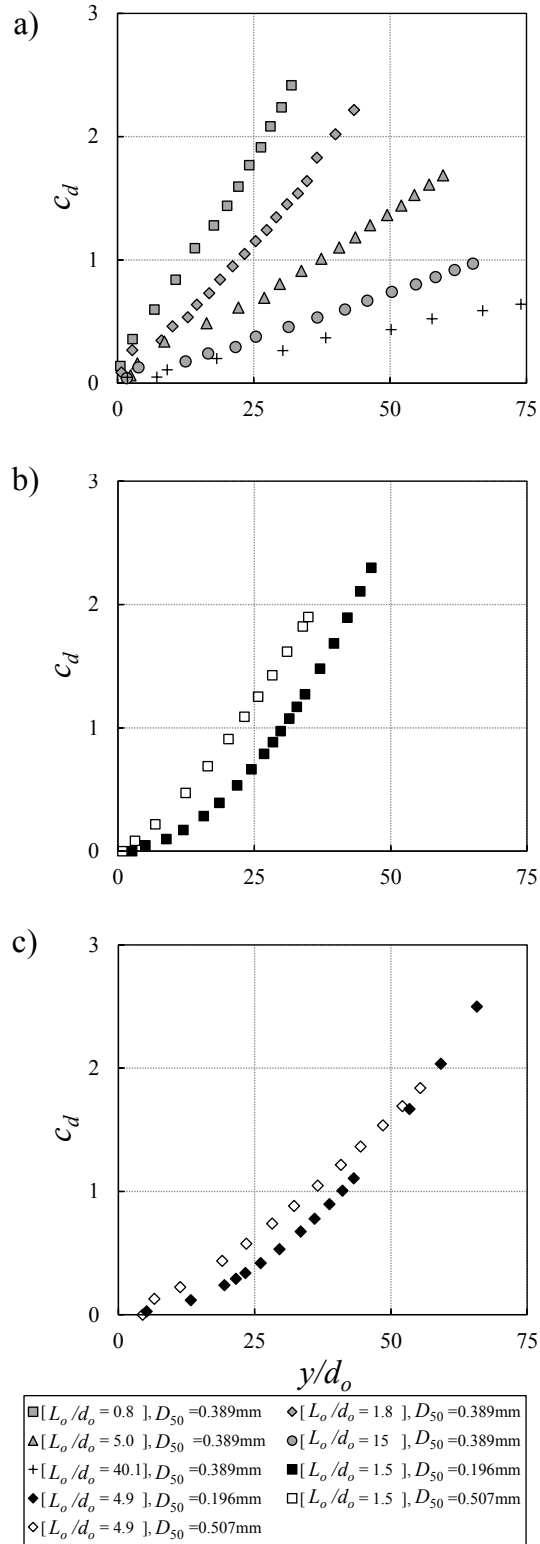
prediction trend for sand. Moreover, for small particle sizes (i.e.,  $D_{50}=0.196$  mm),  $c_d$  is lower than the  $c_d$  for the spherical particle.

Fig. 4.14 shows the variation of drag coefficient along normalized depth. The effect of aspect ratio on drag coefficient of particle cloud with medium size ( $D_{50}=0.389$  mm) can be seen in Fig. 4.14a where larger aspect ratios have smaller drag coefficient. For example, for normalized depth of 25, the  $c_d$  of particle cloud with the aspect ratio of 0.8 is almost eight times of the aspect ratio of 40.1. The wave effect for larger aspect ratios is greater than smaller aspect ratios; therefore, the amount of force exerted to each particle by the surrounding fluid is smaller compared to lower aspect ratios.

Fig. 4.14b and 4.14c show the effect of particle size on drag coefficient of particle cloud for small and medium particle sizes (i.e.,  $D_{50}=0.196$  and 0.507 mm). Hollow points in the figure reflect the data for large particle sizes and solid point are the data for small particle sizes. From Fig. 4.14b, it can be seen that for small aspect ratio (i.e., 1.5), small particle sizes have lower drag coefficient. The reason is that the number of particles  $N$  in the cloud with small particle size is higher compared to large particles. Therefore, the drag force exerted to each particle in the cloud is smaller. The same result was also observed for medium aspect ratio (i.e., 4.9) as shown in Fig. 4.13c.



**Figure 4.13:** Variation of the drag coefficient of particle cloud along the particle Reynolds number,  $Re_p$ .



**Figure 4.14:** Effect of aspect ratio and particle size on drag coefficient of particle cloud. a) Variation of drag coefficient along normalized depth  $y/d_o$  for different aspect ratio b) Effect of particle size on drag coefficient for small aspect ratio of 1.5

#### 4.5 Summary and Conclusion

Experimental study was carried out to consider the behavior of oblique particle cloud in water. Effect of experimental parameters such as particle size, aspect ratio, drop angle and drop height on evolution of the oblique particle cloud were studied in detail over 30 experiments.

It was observed that aspect ratio can considerably control the velocity of oblique particle cloud. For higher aspect ratio, a greater vertical velocity was observed due to higher amount of initial momentum. Moreover, for two particle sizes of 0.389 and 0.507 mm and different aspect ratio, it was observed that the cloud reaches to maximum horizontal displacement at approximately  $t/T=3$ . Furthermore, the aspect ratio affect the trajectory of oblique particle cloud. Higher aspect ratio resulted the clouds to travel longer in horizontal direction compared to smaller aspect ratios. For the oblique particle cloud, three phase of motion includes initial, thermal and swarm was observed. During the swarm phase, the oblique particle cloud settles in vertical direction with particle settling velocity,  $u_{\infty}$ .

Different particle sizes of 0.196 mm, 0.389 mm and 0.507 mm with aspect ratio of 4 were used to consider the effect of particle size on behavior of oblique particle cloud. It was found that larger particle sizes travel longer in x direction compared to smaller particle sizes.

For considering the effect of drop angle, two particle sizes of 0.389 and 0.507mm with releasing angles of 15, 30, 45 and 60 degree were used. Higher release angle resulted in a higher travel distance in horizontal direction but with a lower velocity in depth direction.

The drop height also affects the evolution of oblique particle cloud. For small aspect ratio (i.e.,  $L_o/d_o=1.2$ ), particle cloud travels less in the horizontal direction as the height increases. For the aspect ratio larger than 7.5, it was found that the cloud travels longer in the horizontal direction with increasing the height.

To study the entrainment of vertical particle cloud, an equation was developed to consider the entrainment coefficient in particle clouds. The effect of particle size on entrainment of particle clouds was also studied. It was observed that the entrainment coefficient for small particle sizes (i.e.,  $D_{50}=196$  mm), is greater compared to entrainment coefficient of plumes. For medium and large particle sizes ((i.e.,  $D_{50}=196$  and  $507$  mm), it was found that  $\alpha_e$  decreases with time and varies in a range between the entrainment coefficient of plumes and jets. Moreover, the small particle sizes have higher tendency to mix with water; therefore, the entrainment coefficient of small particle sizes are greater than medium and large particle sizes.

The drag coefficient of particle cloud was also studied in this research. The drag coefficient for particle cloud with small particle sizes (i.e.,  $D_{50}=196$  mm), was lower than the  $c_d$  for the spherical particle. Moreover, due to the higher number of particles in the cloud for small particle sizes, a lower drag coefficient was resulted for small particle sizes. It was also observed that aspect ratio can affect the drag coefficient where larger aspect ratio resulted in a larger drag coefficient.

#### 4.6 Notation

*The following symbols are used in this paper:*

$A_s$  = Surface area of the cloud,  $m^2$

$A_p$  = Projected frontal area,  $m^2$

$b$  = Width of particle cloud, m

$c_o$  = Initial concentration of Sand Jet in tube

$c_d$  = Drag coefficient of particles

$d_o$  = Nozzle size, mm

$D_{50}$  = Particle Size, mm

$F_B$  = Normalized buoyancy, N

$\overline{F_D}$  = Average drag force, N

$g$  = Acceleration due to Gravity,  $m/s^2$

$g'$  = Reduced gravity,  $m/s^2$

$H$  = Release height, mm

$m$  = Sand mass, g

$N$  = Number of particles in the cloud

$L_o$  = Length of sand occupied in release tube, mm

$L$  = Distance travels by piston, mm

$Q_e$  = Entrained flow rate,  $m^3/s$

$Re_p$  = Particle Reynolds number

$T$  = Time of the initial phase, s

$t$  = Time, s

$u_\infty$  = Terminal settling velocity, m/s

$u_f$  = Sand jet frontal velocity, m/s

$u_y$  = Sand jet vertical velocity, m/s

$u_e$  = Water velocity entering the cloud during the entrainment process, m/s

$V$  = Volume of Sand Jet,  $mm^3$

$V_o$  = Initial volume of sand jet in tube,  $m^3$

$v_o$  = Initial velocity at the nozzle, m/s

$v_j$  = Velocity at the water surface, m/s

$x$  = Horizontal distance of cloud from nozzle, m

$x_{max}$  = Maximum horizontal distance of cloud from nozzle, m

$y$  = Vertical distance of cloud from nozzle, m

$\alpha$  = Initial drop angle, degree

$\alpha_e$  = Entrainment coefficient

$\mu$  = Dynamic viscosity, m<sup>2</sup>/s

$\rho_p$  = Densities of sand particles, kg/m<sup>3</sup>

$\rho_w$  = Densities of water, kg/m<sup>3</sup>

## Chapter 5: General Conclusions and Recommendations for Future Research

### 5.1 General Conclusions

In the preceding chapters, a comprehensive experimental study was presented on the dynamic behavior of particle cloud in the water.

In chapter 2, the literature review of the current study was presented. In chapter 3, an experimental study on sand jets and particle cloud in water was conducted. A total of 36 experiments were done to consider the effect of  $L_o/d_o$  ratio, sand particle size, and sand released height. In order to study the effect of  $L_o/d_o$  ratio, six different masses of 1, 3, 6, 9, 12, 18 grams and five different nozzle diameters of 5, 8, 10, 12 and 14mm were used to form different  $L_o/d_o$  ratios ranging from 0.8 to 40.1. Different sand particle sizes were used to consider the effect of particle size with median grain sizes of  $D_{50} = 0.1375, 0.196, 0.389, 0.507, \text{ and } 0.718$  mm. To investigate the effect of released height, 5 different levels of  $H = 0.1, 0.2, 0.3, 0.75$  and 1.3 m were considered and the following results were concluded:

- All range of particle size finally reached their terminal settling velocity.
- Small particle sizes (i.e.  $D_{50} = 0.1375$  and 0.196mm) have small terminal settling velocity; therefore, particles should travel a longer distance to reach terminal settling velocity compared to large particle sizes ( $D_{50} = 0.507$  and 0.718mm).
- To study the evolution of particle clouds in stagnant water, a non-dimensional time scale  $t^* = t/T$  is proposed where  $T$  is the time of initial phase.
- Increasing  $L_o/d_o$  ratio caused the particle cloud to progress faster in water.
- For small particle sizes (i.e.,  $D_{50} = 0.196$  mm), two phases of initial and thermal phases were observed.

- For medium and large particle sizes (i.e.,  $D_{50}=0.389$  and  $0.507$  mm), three phases of initial, thermal and swarm were observed. The swarm phase was observed when the particles travel with their particle settling velocity.
- Larger particle sizes, had shorter thermal region, because they do not tend to follow eddies.
- A power law correlation was found to be suitable for the depth progression with time as  $x/d = a(t/T)^b$  where  $a$  and  $b$  are constants. The constant  $a$  was found to be 17.72, 18.1 and 19.42 for the initial, thermal and swarm phases, respectively. The average exponent of the power law correlation  $b$  was found to be 0.65, 0.60 and 0.58 for the initial, thermal and swarm phases, respectively.
- It was found that frontal velocity of particle cloud is between the frontal velocity of sand jet and particle settling velocity.
- The initial width of particle cloud for small particle sizes was larger than clouds with medium and large particle sizes.
- Particle clouds were classified into three different shapes based on particle size. An arc-shaped for large particle sizes, a bowl shape for medium and a semi-spherical shape for small particle sizes.
- It was observed that cloud with small particle sizes have more tendency to mix with water and follow the eddies which cause a wider cloud compared to large particle clouds.
- The dilution in particle clouds was much greater than sand jets and sand concentration decreased rapidly after releasing particle from the nozzle.

- Release height  $H$  doesn't have a significant impact on the frontal velocity of particle cloud in the water.
- For the effect of initial sand velocity, it was found that for the small  $L_o/d_o$  ratios (i.e.,  $L_o/d_o \approx 1.5$ ), sand particles disperse more compared to large  $L_o/d_o$  ratios and it is due to the air resistance which concludes to the generation of a wide cloud reaching the water surface. For medium  $L_o/d_o$  ratio (i.e.,  $L_o/d_o \approx 5$ ), the momentum force produced by higher impact velocity became dominant. As a result, a cloud with smaller width was formed. For large  $L_o/d_o$  ratios (i.e.,  $L_o/d_o \approx 20$ ), impact velocity doesn't have a great effect on the width of the cloud.

In chapter 4, a total of 30 experiments were conducted to study the oblique particle cloud behavior in water. The experiments were done in a glass tank filled with tap water with length, width and height of 1.65 m, 0.85 m, and 0.85 m respectively. To consider the effect of aspect ratio  $L_o/d_o$ , a relatively wide  $L_o/d_o$  ratio ranging from 1.2 to 15 was used. Moreover, the effect of drop angle  $\alpha$  and release height  $H$  on behavior of oblique particle cloud was also studied and the following results were concluded:

- It was found that entrainment in particle cloud is a function of nozzle diameter  $d_o$ , particle size  $D_{50}$ , initial time  $T$ , aspect ratio  $L_o/d_o$ , normalized time  $t/T$ , and particle settling velocity  $u_{\infty}$  (Eq. 4.14).
- A correlation was performed to estimate the drag coefficient of each particle in the cloud (Eq. 4.23) which is a function of particle velocity, the projected frontal area of each particle  $A_p$ , the number of particles in the cloud  $N$ , water density, and the average drag force (from Eq. 4.21).

- Three phases of motion were observed during the experiments on oblique particle cloud include initial, thermal and swarm phase.
- Larger aspect ratio resulted in a faster particle cloud in a vertical direction.
- Regardless of particle size and aspect ratio, the clouds reached to the maximum horizontal displacement at  $t/T \sim 3$ .
- For all particle sizes, as the aspect ratio  $L_o/d_o$  increased, the maximum horizontal displacement was also increased.
- It was found that large particles (i.e.,  $D_{50} = 0.507$  mm) travel longer in horizontal direction compared to small particle sizes (i.e.,  $D_{50} = 0.196$  mm).
- Higher initial drop angle  $\alpha$ , was resulted in a longer maximum horizontal distance.
- Increasing the drop height decreased the maximum horizontal displacement for small aspect ratio  $L_o/d_o$  (i.e.,  $L_o/d_o = 1.2$ ). However, for medium and large aspect ratios (i.e.,  $L_o/d_o = 7.5, 11$  and  $15$ ), particle clouds traveled a longer distance in the horizontal direction as the drop height increased.
- The entrainment coefficient of small particle sizes (i.e.,  $D_{50} = 0.196$  mm) was found to be greater than medium and large particle sizes (i.e.,  $D_{50} = 0.389$  and  $0.507$  mm).
- It was found that the entrainment coefficient of small particle sizes (i.e.,  $D_{50} = 0.196$  mm) was always greater than single-phase plumes.
- The entrainment coefficient  $\alpha_e$  of medium and large particle sizes (i.e.,  $D_{50} = 0.389$  and  $0.507$  mm) decreased as the cloud travels in the tank. For medium particle sizes, the  $\alpha_e$  varied in a range between the entrainment coefficient of single-phase

plumes and jets while for the large particle sizes it reached the entrainment coefficient of jets at the normalized time of 5.

- It was resulted that particles in the cloud with the larger aspect ratio have smaller drag coefficient  $c_d$ .

## 5.2 Future Research Studies

Since the behavior of particle cloud in water is so complex, further research can enhance our current understanding. A list of possible applied research topics with a brief introduction is described below.

- *Effect of Aspect Ratio and Particle Size on Sediment Deposition of Particle Cloud*

Effect of aspect ratio and particle size on the behavior of particle cloud was studied in this research and the results were shown in chapter 3. Particle clouds have three phases of motion includes initial, thermal and swarm phase. Each phase may lead to a different deposition shape. Because of acceleration that the particles have in the initial phase (i.e. when the sand is still entering into the water), the cloud will hit the bottom of the tank and the deposition will start and the deposition form may be different with other phases such as swarm. In this process, the aspect ratio can control the time of the initial phase. For example, for a specific amount of sand, one can release the sand with a small aspect ratio  $L_o/d_o$  (If we consider a large nozzle diameter, a small aspect ratio  $L_o/d_o$  will be formed). The other time, the same amount of sand is released with a large aspect ratio in a way that the initial phase time is greater than the time the sands reach to the bottom, so the hitting would occur and the cloud will deposit like a sand jet. This two different approaches may lead to different shapes of deposition.

- *Deposition of the Oblique Particle Cloud*

The effect of drop angle on the behavior of particle cloud was studied in this research. It was found that aspect ratio can control the trajectory of the oblique particle cloud. We can form two different shapes of particle cloud with the same amount of sand, one with a large aspect ratio and the other with a small one. The cloud with the larger aspect ratio will generate a longer cloud with a small width while the smaller aspect ratio will settle with a larger width and a shorter length. So it may be concluded that the deposition form of oblique particle cloud can be controlled by the aspect ratio. Moreover, the drop angle may also change the deposition form. For the drop angles close to zero (i.e. vertical particle cloud), a circular shape is expected, while for greater  $\alpha$ , an elliptical shape may be formed. Finally, a relationship may be found between the dimension of the elliptical, initial aspect ratio of the cloud and the drop angle.

- *Effect of Water Depth on Deposition of Oblique Particle Cloud*

In this research, it was found that the growth rate of the cloud depends mainly on particle size and aspect ratio. Therefore, it can be concluded that the form of deposition can be controlled by these two factors. The water depth is another important factor that can change the form of deposition. For example, particle cloud in thermal phase tends to grow fast while in swarm phase, particles do not mix with water and tend to settle with their particle settling velocity. Therefore, it is very important that in which phase the particles reach the bottom of the tank. It seems that after the swarm phase, the depth doesn't have a great effect on the deposition form of the cloud.

- *Experimental Study of Particle Cloud in Current Water*

This research mainly focuses on still-water bodies such as enclosed lakes without a strong current. The equations that were proposed for velocity, width, trajectory, entrainment, and

drag coefficient is applicable for particle cloud in still-water. In some practical problems such as dropping sand in rivers and sea, we deal with flowing water or considerable current in the water. Therefore, depending on the velocity and direction of the flow, the particle cloud behavior such as velocity, dilution, trajectory and entrainment may be different. Predicting the trajectory and deposition form of the cloud with the presence of current seems an interesting area of study. The current may lead to a wider particle cloud that settles with a lower velocity and a tendency to move in the flow direction.

- *Effect of Particle Density on Behavior of Oblique Particle Cloud*

In this research, the effect of different parameters such as particle size, aspect ratio and oblique angle on dynamics of particle cloud was studied. Another parameter that can affect the particle cloud's behavior is the density of particles. The current project was based on sand particles with the density of  $2540 \text{ kg/m}^3$ . The industry may spill some sources of pollutant with different particles density and particle shape. Higher density makes the cloud to settle faster and mix less with water.

## References:

- Arakeri, J. H., D. Das, A. Krothapalli, and L. Lourenco. (2004) "Vortex ring formation at the open end of a shock tube: a particle image velocimetry study." *Physics of Fluids* 16, no. 4.
- Azimi, A. H., Zhu, D. Z., Rajaratnam, N. (2012a). "Experimental study of sand jet front in water" *Int. J. Multiphase Flow*, 40, 19–37.
- Azimi, A. H., Zhu, D. Z., Rajaratnam, N. (2012b). "Computational investigation of vertical slurry jets in water" *Int. J. Multiphase Flow*, 47, 94-114.
- Azimi, A. H., Qian Y., Zhu, D.Z., Rajaratnam, N. (2011). "Effect of particle size on the characteristics of sand jet in water" *J. Eng. Mech.*, 137, 1–13.
- Azimi, A. H., Zhu, D. Z., Rajaratnam, N. (2014). "Experimental Study of Subaqueous Sand Deposition from Slurry Wall Jets" *J. Eng. Mech.*, 140, 296-314.
- Azimi, A. H., Zhu, D. Z., Rajaratnam, N. (2015). "An experimental study of circular sand–water wall jets" *Int. J. Multiphase Flow*, 74, 34–44.
- Batchelor, G. K. (1954). "Heat convection and buoyancy effects in fluids" *Quarterly journal of the royal meteorological society*, 80, 345, 339-358.
- Bin, A.K., 1984. "Air entrainment by plunging liquid jets", In: Proc. of the Symposium on Scale Effects in Modeling Hydraulic Structures, Esslingen, 3–6 September, Paper 5.5, pp. 1–6
- Bond, D., Johari, H. (2005). "Effect of initial geometry on the development of thermals" *Experiments in fluids*, 39, 589–599.
- Bond, D., and H. Johari., (2010), "Impact of buoyancy on vortex ring development in the near field." *Experiments in fluids* 48, no. 5: 737-745.
- Bush, J.W.M., Thurber, B.A., Blanchette, F. (2003). "Particle clouds in homogeneous and stratified environments" *J. Fluid Mech.*, 489, 29–54.
- Cai, J., Hall, N., Elenany, M., Zhu, D.Z., Rajaratnam, N. (2010). "Observations on sand jets in air" *J. Eng. Mech.*, 136, 1181–1186.
- Cai, Jianan, David Z. Zhu, and N. Rajaratnam, (2012). "Observations on sand jets in viscoplastic fluids." *Theoretical and Applied Mechanics Letters* 2, no. 5.
- Chanson, H., 1997. "Air Bubble Entrainment in Free-Surface Turbulent Shear Flows", Academic Press, London.
- Chanson, H., 2004. "Environmental Hydraulics of Open Channel Flows." Elsevier/Butterworth-Heinemann, Oxford, UK.

Chin, D. A. (2012). “*Water-Quality Engineering in Natural Systems: Fate and Transport Processes in the Water Environment*” John Wiley & Sons.

Crowe, C. T., (2000). “On models for turbulence modulation in fluid – particle flows.” *Int. J. Multiphase Flow*, Vol. 26, 719-727.

Energy, Alberta. (2009). "Alberta's Energy Industry." *An Overview*.

Fischer, H.B., List, E.J., Koh, R.C.Y., Imberger, J., Brooks, N.H. (1979). “*Mixing in Inland and Coastal Waters*” Academic press, San Diego, California, USA, 483p.

Friedman, P. D., and J. Katz. "The flow and mixing mechanisms caused by the impingement of an immiscible interface with a vertical jet." *Physics of Fluids*, no. 9 (1999): 2598-2606.

Gharib, M., Rambod, E. and Shariff, K. (1998). “A universal time scale for vortex ring formation” *J. Fluid Mech.*, 360, 121-140.

Gensheimer, R. J., (2010), “Dynamics of particle clouds in ambient currents with application to open-water sediment disposal.” *MSc. Thesis*, Dept. of Civil and Environmental Engineering, MIT, Cambridge, MA, 260 p.

Gensheimer, R.J., Adams, E.E. and Law, A.W. (2012), "Dynamics of particle clouds in ambient currents with application to open-water sediment disposal" *Journal of Hydraulic Engineering*, 139(2), pp.114-123.

Hall, N., Elenany, M., Zhu, D.Z., Rajaratnam, N. (2010). “Experimental study of sand and slurry jets in water” *J. Hydraulic Eng., ASCE*, 136, 727–738.

Ham, J. M., and G. M. Homsy. "Hindered settling and hydrodynamic dispersion in quiescent sedimenting suspensions." *International journal of multiphase flow* 14, no. 5 (1988): 533-546.

Holdich, R.G. (2002). “Fundamentals of particle technology” *Midland Inform. Technol. Publ.*, 173.

Jiang, J. S., Law, A. W. K., and Cheng, N. S. (2005). “Two-phase analysis of vertical sediment-laden jets” *J. Eng. Mech.*, 131(3), 308–318.

Julien, P.Y. (2010). “*Erosion and Sedimentation*” Cambridge University Press.

Lai, A.C., Zhao, B., Law, A.W.K. and Adams, E.E., (2013) "Two-phase modeling of sediment clouds" *Environmental fluid mechanics*, 13(5), pp.435-463.

Lee, J. H. W., and Chu, V. H. (2003). "Turbulent jets and plumes; A lagrangian Approach." Kluwer Academic Publishers Group, the Netherlands, 390 p.

List, E. J. (1982). "Mechanics of turbulent buoyant jets and plumes" *Turbulent buoyant jets and plumes, HMT, the science and applications of heat and mass transfer*, 6, 1-68.

Luketina D, Wilkinson D (1998) "The transition to the swarm phase for a particle cloud" In: Proceedings of the 13th Australasian fluid mechanics conference, Melbourne, Australia.

Lundgren, T.S., Yao, J. and Mansour, N.N. (1992). "Microburst modelling and scaling" *J. Fluid Mech.*, 239, 461-488.

Mohseni, K. and Gharib, M. (1998). "A model for universal time scale of vortex ring formation" *Physics of Fluids*, 10(10), 2436-2438.

Moreira, D. and Vilhena, M. eds. (2009). "*Air pollution and turbulence: modeling and applications*" CRC Press.

Morton, B. R., Geoffrey Taylor, and J. S. Turner. (1956). "Turbulent gravitational convection from maintained and instantaneous sources" In *Proceedings of the Royal Society of London A: Mathematical, Physical and Engineering Sciences*, 234, 1196, 1-23.

Muste, M., Fujita, I., & Kruger, A. (1998). "Experimental comparison of two laser-based velocimeters for flows with alluvial sand" *Exp. Fluids*, 24, 273-284.

Neto, I. E., Zhu, D. Z., & Rajaratnam, N. (2008). "Air injection in water with different nozzles" *Journal of Environmental Engineering*, 134(4), 283-294.

Nicolai, H., B. Herzhaft, E. J. Hinch, L. Oger, and E. Guazzelli. (1995) "Particle velocity fluctuations and hydrodynamic self-diffusion of sedimenting non-Brownian spheres." *Physics of Fluids (1994-present)* 7, no. 1: 12-23.

Nicolas, M. (2002). "Experimental study of gravity-driven dense suspension jets." *Physics of Fluids*, 14, no. 10.

Noh, Y., Fernando, H.J.S. (1993). "The transition in the sedimentation pattern of a particle cloud" *Physics of Fluids A: Fluid Dynamics*, 5, 12, 3049–3055.

Noh, Y. (2000). "Sedimentation of a particle cloud across a density interface" *Fluid Dyn. Res.*, 27, 129–142.

- Pantzlaff, L. Lueptow, R.M. (1999). "Transient positively and negatively buoyant turbulent round jets" *Experiments in Fluids* 27, 117-125.
- Papanicolaou, P. N., and List, E. J. (1988). "Investigations of round vertical turbulent buoyant jets" *J. Fluid Mech.*, 195, 341–391.
- Parthasarathy, R. N., & Faeth, G. M. (1987). "Structure of particle-laden turbulent water jets in still water" *International Journal of Multiphase Flow*, 13(5), 699-716.
- Philippe, P., Raufaste, C., Kurowski, P., & Petitjeans, P. (2005). "Penetration of a negatively buoyant jet in a miscible liquid." *Physics of Fluids*, 17, no. 5.
- Pignatel, F., Nicolas, M. and Guazzelli, E., 2011. A falling cloud of particles at a small but finite Reynolds number. *Journal of Fluid Mechanics*, 671, pp.34-51.
- Pottebaum, T. S., & Gharib, M. (2004). "The pinch-off process in a starting buoyant plume" *Experiments in fluids*, 37(1), 87-94.
- Qu X. L., Khezzar L., Danciu D., Labois M., Lakehal D. (2011). "Characterization of plunging liquid jets: A combined experimental and numerical investigation" *Int. J. Multiphase Flow*, 37, 722–731.
- Qu, X. L., Goharzadeh, A., Khezzar, L., & Molki, A. (2013). "Experimental characterization of air-entrainment in a plunging jet" *Experimental Thermal and Fluid Science*, 44, 51-61.
- Rahimipour, H. and Wilkinson, D. (1992). "Dynamic behavior of particle clouds" *Eleventh Australasian Fluid Mechanics Conference*, Vols 1 and 2, University of Tasmania, Hobart, Australia, 743-746.
- Rao, K. K., Nott, P. R. and Sundaresan, S. (2008). *An introduction to granular flow*, Cambridge University Press, Cambridge, N.Y.
- Rogers, Michael C., and Stephen W. Morris. (2009) "Natural versus forced convection in laminar starting plumes." *Physics of Fluids (1994-present)* 21, no. 8.
- Ruggaber, G. J., (2000), "Dynamics of particle clouds related to open-water sediment disposal." *Ph.D. Thesis*, Dept. of Civil and Environmental Engineering, MIT, Cambridge, MA, 242 p.
- Scase, M. M., C. P. Caulfield, P. F. Linden, and S. B. Dalziel. "Local implications for self-similar turbulent plume models." *Journal of Fluid Mechanics* 575 (2007): 257-265.
- Sheen, H. J., Jou, B. H., and Lee, Y. T. (1994). "Effect of particle size on a two-phase turbulent jet" *Exp. Therm. Fluid Sci.*, 8, 315–327.
- Sharma, H. D., & Reddy, K. R. (2004). *Geoenvironmental engineering: site remediation, waste containment, and emerging waste management technologies*. John Wiley & Sons, Inc..

Shusser, M., & Gharib, M. (2000a). "Energy and velocity of a forming vortex ring" *Physics of Fluids*, 12(3), 618-621.

Shusser, M. and Gharib, M. (2000b). "A model for vortex ring formation in a starting buoyant plume" *J. Fluid Mech.*, 416, pp.173-185.

Swamee, P.K. and Ojha, C.S.P., (1991) "Drag coefficient and fall velocity of non-spherical particles" *Journal of Hydraulic Engineering*, 117(5), pp.660-667.

Toombes, L., and Chanson, H., (2005). "Air-water mass transfer on a stepped waterway." *J. Environ. Eng.*, 131(10), 1377–1386.

Turner, J. S. 1986 "Turbulent entrainment: the development of the entrainment assumption, and its application to geophysical flows." *J. Journal of Fluid Mechanics*

Tsuji, Y., Y. Morikawa, T. Tanaka, K. Karimine, and S. Nishida. "Measurement of an axisymmetric jet laden with coarse particles. " *International Journal of Multiphase Flow* 14, no. 5 (1988): 565-574.

Turner, J. S. (1969) "Buoyant plumes and thermals" *Annual Review of Fluid Mechanics* 1.1: 29-44.

Wang, H. and Wing-Keung Law, A. (2002). "Second-order integral model for a round turbulent buoyant jet" *J. Fluid Mech.*, 459, 397-428.

Wang, X., & Kikkert, G. A. (2014). "Behaviour of oblique jets released in a moving ambient" *Journal of Hydraulic Research*, 52, 4, 490-501.

Wang H, Law AWK (2002) "Second-order integral model for a round turbulent buoyant jet." *J Fluid Mech* 459:397–428

Wang, R. Q., Law, A. W. K., Adams, E. E., & Fringer, O. B. (2009). "Buoyant formation number of a starting buoyant jet" *Physics of Fluids (1994-present)*, 21(12), 125104.

Wang, R. Q., Law, A. W. K., Adams, E. E., & Fringer, O. B. (2011). Large-eddy simulation of starting buoyant jets. *Environmental fluid mechanics*, 11(6), 591-609.

Wang, R.Q., Adams, E.E., Law, A.W.K. and Lai, A.C., (2015) "Scaling particle cloud dynamics: from lab to field" *Journal of Hydraulic Engineering*, 141(7), p.06015006.

Wörner, M., (2003). "A compact introduction to the numerical modeling of multiphase flows" Forschungszentrum Karlsruhe.

Wynanski, I., Fiedler, H., (1969). "Some measurements in the self-preserving jet." *Journal of Fluid Mech.*, Vol. 38, part 3, pp. 577-612.

Zhao, B., Law, A.W., Eric Adams, E., Shao, D. and Huang, Z., (2012) "Effect of air release height on the formation of sediment thermals in water" *Journal of Hydraulic Research*, 50(5), pp.532-540.